

國立中央大學

應用地質研究所

碩士論文

利用台灣西南部二仁溪之階地分析探討全新  
世構造運動

**Holocene Tectonics Inferred from Fluvial  
Terrace Analysis in the Erhjen River (二仁溪),  
Southwestern Taiwan**

研究生：Hadis Sakti Hasyimi Miftahul Ulum

(哈帝斯)

指導教授：黃文正博士

Maryline Le Béon Ph.D

中華民國一百零八年一月

## 題目

菲律賓海板塊每年以約8cm/year的速率向歐亞板塊聚合，並且形成了台灣造山帶。板塊隱沒造成的縮短變形主要集中於台灣東部的花東縱谷、板塊縫合帶以及西部麓山帶前緣。此板塊聚合作用於西部麓山帶南側形成一系列的逆衝斷層，並藉由2000年至2010年的大地測量數據可觀察到每年6公分的速率向西移動以及每年2公分之速率抬升。本研究的目標為利用局部河流下切速率及水準測量資料來了解古亭坑斷層帶在全新世的變形行為。位於西部麓山帶南段的二仁溪流經數個地質構造，包含古亭坑斷層、龍船斷層及小滾水背斜，本研究將二仁溪河階區分為四個群集與四個子群集，在靠近古亭坑斷層處共有10處的地形面向西北傾斜 $1^{\circ}$ 至 $4^{\circ}$ ，誤差為 $0.02^{\circ}$ 。根據河階沉積物中的碳十四定年結果得知最古老的河階(T1a)老於2200 B.P.、最年輕的河階(T4a)不超過800B.P.，上游至下游的地形剖面顯示河階坡度從T4至T1逐漸增加，T4a傾斜 $1.98^{\circ}$ 、T1a傾斜為 $4.28^{\circ}$ 。我們藉由一組與地形測繪符合之碳十四定年結果來計算二仁溪的河流局部下切速率，計算的結果顯示河流局部下切速率在2ka至1ka期間為 $2\sim 6$  mm/year，而1ka至今則劇增為 $25\sim 27$  mm/year。假設碳十四定年的結果能代表河階沉積物之真實年代，針對二仁溪在1 ka至今下切速率據增之現象，本研究提出了三個可能的假設：(1)河道坡度的改變、(2)存在向西傾斜的逆衝斷層以及(3)斷層活動性的改變。

**關鍵字：**二仁溪、全新世大地構造、河流階地分析

## Abstract

The Taiwan orogenic belt is the result from the westward convergence of the Philippine Sea Plate towards the Eurasian Plate at a rate of ~8 cm/yr. Shortening is mostly consumed along the Longitudinal Valley in Eastern Taiwan, the plate suture, and across the Western Foothills, at the mountain piedmont. In the southern Western Foothills, this convergence caused a series of thrust systems and westward movement reaching up to 6 cm/yr and 2 cm/yr local uplift rate based on geodetic data during 2000 – 2010. The Erhjen River, which is located in the south part of the Western Foothills, flows across several geological structures which are the Gutingkeng fault, Lungchuan fault, and Hsiaokunshui anticline. We found that four groups and four sub-groups of terrace level were developed. By observing these terraces we aim at better understanding the Holocene deformation across the Gutingkeng fault zone. We observe that 10 geomorphic surfaces are tilted with slope values in the range  $1^\circ - 4^\circ \pm 0.02^\circ$  and mostly tilted to the NW direction near the Gutingkeng fault zone. Based on radiocarbon dating from a previous study and from our work, we estimate the age of the oldest terrace (T1a) to more than 2200 Years BP, while the youngest terrace (T4a) is less than 800 Years BP. Euclidian topographic profile from upstream to downstream shows that the terrace slope increases from T4 to T1, with a slope of  $1.98^\circ$  for T4a and  $4.28^\circ$  for T1a. We obtain local incision rate of four geomorphic surface where the radiocarbon dates are consistent with the geomorphic mapping. The calculation results show that the local incision rate at three sites are similar, ranging from 25 – 27 mm/yr, while local incision rate is slower at the fourth site, at 15.3 mm/yr. Leveling data during 2004 - 2016 shows uplift rates of the same order in this area reaching 25.1 – 34.2 mm/yr, with the west side uplifted relative to the east side, while based on geology Gutingkeng fault is an east dipping thrust. We propose three working hypotheses that could explain the Erhjen River local incision rate in our study. These hypotheses include a change in river slope, the existence of a west-dipping thrust fault, and/or a change in the fault activity.

**Keywords:** Erhjen River, Holocene Tectonics, Terrace analysis.

## Acknowledgments

I would like to thank الله (Allah) for His mercy and guidance in giving me the strength to complete this master thesis which entitled “Holocene Tectonics Inferred from Fluvial Terrace Analysis in the Erhjen River (二仁溪), Southwestern Taiwan.

I owe my deepest gratitude to my parents. Without their pray and support, I will not have a spirit to finish this master thesis. They help me to get up when I am down, they remind me to stay low when I am up. Midnight calls with them always make me calm whenever I feel pessimist to my own.

I would like to express my deepest appreciation to my advisor Dr. Maryline Le Béon who guided me through this project from the beginning. She helped me to do my fieldwork. She teaches me anything that I did not know before. Thank you for being patient to teach me, I am deeply grateful to you.

I want to express my gratitude to Professor Wen-Jeng Huang who also become my advisor. He teaches me how to be a graduate student, to be a discipline, and more important he accept me as his student with all of my deficiency. Thank you for letting me in, in the Geomechanics Research Group.

I also want to thank Professor Meng-Long Hsieh and Professor Ching Kuo-En for providing me his unpublished  $^{14}\text{C}$  data and leveling data.

The last, I want to thank all of the Geomechanic Research Group especially Yu-Chun and Yen-Ju. They help me during my two years study in here. We work together as a classmate to finish our study in NCU. It is a great pleasure to acknowledge my deepest thanks to our senior, Mike and Yi-Wei. Our senior take their time to help us to check everything before we submit our master thesis.

# Table of Contents

題目 .....	ii
<b>Abstract</b> .....	<b>iii</b>
<b>Acknowledgments</b> .....	<b>iv</b>
<b>Table of Contents</b> .....	<b>v</b>
<b>List of Figures</b> .....	<b>vii</b>
<b>List of Tables</b> .....	<b>xi</b>
<b>Chapter 1 : Introduction</b> .....	<b>1</b>
1.1 Background of Study .....	1
1.2 Geological Setting of Taiwan.....	3
1.3 Geological Setting of Southwest Taiwan.....	5
1.3.1 Geological Deformation History of Southwest Taiwan.....	10
1.3.2 Rapid Tectonic Deformation in Southwest Taiwan .....	13
1.4 River Terrace study in Southwest Taiwan .....	16
1.5 Geomorphic Setting of the Erhjen River.....	22
1.6 Research Objectives .....	25
<b>Chapter 2 : Methodology</b> .....	<b>27</b>
2.1 Field Survey .....	27
2.2 Erhjen River Terrace Mapping.....	28
2.3 Tilted Terrace mapping .....	30
2.4 Radiocarbon Dating ( <sup>14</sup> C) .....	32
<b>Chapter 3 : Results and Discussions</b> .....	<b>34</b>
3.1 Erhjen River Terrace Classification Map.....	34
3.2 Radiocarbon Dating Results.....	39
3.3 Tilted Terrace at the midstream of Erhjen River .....	45
3.4 Discussion .....	55
3.5 Limitation.....	62

<b>Chapter 4 : Conclusions .....</b>	<b>64</b>
<b>References .....</b>	<b>66</b>
<b>Appendixes.....</b>	<b>72</b>
<b>Appendix A: Terrace Map (Attached) .....</b>	<b>73</b>
<b>Appendix B: Leveling Data Station Map (Attached).....</b>	<b>74</b>

## List of Figures

Figure 1.1 Geodynamic setting and major geological provinces of Taiwan (Modified from F. Mouthereau et al., 2001) .....	3
Figure 1.2 (a) Geological map of Southwest Taiwan (Modified from Biete et al., 2018). Blue frame indicates our research area, bigger scale is in the Figure 1.4. (b) Geological cross-section of E-E' and F-F'. We only consider the E-E' and F-F' sections because they are located near our research area. ChT = Changhua thrust; CiT = Chishan thrust; CT = Chenglungpu thrust; CuT = Chutochi thrust; LT = Lungchuan thrust; PT = Pingchi thrust; ChF = Chauchou fault; HF = Hsinhua fault; ZF = Zuojhen fault; NA = Niushan anticline; NeA = Neiyingshan anticlinorium; SS = Shihchangli syncline; TA = Tainan anticline; TS =Tingpinglin syncline; YS = Yushing syncline; HS = Hsiaolin syncline; KS = Kuanglin synform .....	7
Figure 1.3 (A) Regional geological map of Tainan area, southwestern Taiwan (Le Beon et al., 2017) T= Tainan anticline, C= Chungchou anticline, P = Pitou anticline, N= Napalin anticline, G= Guanmiao Syncline, S = Shihtzuchi syncline. (B & C) Balanced geological cross-section. Red faults are inferred to have activated during the Meinong earthquake (Le Beon et al., 2017) .....	8
Figure 1.4 Geological and structural map of the Southwestern Foothills. The geological units are classified based on the rock ages. The Tawan syncline, Tainan anticline, Chungchou anticline, Houchiali fault, and Hsiaokangshan fault are from Central Geological Survey geological map, 2013 (Modified from CPC Geological Map, 1989).	9
Figure 1.5 The Taiwan orogeny in terms of the geodynamic processes (Modified from Huang et al., 2000) .....	10
Figure 1.6 Correlation between regional and local tectonic evolution in the southwestern foreland thrust belt during the Plio-Pleistocene collision. (A) Timing of local thrust activity. (B) Curves of regional sedimentation rates. (Modified from F. Mouthereau et al., 2001) .....	12
Figure 1.7 (A) Horizontal velocities relative to the station S01R based on GPS measurements during 2002 to 2010 (Ching et al., 2015). Arrows denote the vectors derived by GPS observation. (B) Vertical velocities based on leveling data during 2000 – 2010 (Ching et al., 2015). Red color means uplift, blue color means subsidence. The red	

dash line frame represents research area. HKSF = Hsiaokangshan Fault, LCNF = Lungchuan fault, CHNF = Chisan Fault, CCFU = Chaochou Fault.....	14
Figure 1.8 ALOS coseismic interferograms of $M_w$ 6.4 Jiashan Earthquake in March 4 <sup>th</sup> , 2010. The colors represent the coseismic slant range displacement (Courtesy of Huang Mong-Han, 2017).....	15
Figure 1.9 Location of the Gutingkeng fault trace based on CPC, CGS and comparison with the location of the displacement gradient observed from InSAR (similar dataset as Fig 1.8). Note that the Gutingkeng fault is identified as an east-dipping thrust based on geology, while the footwall was uplifted relative to the hanging wall during the Jiashan earthquake. ....	15
Figure 1.10 Geological and geomorphological framework of the Erhjen River basin. Location of the mud volcanoes is based on Shih (1967); structures are according to Chinese Petroleum (1971); rock chronology is based on Lin (1991) (Modified from Hsieh & Knuepfer, 2001) .....	17
Figure 1.11 Distribution of river terraces in the upstream segment of the Erhjen River (Modified from Hsieh & Knuepfer, 2001).....	18
Figure 1.12 Distribution of river terraces in the midstream segment of the Erhjen River (Modified from Hsieh & Knuepfer, 2001).....	19
Figure 1.13 Distribution of river terraces in the downstream segment of the Erhjen River (Modified from Hsieh & Knuepfer., 2001).....	20
Figure 1.14 (A) Longitudinal profile along the Erhjen River from upstream to downstream to show the distribution of each terrace (B) Proposed correlation of the river terrace sequences in the main-stem Erhjen River. (Modified from Hsieh & Knuepfer, 2001) ..	21
Figure 1.15 Topography in the Erhjen River area based on 5m DEM .....	24
Figure 1.16 Annual Precipitation record of Tainan Station during 1990 – 1996 (CWB climatic data in Hsieh & Knuepfer., 2001) .....	25
Figure 2.1 Classifying terraces in the field. See map Appendix A-1 for the location ....	27
Figure 2.2 Formation of terrace levels due to the river incision and lateral erosion (Burbank, 2012) .....	28
Figure 2.3 Slope map of the Erhjen River area based on 5m DEM.....	29
Figure 2.4 Slope calculation for the tilted terrace .....	30
Figure 2.5 Sketch explaining curvilinear versus euclidian distance .....	31
Figure 2.6 Screen capture of the 1-m DEM based on LiDAR data in the midstream segment of the Erhjen River.....	32

Figure 3.1 Erhjen River terrace map (Appendix A for bigger scale).....	35
Figure 3.2 (A) 3D morphotectonic map of the upstream segment of the Erhjen River upstream with vertical exaggeration of 1.5x (times). (B) Topographic profiles showing two different levels of terrace deposit.....	36
Figure 3.3 (A) 3D morphotectonic map of the Erhjen River midstream segment with vertical exaggeration of 1.5x (times). (B) Topographic profiles of 4 within frame A showing morphology of the Erhjen River midstream area .....	37
Figure 3.4 Midstream of Erhjen River terrace map. (B) Aerial photo of Erhjen River midstream segment.....	38
Figure 3.5 Stratigraphic column for each radiocarbon dating sites. (Lithology symbols and colors – USGS, 2006).....	41
Figure 3.6 Outcrop photos where the C2, C9, C62, and C68 samples were taken. ....	43
Figure 3.7 Topographic profiles of A-A', and D-D'. The age in C68 is projected into A-A' section (Map view in figure 3.4).....	44
Figure 3.8 (A) The “B” terrace landscape field photo (B) Abandoned channel of Erhjen River (C) Shear zone of Gutingkeng fault .....	47
Figure 3.9 Interpretation on the fault trace based on the tilted terrace. (A) 1m DEM map. (B) 5m DEM map .....	48
Figure 3.10 (A) Topographic profiles of frame “A” located in map <b>Figure 3.9</b> . (B) Field photograph of the topographic scarp.....	49
Figure 3.11 Euclidian section of A-A' used to project the terraces along the Erhjen River (Appendix A for bigger scale).....	50
Figure 3.12 Projected topographic profile A-A' (See location in <b>Figure 3.11</b> ). The code number of radiocarbon dates refers to table 3.1. The number on each borehole represents the conventional age with Years Before Present (YBP) as the unit. Location of CGS borehole data in appendix: A. Details of each borehole data are in the table 3.3 .....	51
Figure 3.13 Curvilinear topographic profile along the Erhjen River .....	52
Figure 3.14 Schematic diagram of <sup>14</sup> C dates for each group of terrace age based on Hsieh & Knuepfer (2001) and this study.....	53
Figure 3.15 Sea level observation around Taiwan based on Kaohsiung & Penghu Station (Tseng, 2009) .....	57
Figure 3.16 Generalized curve of sea level rise since the last ice age (Courtesy of Vivien Gornitz - NASA, 2007).....	57

Figure 3.17 Location of the leveling benchmark and 280° azimuth projection axis Z-Z' with geological map as the background (Appendix: B for bigger map).....	58
Figure 3.18 Projection of benchmark leveling point position to the Z-Z' axis. The colors in the graph and the geological structure are based on the CPC geological map .....	59
Figure 3.19 The location of the highest uplift leveling benchmark point in the midstream segment of the Erhjen River.....	60
Figure 3.20 Leveling data time series for benchmarks G477, G478, J109 and J110 (Courtesy of Ching Kuo-En, 2018).....	60
Figure 3.21 The location of interpreted reverse fault.....	61

## List of Tables

Table 2.1 Absolute dating methods (Burbank, 2012). Red frame indicates the method that is used in this study .....	33
Table 3.1 Radiocarbon dates along the Erhjen River. The number of the sample correlates with the map in Appendix A. Samples with a number starting with capital “C” (grey column) are the samples from this study (conventional ages) while the others are from a previous study (Meng-Long Hsieh conventional ages – Unpublished data) .....	40
Table 3.2 Slope measurements for the tilted terrace in the midstream segment of the Erhjen River. (Refers to <b>Figure 3.9</b> ).....	46
Table 3.3 Central Geological Survey borehole data (Central Geological Survey, borehole sites refer to map in Figure 3.13) .....	53

# Chapter 1 : Introduction

## 1.1 Background of Study

A river valley has features which contain a record of a past geomorphic event. It can be formed of the drainage basin, drainage system, and landforms associated with a stream. The study of all these landforms helps to interpret the geomorphic history of the river valley. Characteristics of landform such as topography imbalances, uplifted peneplains, incised meander, and alluvial terrace can be used as a past events geomorphic indicator.

River terraces are the feature of landforms formed by river action. River terraces are located along the river floodplains (Kumar, 2005). It is a flat platform on one or both sides of the river and may have many such levels. Multi-level river terraces appear like step-like forms on one or both sides of the river. Two consecutive terrace levels are generally separated by a vertical distance termed as terrace risers. The shape, size and vertical distance of flat surface between two consecutive terrace levels vary spatially. The terrace usually composed of material deposited by the river. This material includes alluvium, boulders, fossils, paleosols, and tools of paleo-civilizations. River terraces usually formed by the former river floodplains, the formation of river terraces is relating with the processes of erosion and deposition. No erosion and deposition take place when the ratio of stream power and resisting power is equal to one. But the increase in stream power favors degradation and increase in resisting power leads to aggradation (Kumar, 2005). When the process of aggradation is followed by degradation, this leads to the abandoning of depositional surfaces and creation of fill or depositional terraces. Thus fill terraces record the perturbations of catchment's sediment. The study of these deposits and the processes of terrace formation are interpreted to study about climate and tectonics. Hence the study of river terraces is a multi-disciplinary field of investigation and has attracted the attention of researcher across subject lines.

The progress of the fluvial terrace study is one of the most prominent geomorphic features in Taiwan. The study of fluvial terraces is essential in revealing the neotectonic and the geomorphological evolution in Taiwan. However, such studies are limited by the limitations of dating methods.

In the Southwestern part of Taiwan where the geological structure and the development of tectonic deformation are rapid, a knowledge about terrace is necessary to analyze this. In the GPS velocity map and Leveling map by Ching et al., 2015 shows the velocity of the horizontal deformation in the eastern part of Southwest Taiwan reaching up to 6 cm/year locally to the west and 2cm/yr in the western part due to the tectonics of the Philippines sea plate colliding with the eastern Eurasian plate. This velocity differences resulting in an N-S trend major fault. Two of these faults are Qishan Fault and Lungchuan Fault. Based on the leveling data in the Lungchuan fault area the footwall part uplifted ~2 cm/yr which make this phenomenon is interesting. The Lungchuan fault is N-S trend east-dipping thrust fault. This fault brought the Miocene age sandstone over the Pliocene age Mudstone.

Lungchuan fault branched off into 2 faults in the southern part become Gutingkeng fault and Lungchuan fault itself. The uplifted footwall phenomenon propagate to the Gutingkeng fault. Lungchuan fault trace line passes through several major rivers in southwest Taiwan. One of them is Erhjen River. Erhjen River is a westward flowing river from Western Foothills to the Taiwan Strait. This river produces a river terrace then developed to be a terrace deposit. This terrace deposit can be studied in more detail to analyze the river response to the geological structure which developed in southwest Taiwan especially along the Erhjen River.

In the Southwestern part of Taiwan itself, the existence of fluvial terraces has been known for a long time. But these terraces have not yet been studied in detail. This research studies about the river terraces in the Southwestern part of Taiwan along the Erhjen River aided with complementary radiocarbon  $^{14}\text{C}$  dating and several  $^{14}\text{C}$  dates from the previous study. These radiocarbon dates will help to classify multiple terraces which developed along the Erhjen River. This classification is used to analyze the river response to climate change and active tectonic uplift.

## 1.2 Geological Setting of Taiwan

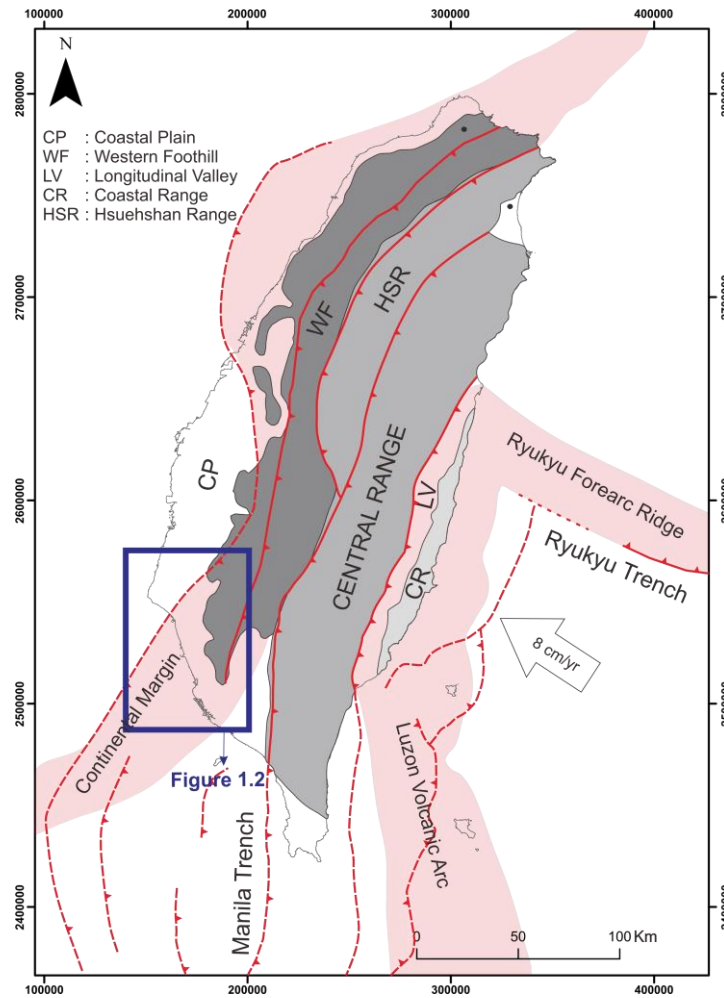


Figure 1.1 Geodynamic setting and major geological provinces of Taiwan (Modified from F. Mouthereau et al., 2001)

In the western part of Pacific, the island of Taiwan located at the junction between the Luzon and Ryukyu arcs. The Chinese passive margins formed as a result of rifting during the early Cenozoic time and Luzon arc collisions with passive margins, starting at late Miocene, resulted in the formation of Taiwanese orogeny which actively propagates to the South (Chou, 2002). Taiwan mountain belt has been presented as an example to understand the evolution of active structures in the foreland thrust belt (Mouthereau et al., 2001) because of the collision between the Philippine Sea Plate and the Eurasian block of South China Sea since late Miocene (Sibuet & Hsu, 2004). According to GPS survey (Yu et al., 1999), the present-day convergence rate of the Philippine Sea Plate towards the Eurasian block of South China Sea is about 8 cm/yr. This causes the rise of the mountainous area reaching up to 3950 m in elevation with N-S trend. The metamorphic basement of Taiwan is the oldest geological-tectonic element. Formed in the late

Paleozoic to the Mesozoic era when the sequences of sandstone, shale, siltstone, limestone, and thick volcanic rocks are deposited along with the association of acids to the intermediate magmatic activity. This old geological-tectonic element encounter several phases of orogenic deformation, magmatism, and metamorphism, culminating in the late Mesozoic orogeny known as Nanao Orogeny. These Pre-Cenozoic rocks were then folded into the mountains and deeply metamorphosed to form Taiwan's Major metamorphic complex (CGS website).

Taiwan Island also divided into several major geologic terrains from west to east: Coastal Plain, Western Foothills, Hsuehshan Range, Central Range, Longitudinal Valley, and Coastal Range.

Coastal Plain located in the western part of Taiwan Island consists of Holocene sediments and alluvial deposits from the mountainous area brought by the river bordered by Western foothills in the east. The Western Foothills composed of Oligocene to Pleistocene clastic sediments. The Western Foothills consist of a series of mountains and hills flanking to the west margin of the Central Range. The boundary between the Western foothills and Coastal plain is hard to define topographically.

Hsuehshan Range is part of Central Range which forms the backbone ridge of the island. This region consists of Pre-Tertiary continental basement uncomfortably with the Eocene to Miocene metamorphosed clastic deposit during the Paleogene rifting and Oligocene-Miocene post-breakup phases associated with the opening of the South China Sea (Lin et al., 2003). Hsuehshan range mostly composed of low-grade metamorphic rocks. The grade of the metamorphic rocks is higher towards the east.

At the east of Central Range, there is the Longitudinal Valley bordered by Longitudinal Valley fault. Longitudinal Valley mostly composed of Sediments which deposited from the Central Range metamorphic area and Coastal Range. Longitudinal Valley also recognized as the suture zone between Eurasian plate and Philippine Sea Plate. Two major structures dominate the Longitudinal Valley which is the Longitudinal Valley fault and Central Range fault.

The Coastal Range includes two main units of different origin, which are the volcanic basement (Tuluanshan Formation). And a thick terrigenous sequence (Takangkou Formation). The Tuluanshan Formation make up the basement for the Coastal Range. It is mainly composed of volcanic of andesitic origin, mainly agglomerates associated with dikes and intrusions. Available radiometric dating shows the main andesitic intrusion and lava flows are Miocene in age (Ho, 1969; Richard, 1983).

The terrigenous sequences represent several thousand meters of sediments which overlie the Tuluanshan Formation. The Stratigraphy of the Coastal Range records the evolution of the Taiwan orogeny and the Plio-Quaternary collision process (Barrier et al., 1985).

The research area of this study is located in the south part of the Western foothills and Coastal Plain. Mudstone and sandstone are the dominant lithologies which made this place occupied by several small badlands area.

### **1.3 Geological Setting of Southwest Taiwan**

The southwestern Taiwan fold and thrust belt are formed on the outer shelf and slope of the Eurasian continental margin. It comprises a roughly N-S striking, west verging imbricate thrust system that has been developing since the Late Miocene (Biete et al., 2018). This west verging imbricate thrust system yield a roughly N-S striking lithology and geological structures.

The geological map from Biete et al., 2018 & Le Béon et al., 2017 (Error! eference source not found. & Error! Reference source not found.) shows that the distribution of the lithology is the rocks are younger towards the west. E-E' and F-F' geological cross-sections show that in the foreland basin (western part of Xuxian antiform) characterized by low dipping angle and dominated by west dipping direction. As we go near the Xuxian antiform, the dipping angle starts to steep and where the Lungchuan thrust occurred, the dip direction change to the east. The geological cross-section from the Biete et al., 2018, they uses the uncertainty of Vp 5.2 km/s to represents the top of the metamorphic basement layer. Another balanced geological cross-section (**Figure 1.3**) also shows a similar result regarding the dipping angle it becomes steeper as we go near the Lungchuan back-thrust. This Lungchuan back-thrust is part of a fault that activated during the Meinong earthquake (February 5<sup>th</sup>, 2016) together with the Tainan Detachment, Pitou back-thrust, Napalin back-thrust, and Changchihkeng detachment. The movement of Lungchuan back-thrust also can be seen in the InSAR co-seismic map of M<sub>w</sub> 6.4 Jiashan earthquake where the west side of the Lungchuan fault trace show sharp uplift relative to the east side ( Courtesy of Mong-Han Huang., 2017) .

The Miocene rocks emerge on the earth surface as the shape of ridges. These ridges mostly composed by high dipping angle due to the thrust fault system caused by the westward movement of Manila Plate in the East coast of Taiwan. The Miocene rocks consist of several formations from Late Miocene to Early Miocene such as

Changchihkeng Formation, Tangenshan Formation, Wushan Formation, and Yenshuikeng Shale.

In the top of Miocene rocks, there are Pliocene Rocks which is dominated by mudstone from Gutingkeng Formation. This mudstone intercalated with a thin layer of medium – fine sandstone. High dipping angle to the overturned bedding of Pliocene rocks also can be found both in the hanging-wall and foot-wall of Lungchuan Fault. Lungchuan Fault brings the Miocene rocks on the top of Pliocene Rocks, it brings Wushan Sandstone to the top of Gutingkeng Mudstone. As we can see at fault No. 1 in **Figure 1.4**. The Lungchuan Fault is an N-S striking with east dipping ( $70^{\circ}$  -  $80^{\circ}$ ) thrust fault (Central Geological Survey, 2013). However, Lungchuan fault in Figure 1.2 and Figure 1.3 is different. Biete et al. (2018) in their map shows that only Lungchuan thrust, but in Le Béon et al. (2017) the south part of Lungchuan fault is branched off into another fault which is Gutingkeng fault. If we take a look on the geological section in Le Béon et al. (2017) they proposed the west-dipping Lungchuan back-thrust based on InSAR data that shows a sharp uplift at the Lungchuan fault trace and Gutingkeng fault trace, with the west side going up relative to the east side.

Pliocene Rocks comprises several formations from Early - Pliocene to Late Pliocene such as Ailiaochiao Formation, Maopu Shale, and Chutouci Formation. Followed by Pleistocene rocks that still dominated by mudstone from Gutingkeng formation. On the top of Gutingkeng mudstone, Sandstone from Erchungci formation was deposited on the Chinese continental margin after the rifting of South -China Sea during the late uplift of the Peikang basement high (Mouthereau et al., 2001).

The youngest lithology in this area is the Holocene Rocks which consist of Quaternary deposit from the Western Foothills and Central Range brought by the modern channel to the lower elevation.

In the middle to late Miocene, this area was situated in an inner shelf to outer shelf environment and deposited the Changchihkeng formation and the Tangenshan Sandstone. Followed by the deposition of mud-dominated strata and the overlying Wushan Formation. In the meanwhile, the central part of the map area was situated in a sub-bathyal to outer shelf environment (Central Geological Survey, 2013). The main geological structures were caused by the tectonic force of the Penlai Orogeny and developed during Pleistocene.

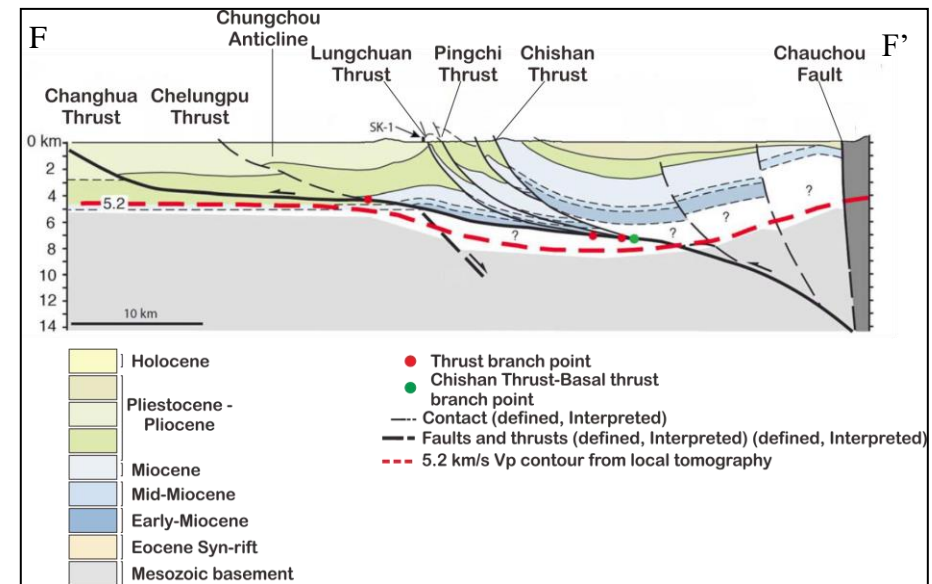
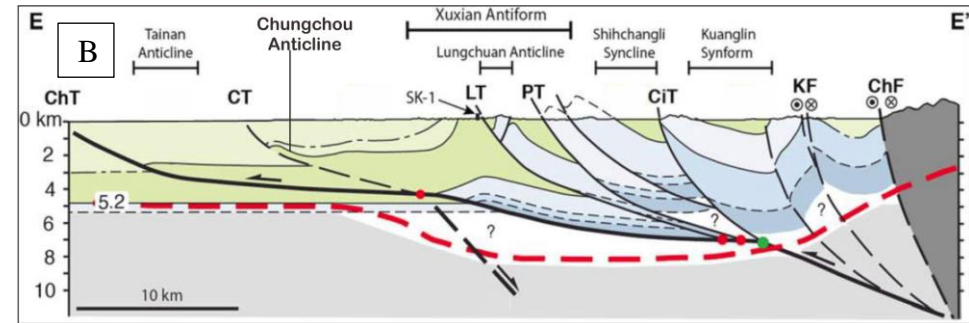
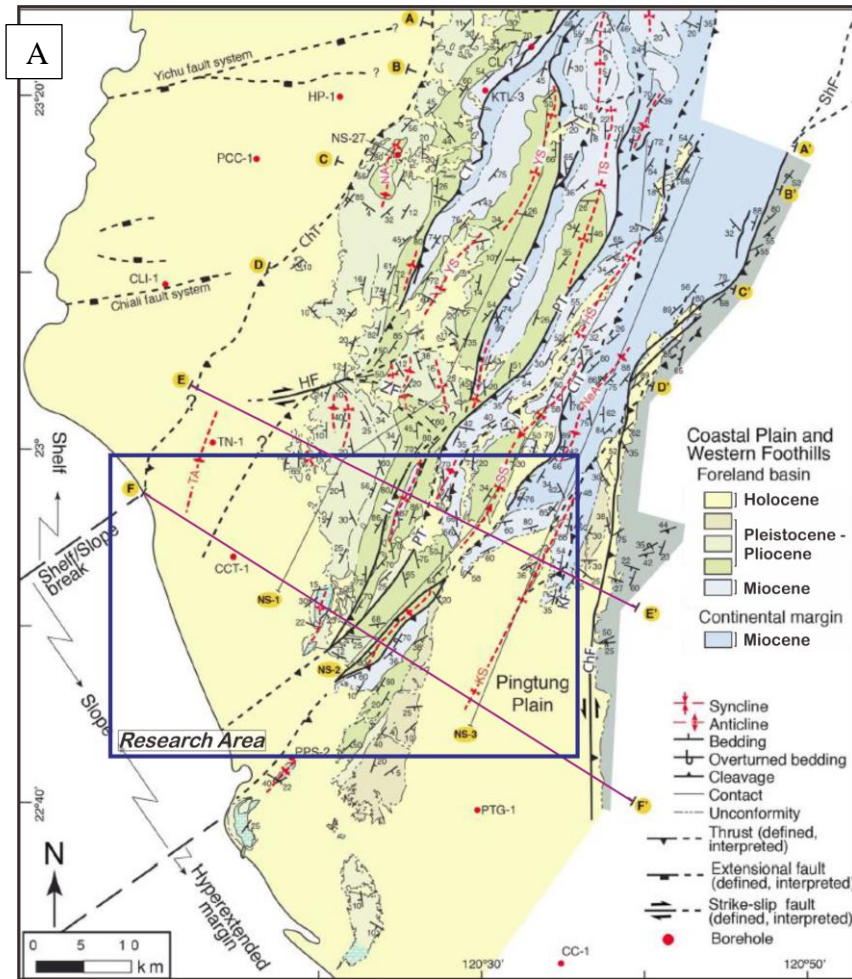


Figure 1.2 (a) Geological map of Southwest Taiwan (Modified from Biete et al., 2018). Blue frame indicates our research area, bigger scale is in the Figure 1.4. (b) Geological cross-section of E-E' and F-F'. We only consider the E-E' and F-F' sections because they are located near our research area. ChT = Changhua thrust; CiT = Chishan thrust; CT = Chenglungpu thrust; CuT = Chutochi thrust; LT = Lungchuan thrust; PT = Pingchi thrust; ChF = Chachou fault; HF = Hsinhua fault; ZF = Zuoqjen fault; NA = Niushan anticline; NeA = Neiyingshan anticlinorium; SS = Shihchangli syncline; TA = Tainan anticline; TS = Tingpinglin syncline; YS = Yushing syncline; HS = Hsiaolin syncline; KS = Kuanglin synform

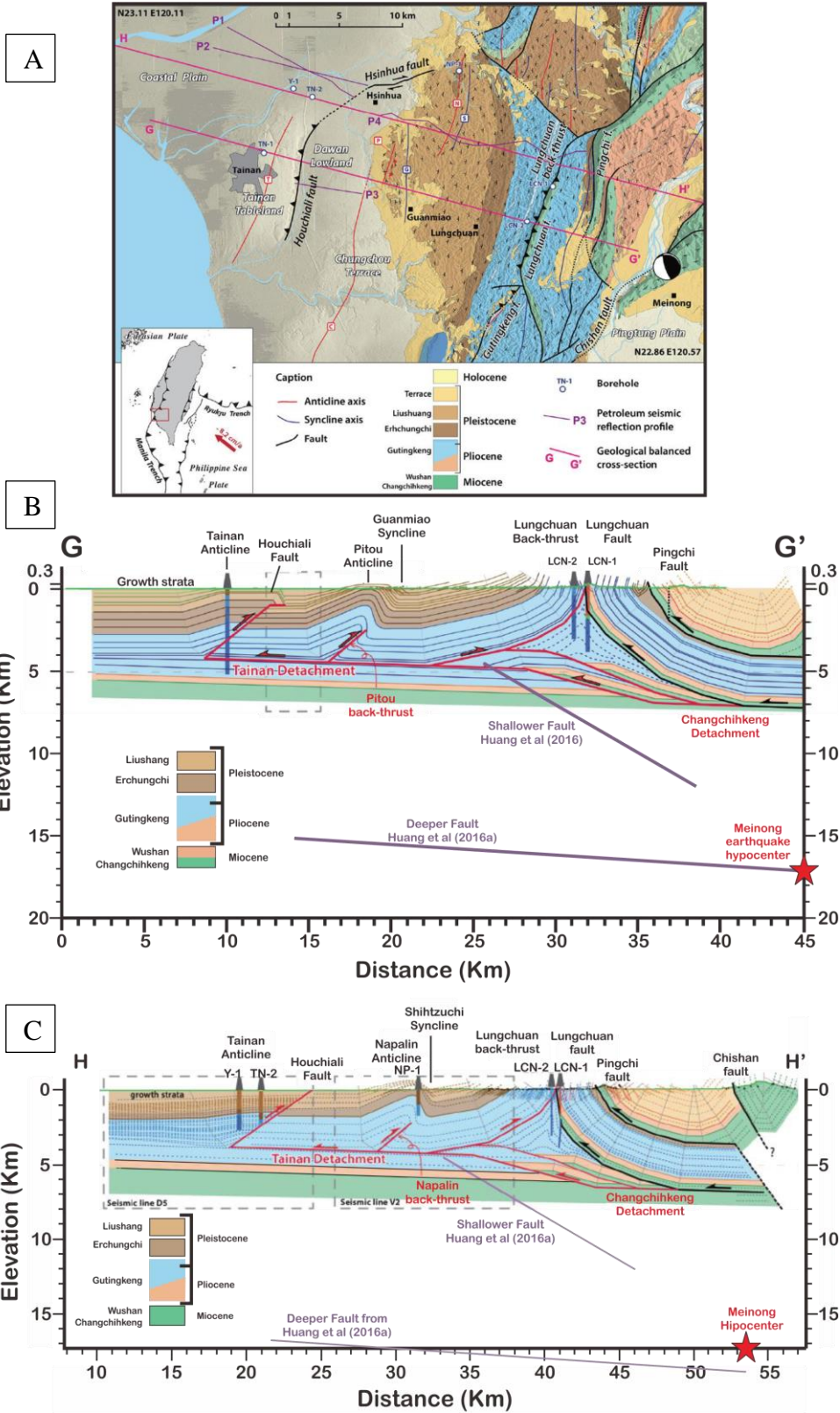


Figure 1.3 (A) Regional geological map of Tainan area, southwestern Taiwan (Le Beon et al., 2017) T= Tainan anticline, C= Chungchou anticline, P = Pitou anticline, N= Napalin anticline, G= Guanmiao Syncline, S = Shihztzuchi syncline. (B & C) Balanced geological cross-section. Red faults are inferred to have activated during the Meinong earthquake (Le Beon et al., 2017)

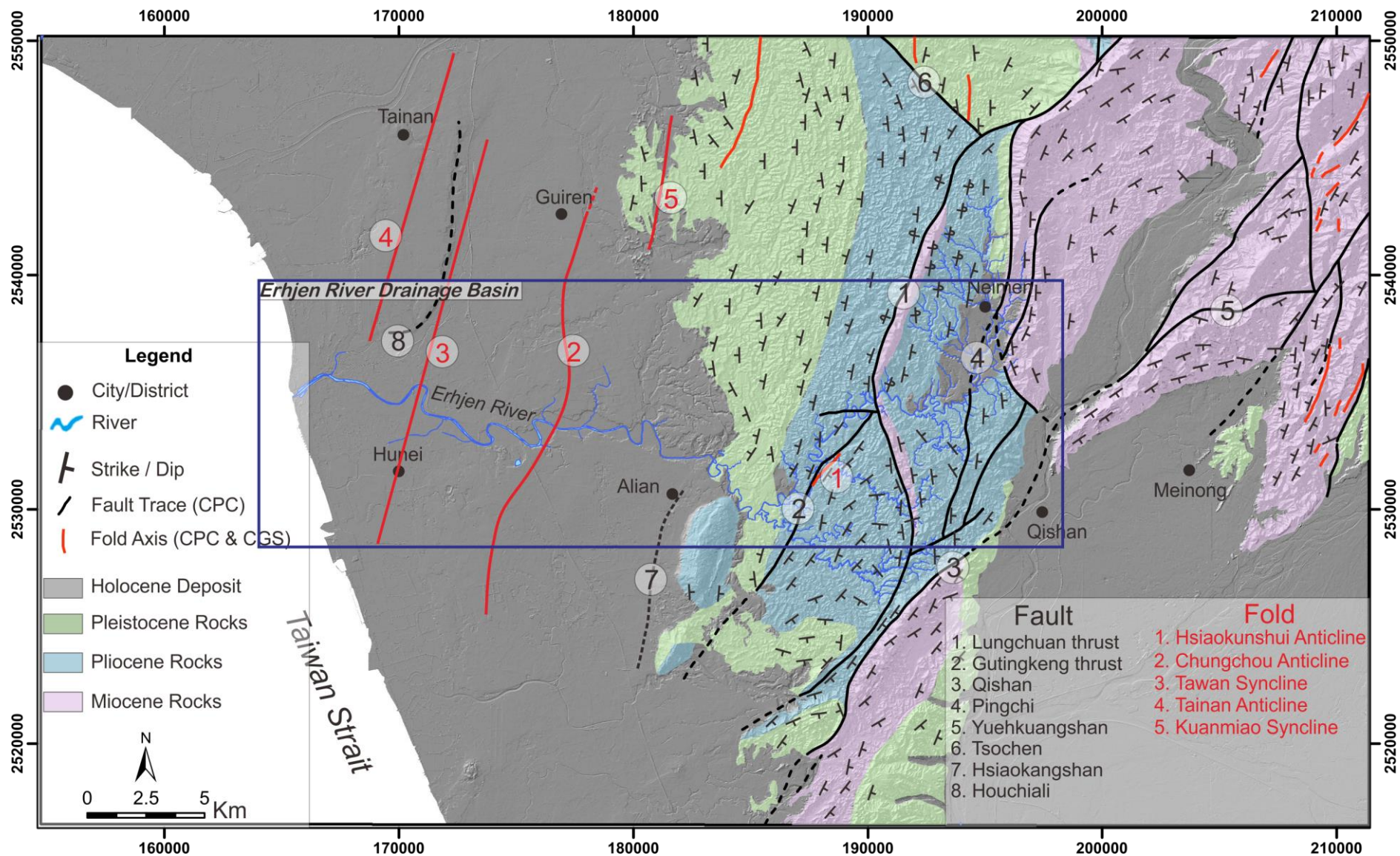


Figure 1.4 Geological and structural map of the Southwestern Foothills. The geological units are classified based on the rock ages. The Tawan syncline, Tainan anticline, Chungchou anticline, Houchiali fault, and Hsiaokangshan fault are from Central Geological Survey geological map, 2013 (Modified from CPC Geological Map, 1989)

### 1.3.1 Geological Deformation History of Southwest Taiwan

Basin-scale analysis with local deformation history and estimated level of shortening rates are performed in the southwestern foreland thrust belt of the Plio-Pleistocene Taiwan Orogen (Mouthereau et al., 2001). Over the years, the Taiwan mountain belt has been presented as the example to understand the evolution of active foreland thrust belt. A model showing the sketches of the evolution of Taiwan Orogeny when the initial arc-continent collision occurred since 2 Ma to recent regarding the fold-thrust evolution belt (**Figure 1.5**).

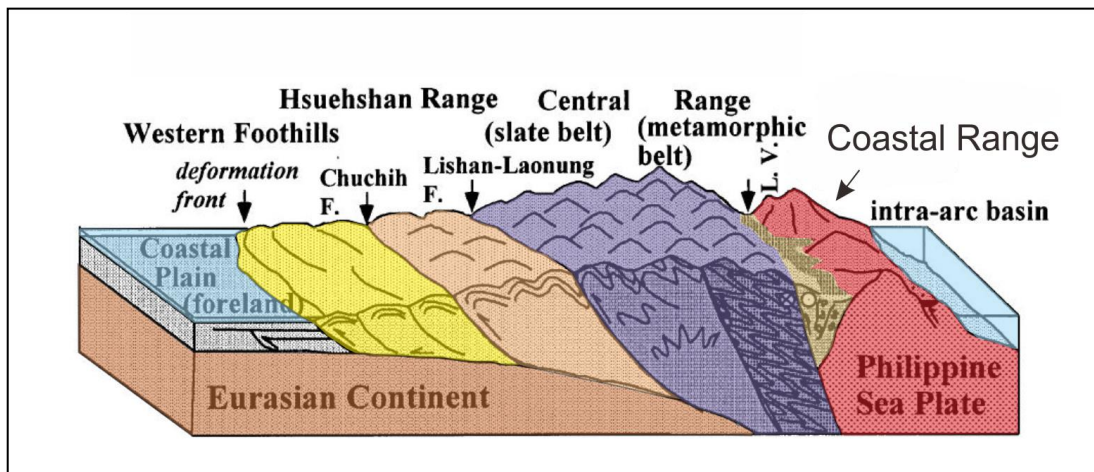


Figure 1.5 The Taiwan orogeny in terms of the geodynamic processes (Modified from Huang et al., 2000)

From this model, we can see the foreland basin, where is the research area conducted receives sediments from the growing orogen of Central Range due to the thrust fault system created by the Philippine Sea Plate movement towards west. In the Middle Pleistocene the foreland basin start to progressively fill with the synorogenic deposits, the basin evolves from dominant marine – submarine sediments to terrestrial sediments associated with the coarsening upward grain size. This has been proven by the geological map at the Western Foothills where is the research area conducted as we go to the west, the rock ages become older and the grain size is increasing from mudstone to sandstone. The oldest sediments are found in the deep part of Qishan thrust sheet limited by the boundary of Western Foothills and Hsuehshan Range (**Figure 1.5**).

Three major tectonic deformation stages occur in the southwest part of Western Foothills related to the evolution of foreland basin and fold-thrust belt. The first stage of major tectonic deformation is the initial movement of thrust activity of Qishan Fault in near 5 Ma and Pingchi Fault between 3 – 3.4 Ma. In this era, the tectonic activity still

weak followed by the deposition of shallow marine sediments which continuously deepening the basin with low sedimentation rates  $< \sim 1$  Ma. The submarine accretionary stage occurs when the foreland basin is mostly underfilled with the sediments based on a local and large scale of tectono-sedimentary data.

The second stage occurs in late Pliocene – Early Pleistocene (2 – 1.6 Ma). This is the transitional stage towards higher energy depositional sediments. In this stage the rates of deposition increase, reaching 1.8km/ma followed by the initiation of Lunhou Thrust in the Early Pliocene and Lungchuan thrust in 1.6 Ma. During the initiation of Lunhou Thrust, Phingchi thrust is reactivated followed by the Qishan thrust. This stage also marked by the grain size of this sediments is increasing since the distance between the source of the sediments and the place of deposition become shorter.

The last major stage is called overfilled basin. This is where the condition of the basin become overfilled with the sediment. In this stage, the sediments deposition rate increasing up to 3km/ma. Occurs in middle Pliocene up to recent days which lead to the construction of the mountainous area in southwest Taiwan. The grain size which deposited in this stage also increasing become bigger. At this stage, most of the geological structures are reactivated except the Meilin and Niushan thrust which occurs in 0.8 and 0.5 Ma. Gutingkeng thrust also begins to initiate in the midstream of Erhjen River in near 0.5 Ma. All of the major tectonic stages are simplified in **Figure 1.6**.

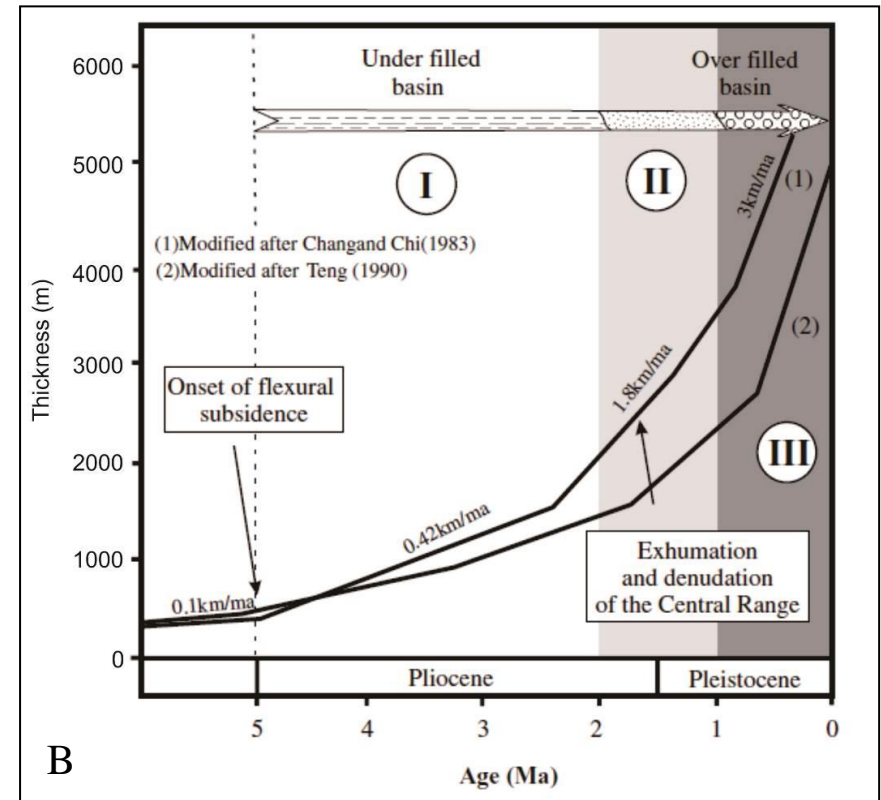
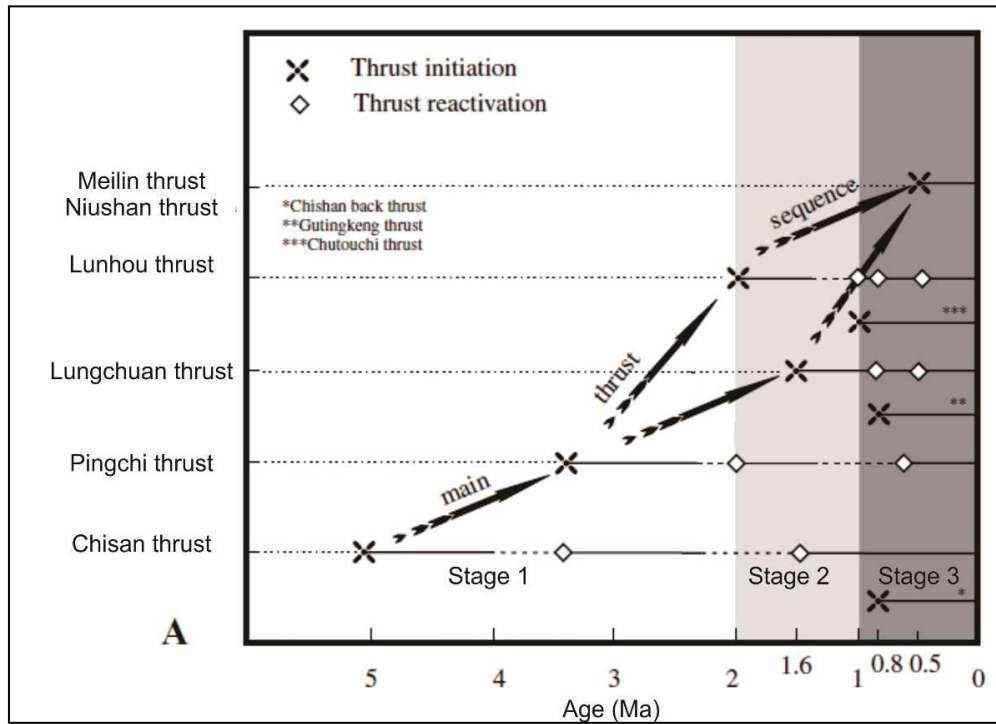


Figure 1.6 Correlation between regional and local tectonic evolution in the southwestern foreland thrust belt during the Plio-Pleistocene collision. (A) Timing of local thrust activity. (B) Curves of regional sedimentation rates. (Modified from F. Mouthereau et al., 2001)

### *1.3.2 Rapid Tectonic Deformation in Southwest Taiwan*

After we learn about the geological deformation history of Southwestern Taiwan, we have to know the rate of tectonic deformation. Geodetic measurements play a key role in order to measure the rate of tectonic deformation in Southwest Taiwan. 106 campaign-mode GPS observation and 310 leveling vertical measurements from 2000 – 2010 had been conducted in by the Central Geological Survey to measure the tectonic deformation rate of both vertical and horizontal movement.

The result of this measurements is two maps showing vertical and horizontal velocity (**Figure 1.7**). From the horizontal velocity maps, we can see the eastern part of Southwest Taiwan moves towards the west at a rate of 6 cm/yr and the Northeast part moves at a rate about 2 cm/yr, with the Penghu Island as the reference. The area which has a sharp gradient of velocity rate showed by the green color, mark that this place encounters high strain with ~4 cm/yr shortening rate.

However, not all area have the same horizontal velocity rate which causes the east part of this area is pushing westward faster than the west part. The consequences from this phenomenon are the vertical movement at the green area at a rate ~2 cm/yr showed by the vertical velocity map.

As they put the geological information both in the vertical and horizontal velocity map, three main structures which are Hsiaokangshan fault, Lungchuan fault, and Qishan fault suit very well with both of the maps. Since our research area is in Erhjen River, we only focus on the geological structures that passed by the Erhjen River. We can see Erhjen River is located in the high strain area, especially the midstream part where the leveling data shows the highest velocity rate and also passed by the Lungchuan fault (**Figure 1.7**). A precise InSAR co-seismic map (**Figure 1.8**) of  $M_w$  6.4 Jiashan earthquake also shows Line of Sight (LOS) displacements with red color in the midstream means that this area is moving up and westward reaching up to 2.5 cm. As we overlay the Gutingkeng fault trace and Lungchuan fault trace from CPC and CGS, the sharp gradient red color in the InSAR co-seismic map lies between these two fault traces (**Figure 1.8**).

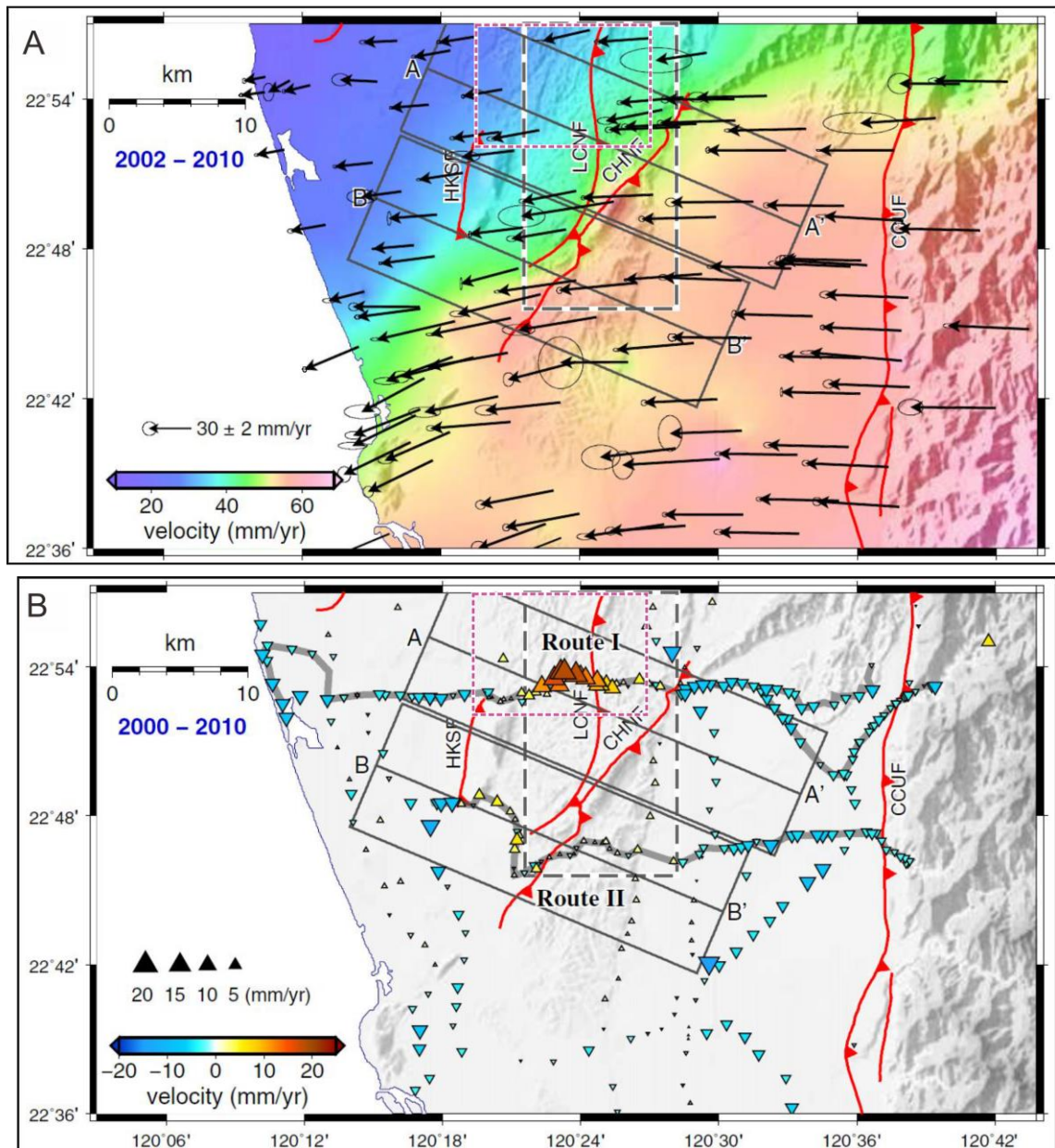


Figure 1.7 (A) Horizontal velocities relative to the station S01R based on GPS measurements during 2002 to 2010 (Ching et al., 2015). Arrows denote the vectors derived by GPS observation. (B) Vertical velocities based on leveling data during 2000 – 2010 (Ching et al., 2015). Red color means uplift, blue color means subsidence. The red dash line frame represents research area. HKSF = Hsiaokangshan Fault, LCNF = Lungchuan fault, CHNF = Chisan Fault, CCUF = Chaochou Fault.

The Jiashian earthquake epicenter located 5 km east of the Chaochou fault which represents the tectonic boundary of the Taiwan orogenic belt between the metamorphosed slate belt to the east and the foreland fold-and-thrust belt to the west (Hsu et al., 2011).

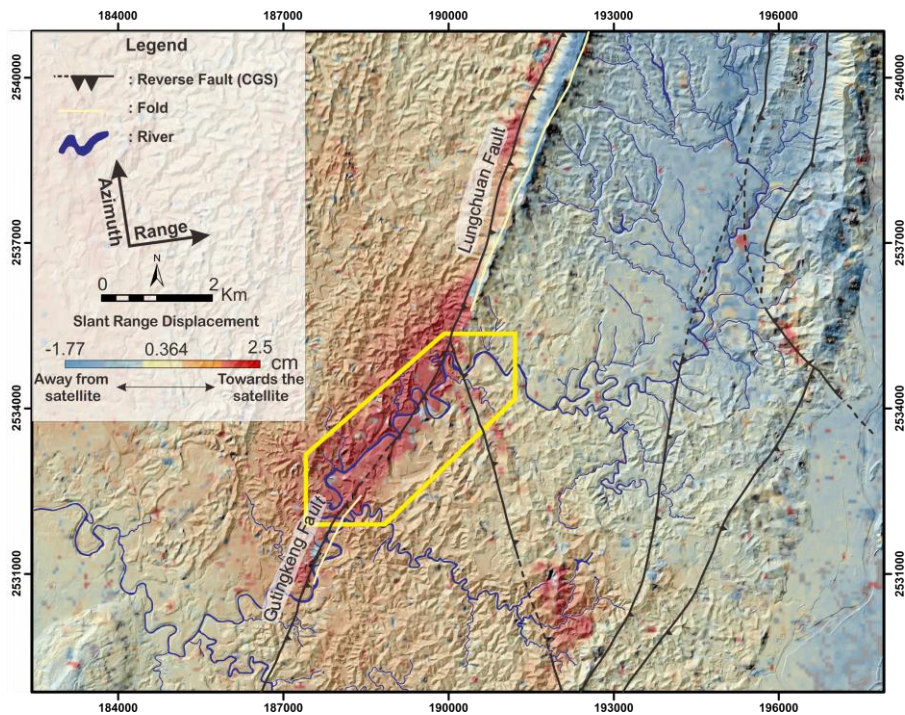


Figure 1.8 ALOS coseismic interferograms of  $M_w$  6.4 Jiashian Earthquake in March 4<sup>th</sup>, 2010. The colors represent the coseismic slant range displacement (Courtesy of Huang Mong-Han, 2017)

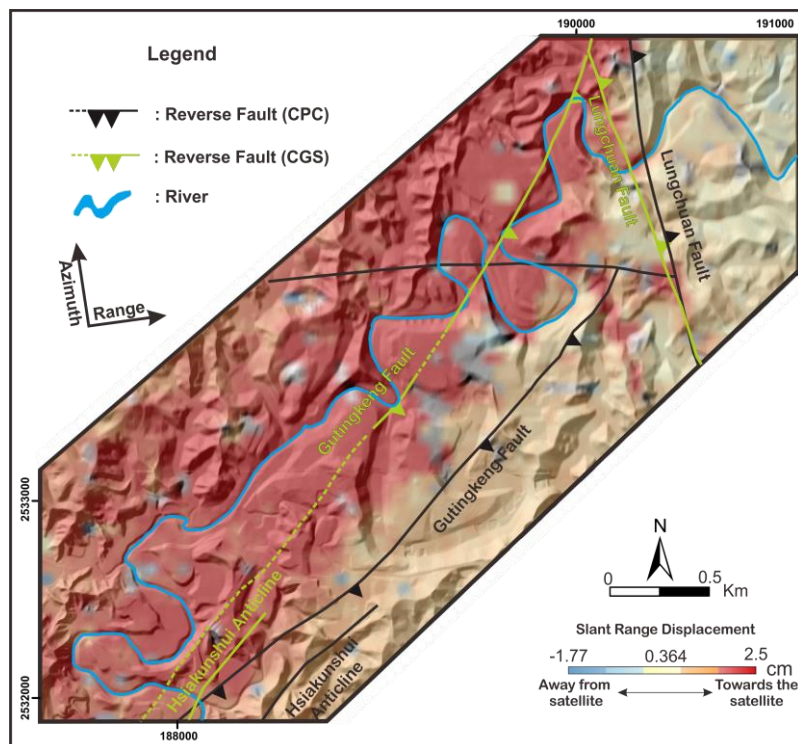


Figure 1.9 Location of the Gutingkeng fault trace based on CPC, CGS and comparison with the location of the displacement gradient observed from InSAR (similar dataset as Fig 1.8). Note that the Gutingkeng fault is identified as an east-dipping thrust based on geology, while the footwall was uplifted relative to the hanging wall during the Jiashian earthquake.

## 1.4 River Terrace study in Southwest Taiwan

After we know the geology and the rate of tectonic movement in southwest Taiwan we should know how these events give some effects to the modern geologic activity, in this case, is a river. Several big rivers located in the southwestern area which are Tsengwen, Tsailiao and Erhjen River has already become an object to study terrace. Each of the rivers has its own interpretation. This study will focus on one of the river in Southwest Taiwan which is Erhjen River. We will interpret the terrace based on how much changed in the river terraces based on the tectonic event (fault and fold). River terraces were first mapped from aerial photographs through stereoscopes and plotted onto photograph based, 1:5000-scaled topographic maps issued by the Department of Agriculture and Forestry of Taiwan. The elevation of each terrace surface was directly determined from these maps and referenced to the elevation of the active channel as defined on the maps. Because the maps have a 5m contour interval, any location which is between two contour lines has an elevation uncertainty of 5m. The stratigraphy of terrace deposits and the underlying bedrock configuration were then examined in the field.

The study of terrace analysis in Southwest Taiwan is mostly to illustrate the development of river terraces across growing anticline (Hsieh & Knuepfer, 2002). We can see the three rivers which has been studied is passed by several geological structures

*In the Erhjen River*, where this research is conducted also has been studied from in 2001 by Hsieh & Knuepfer while the tools are limited to analyze the terrace and 5m DEM along with the leveling data has not been set. Four groups of the terrace are classified which are a low terrace, Major terrace, Minor and High terrace. These four groups of terrace then have their own classification. Low terrace interpreted as a modern floodplain. This terrace composed of vegetated or mudrock banks. Followed by the Major terrace, located higher than low terraces labeled as KT in the downstream and CP in the upstream of the Lungchuan Fault. Hsieh & Knuepfer differentiate the terrace label of KT and CP due to the uncertainty of correlation between the terraces from upstream Erhjen River to the Downstream of Erhjen River and the last terrace is Minor and high terraces, most of the minor and high terraces developed in the main stem between Chungte and the Lungchuan fault (**Figure 1.11**). Minor and high terraces cannot be correlated as extensively as a Major terrace. Minor terrace labeled by a small letter while high terrace labeled by capital H.

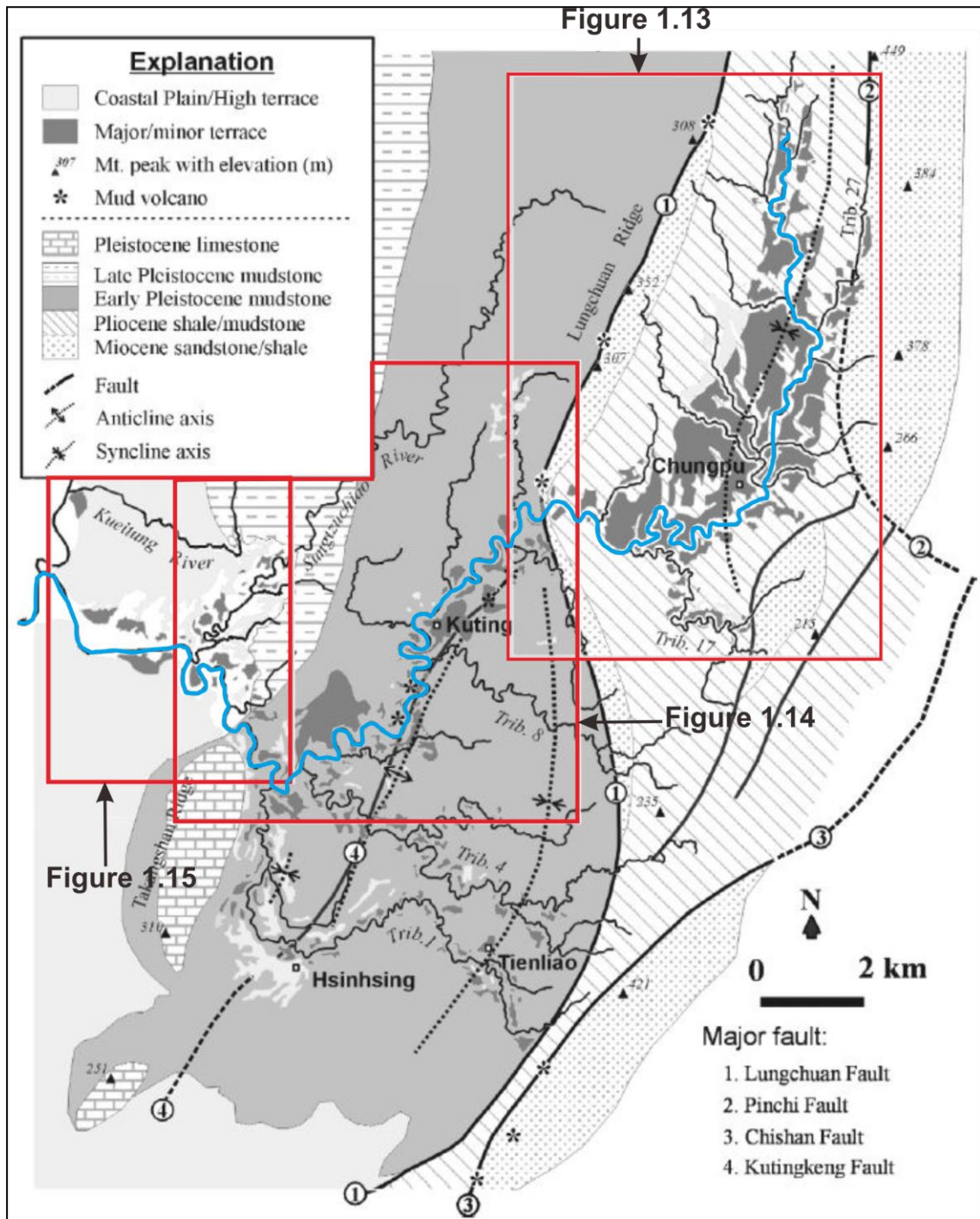


Figure 1.10 Geological and geomorphological framework of the Erhjen River basin. Location of the mud volcanoes is based on Shih (1967); structures are according to Chinese Petroleum (1971); rock chronology is based on Lin (1991) (Modified from Hsieh & Knuepfer, 2001)

Erhjen River terraces are well-distributed from other rivers in the north. It spreads more than in 25 km in length from upstream to downstream. This river passed by several geological structures, but only in the midstream part affected by them. As we can see in the geological map from the Hsieh & Knuepfer (**Figure 1.10**). In the upstream, it near the Pingchi fault while in the midstream two N-S striking reverse faults which are Gutingkeng

and Lungchuan passed by this river. In the upstream near the Neimen plain, the river is meander-less compare to the midstream where there is an abandoned channel.

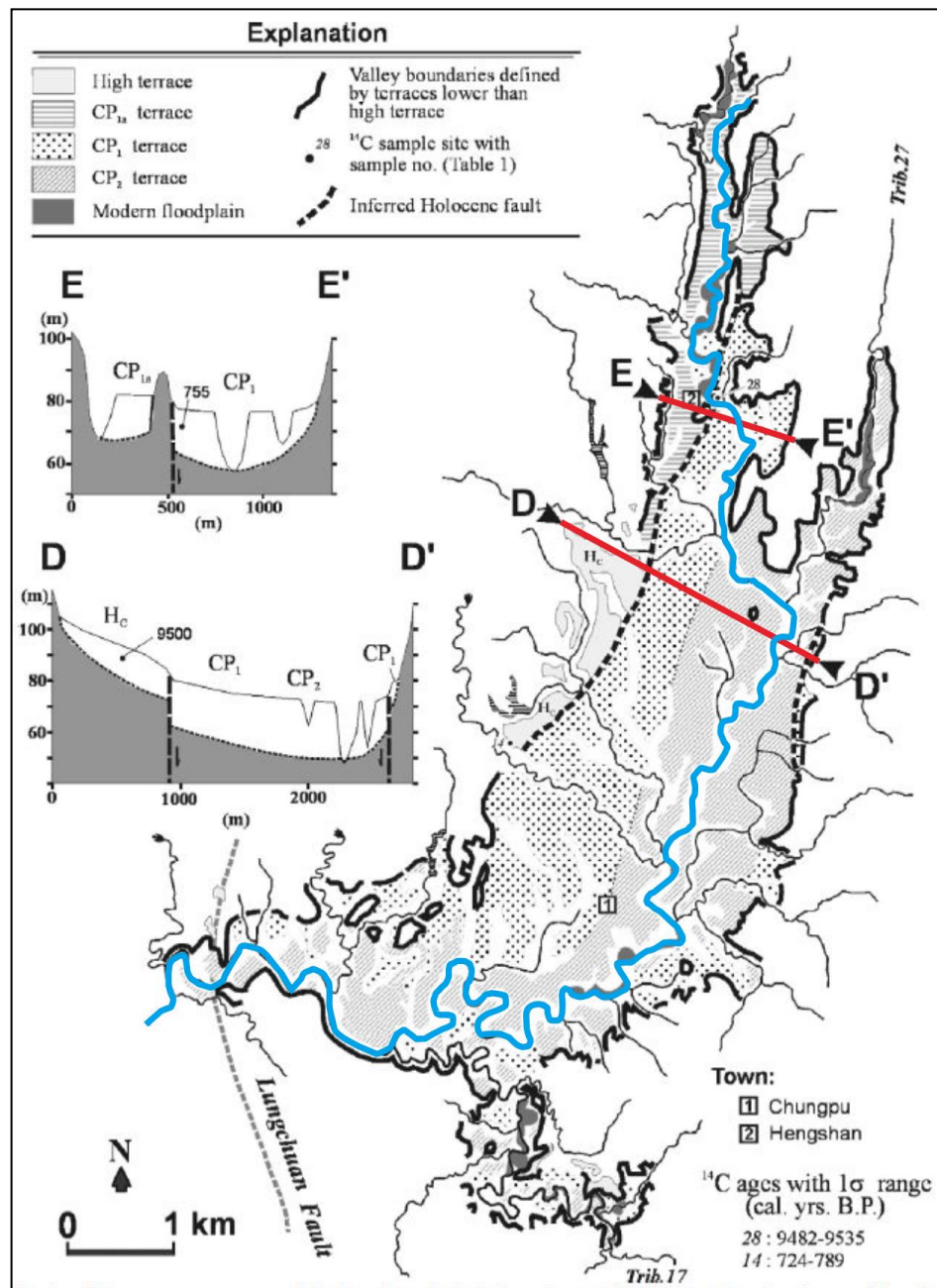


Figure 1.11 Distribution of river terraces in the upstream segment of the Erhjen River (Modified from Hsieh & Knuepfer, 2001).

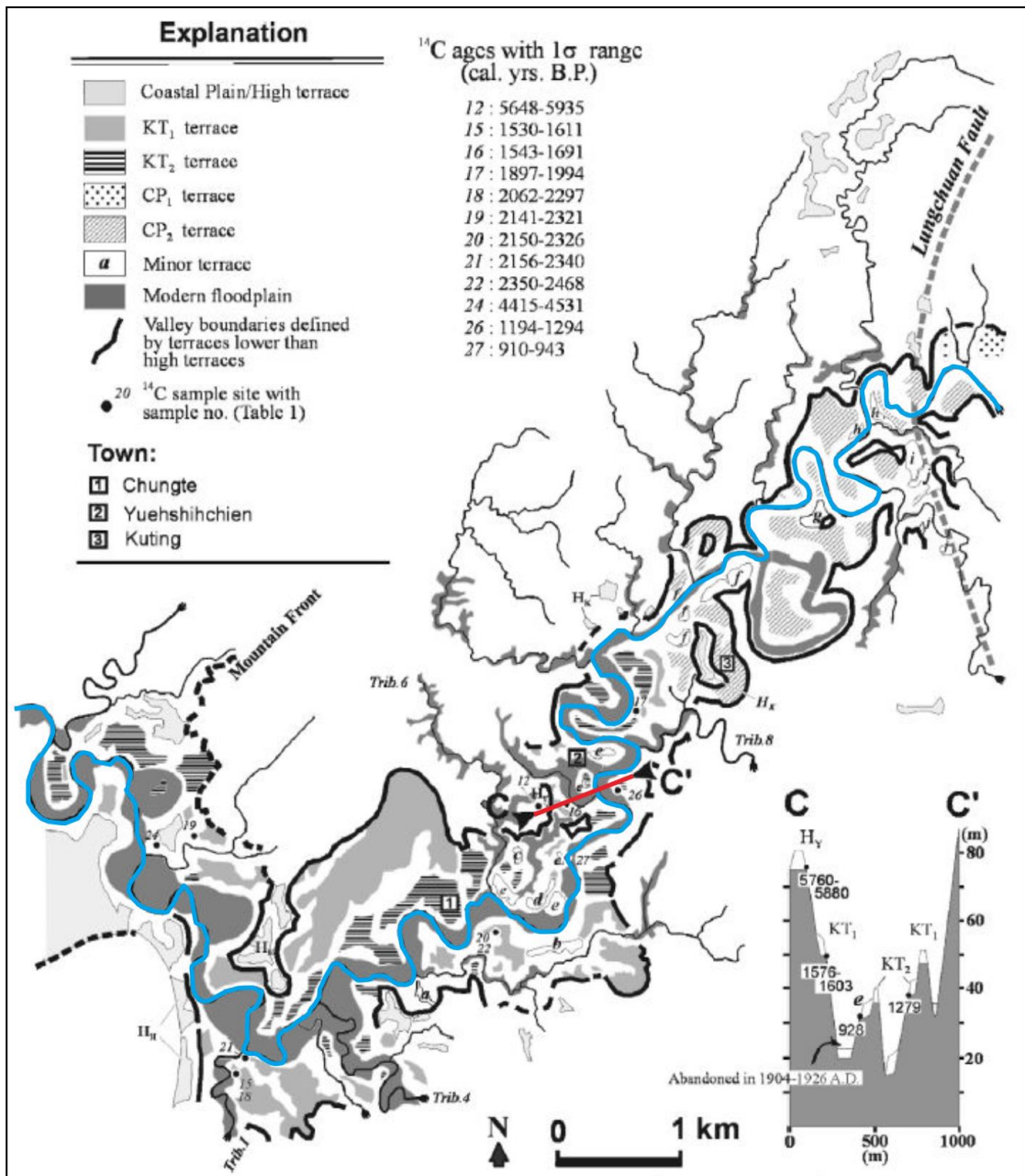


Figure 1.12 Distribution of river terraces in the midstream segment of the Erhjen River (Modified from Hsieh & Knuepfer, 2001).

In the upstream of Erhjen River, the terrace developed very well and dominated by CP terrace, it spreads for more than 2 km in width. Based on the topographic profiles from the Hsieh & Knuepfer there are two Holocene structures both on the west side and east side of the river. This Holocene structures marked by the significant elevation differences in the topographic profiles. Although Pingchi fault passed by the upstream part of the river, it does not show some offset in the topography. Thus, it does not affect the terrace.

While in the midstream the CP terrace gradually disappears and KT starts to develop as we go to the downstream due to the uncertainty of the correlation between the major terraces. At that time the radiocarbon dates still limited at the north part of the midstream river. Based on the geological map (**Figure 1.10**) three geological structures are developed which are the Lungchuan fault, Gutingkeng fault, and Hsiaokunshui anticline.

CP terrace starts to fully disappear at the downstream of the Erhjen River. In the downstream CP and KT terrace stop developing at the edge of the Western foothills and Chungchou terrace starts to develop in the Coastal Plain (**Figure 3.1**).

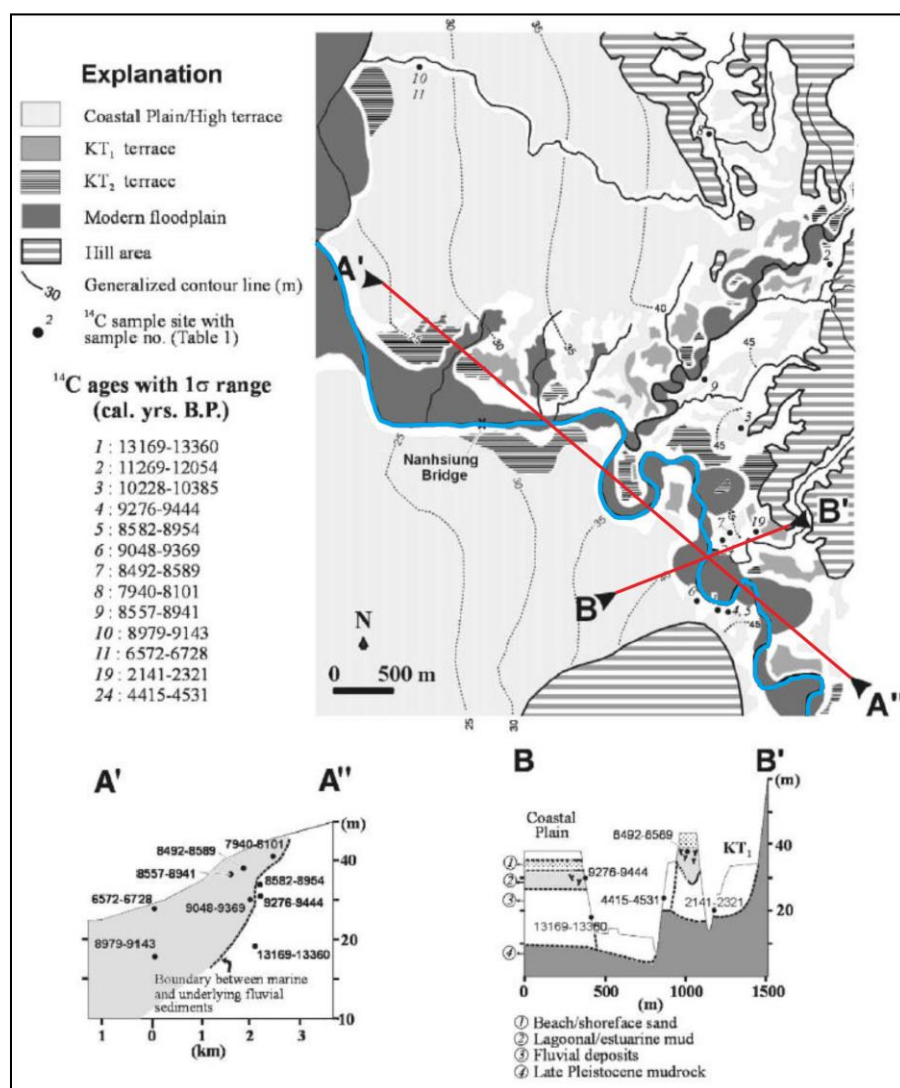


Figure 1.13 Distribution of river terraces in the downstream segment of the Erhjen River (Modified from Hsieh & Knuepfer., 2001).

A long profile of Erhjen River from upstream to downstream showing an uplift terrace in the midstream west side of the Lungchuan fault. This uplift terrace interpreted

due to the results of Holocene tectonic activity which called as “*doming structure*”. This doming structure is suggested by the convergence of KT1 terrace to the KT2 and the modern channel, by steeper long profiles of terraces KT1 and KT2, by apparent of the Lungchuan fault, and by the upstream convergence of CP1 and CP2. The orientation of this doming structure is roughly NNS-SSW direction and plunges to the south downstream from the Kuting. It is hard to determine the orientation since the limitation of the terraces correlation.

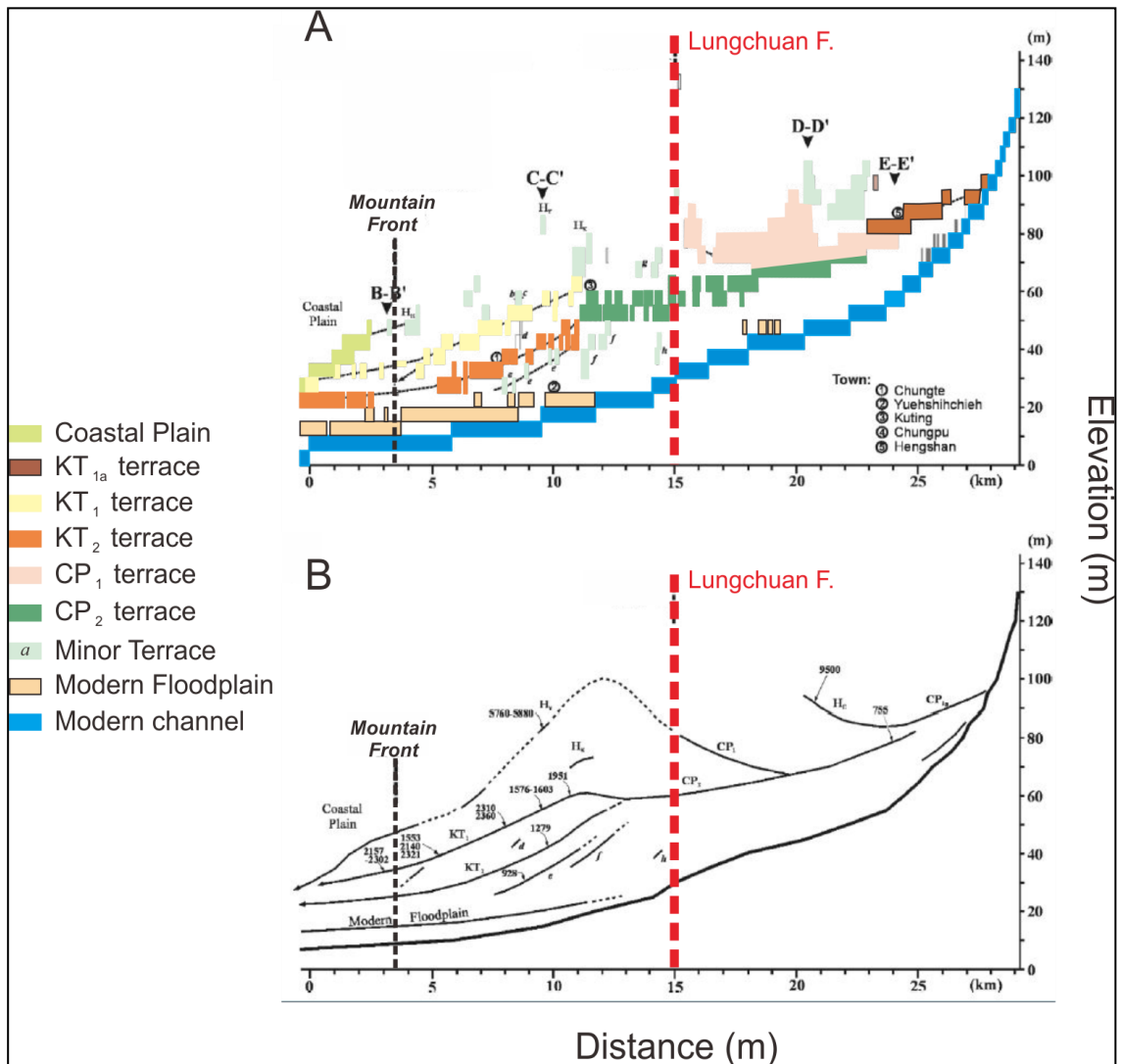


Figure 1.14 (A) Longitudinal profile along the Erhjen River from upstream to downstream to show the distribution of each terrace (B) Proposed correlation of the river terrace sequences in the main-stem Erhjen River. (Modified from Hsieh & Knuepfer, 2001)

28 radiocarbon dates which have been conducted by Hsieh & Knuepfer (2001) are very useful for correlating the terraces and as a parameter to calculate the local incision rate on Erhjen River. The oldest age, 13169 – 13360 years BP located in the north

tip of Takangshan Hill (downstream, Figure 1.15) while the youngest age,  $597\pm 47$  Years BP located in the upstream. Based on a radiocarbon date results at Yuehshihchieh (**Figure 1.12**) the local incision rate of Erhjen River is 7-8 mm/year during 5 - 2.5 ka. After 2.5 ka two major terraces which are CP and KT with hundreds of meter width converge downstream to the Chungchou marine terrace surface. At this time, the incision rate increases to 5 cm/yr. Hsieh & Knuepfer stated the channel incision processes are strongly controlled by such climatic-driven discharge and bedload condition (Hsieh, 2001).

The three rivers in Southwest Taiwan that have been studied, three of them have the similarity characteristics. Three of the rivers provides evidence of the development of river terraces across growing anticline. We can see from the terrace correlation in the terrace profile from upstream to downstream of each river. The previous study determines that there are three major Holocene anticlinal structures located in the Yuching and Tsochen area. All of these structures can be recognize by the converging and diverging terrace sequence with chronologic control provided by more than 20 radiocarbon dates.

In this study, we will focus more on the Erhjen River. The terrace deposit in this river is well-developed and spread very wide, reaching up to more than 2 km wide in the upstream. This study will also propose a Gutingkeng fault trace that has not been explained in detail in the previous study.

## **1.5 Geomorphic Setting of the Erhjen River**

The Erhjen River is a westward flowing meandering river located in southwestern Taiwan that flows from the Neimen District to the Taiwan Strait. The Erhjen River has different names for each location from upstream to downstream. In the upstream near Gangshantou, people call it the Shuishui River. In the midstream, the name changes to Gangshan River and in the downstream the name changes again to Erzangxingxi. The mountainous region of the Erhjen River consists of two sets of sedimentary rocks: pre-collisional, late Miocene sandstone and shale formed on the stable continental margin and a syn-collisional Plio-Pleistocene foreland sequence; the latter is dominated by mudstone at least 4 km in thickness (Hsieh & Knuepfer., 2001).

The length of Erhjen River from upstream to the river mouth is about 61 km with the 340 km<sup>2</sup> basin area size and carries 3600 m<sup>3</sup>/s fine-grained sediments from the Miocene rocks in the Western Foothills to be deposited in the Taiwan Strait (Water

Resources Agency – Ministry of Economic Affairs, 2016). The valley width in the upstream reaching up to 2.5 km measured from the major river terraces which are double from the midstream.

The morphology of the Erhjen River Basin is strongly controlled by the underlying bedrock lithology. We can know from the drainage pattern that showing a dendritic pattern in the upstream and sub-dendritic pattern in the midstream. In the upstream, where the dendritic pattern occurred it represents the variety-less underlying rock resistance and it has a gentle slope while the geological control is not developed very well. The sub-dendritic pattern in the midstream represents that this area is controlled by the increasing slope value, topography and geological structures (Howard, 1967).

The Erhjen River precipitation comes mainly from rainfall in the summer season especially associated with tropical typhoons (Wu, 1992 in Hsieh & Knuepfer., 2001). This river's mean annual rainfall of 2000 – 2500 mm, and it decreases as we go to the coastal plain to 1750 mm in the Tainan area (**Figure 1.16**)

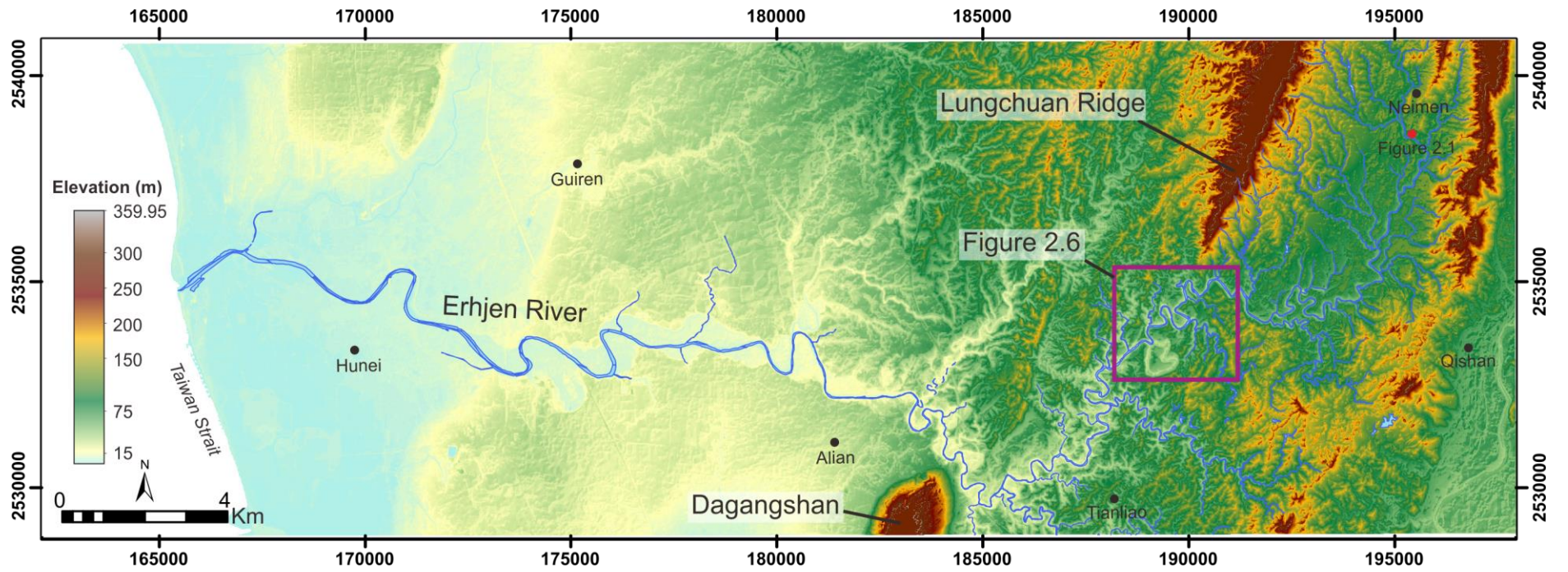


Figure 1.15 Topography in the Erhjen River area based on 5m DEM

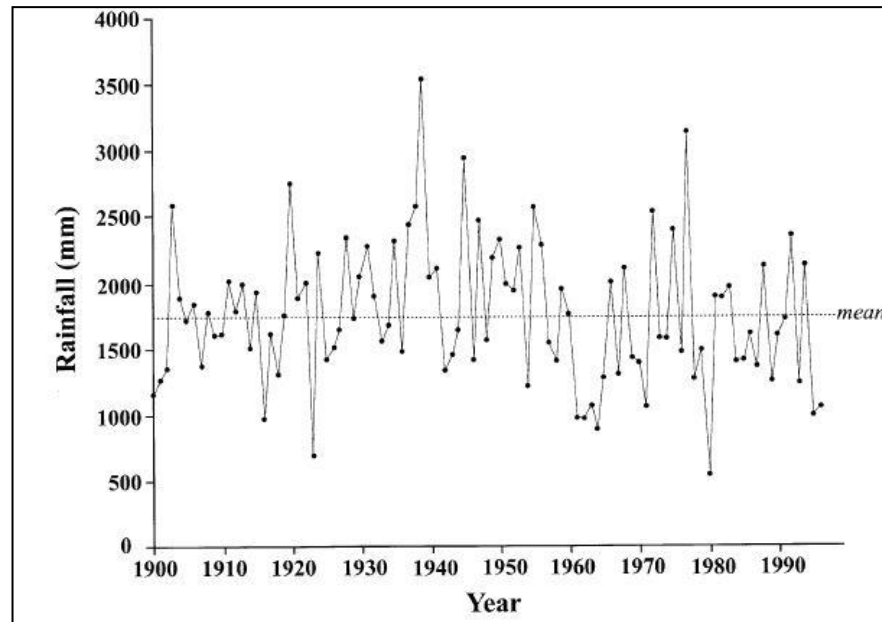


Figure 1.16 Annual Precipitation record of Tainan Station during 1900 – 1996 (CWB climatic data in Hsieh & Knuepfer., 2001)

## 1.6 Research Objectives

Our research will focus on the Erhjen River terrace because the distribution of the terrace is well-developed from upstream to downstream and there are more than 20 radiocarbon dating data which we can rely on as our database from Hsieh & Knuepfer et al., 2001. In our study, we will also add complementary radiocarbon dates in the midstream area of the river where there is a lack of radiocarbon dates. We also learn that from the curvilinear profile of Erhjen River shows there is a terrace that encounters some uplift in the midstream of Erhjen River. This uplift terraces somehow is interpreted with the dashed line connecting with the terraces in the upstream. We will try to update the curvilinear profiles with new terrace classification based on the precise 5m DEM and complementary radiocarbon dating. The uplifted area showed by Sharp gradient difference color in the co-seismic deformation of Jiashan Earthquake showing an uplift area on the west side of Gutingkeng and Lungchuan fault during Jiashan Earthquake. From the brief introduction in **section 1.1**, we know that Lungchuan fault is an east-dipping reverse fault with the branch in the south part. Which means the east side of Gutingkeng and Lungchuan should be going up relative to the west side. This phenomenon raises the problem that we want to observe.

With this study, we will use Erhjen River terrace which is passed by the Gutingkeng and Lungchuan fault to detect this phenomenon. The aims of this study are to get a better understanding of the Holocene deformation in the Gutingkeng fault zone which has not been explained in detail from the previous study using updated terrace deposit along the Erhjen River added with quantifying local uplift rate and incision rate on the terrace. We calculate the incision rate on the terrace using leveling data from the previous study and  $^{14}\text{C}$  radiocarbon dating. Several borehole data also provided by Central Geological Survey in the lower Erhjen River to help us correlate the terrace in the midstream of Erhjen River with the Terrace in the Chungchou plain. Since we are using terrace analysis, the deformation of the fault is limited by the Holocene period.

We know the previous study already did the terrace deposit analysis, but in this research, the main focus is updating the information since the last research is done 19 years ago. We use modern tools which have not been set in that time. Precise 5m DEM, complementary radiocarbon dates, and leveling data become our tools to update the information in this area.

## Chapter 2 : Methodology

### 2.1 Field Survey

Geomorphology fieldwork in the early period of this research consists of physiographic mapping and description of the landscape under the rubric of physical geography. We did the field surveys where there is lack of data in a certain area. We survey the terrace deposit that we are unable to see clearly in the DEM in several areas of the Erhjen River from upstream to downstream. This field survey also will help us to determine the uncertainty of the 5m DEM as our base map to classify the terrace. Before we conduct the field survey we need to decide what kind of data that we have to acquire. Data acquisition is substantial before we choose the tools for the field work. As for some data that we took on the field are: geomorphological features (scarp, terrace risers, river meandering), geological features (bedding attitude, lithology, stratigraphic column, fault attitude, and fold), and radiocarbon dating sample.

Field survey is conducted in order to check the small terrace that is hard to recognize. In the midstream area of Erhjen River where the meandering starts to developed, small terrace formed in several places. These small terraces will be the key to correlating the terrace from upstream to downstream. We use 5m DEM map to classify the terrace based on the elevation in the field survey.

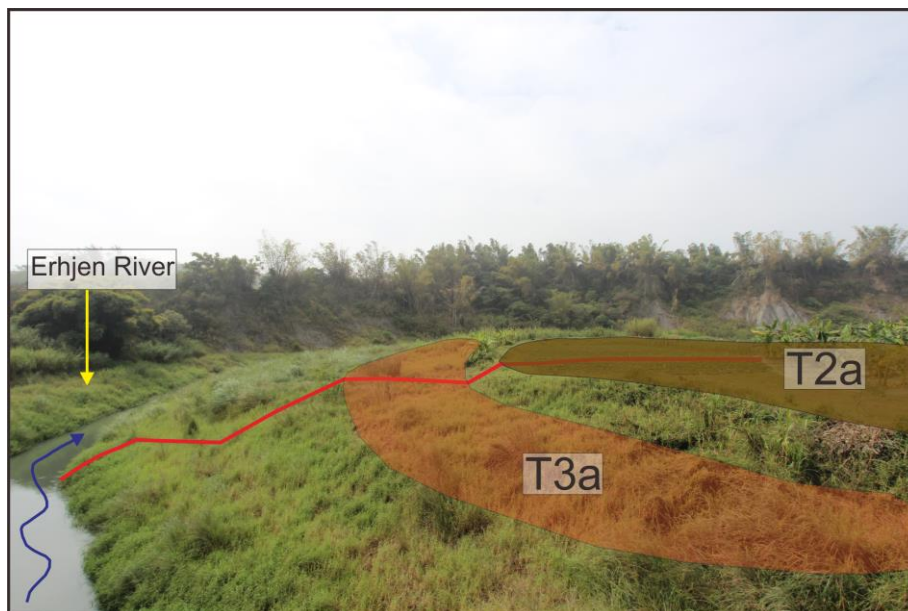


Figure 2.1 Classifying terraces in the field. See map Appendix A-1 for the location

## 2.2 Erhjen River Terrace Mapping

The availability of high-resolution digital elevation models (DEM) survey has spurred the development of several methods to identify and map fluvial terraces (Hopkins et al., 2016). We mapped Erhjen River terraces based on 5m DEM using ArcGIS software to process the data. The early stage of terrace mapping is we have to decide the flat area along the Erhjen River from upstream to downstream by making a topographic section perpendicular to the river flow direction. Since the river terrace was a deposit from the river, the terrace will have several levels of elevation due to the change of river water level (figure 2.2). Terrace with the highest elevation level in reference with the river will be the oldest terrace, thereby we call this terrace as T1a. The name of the terraces changing as the terrace level decreasing to the T2a, T3a, and T4a.

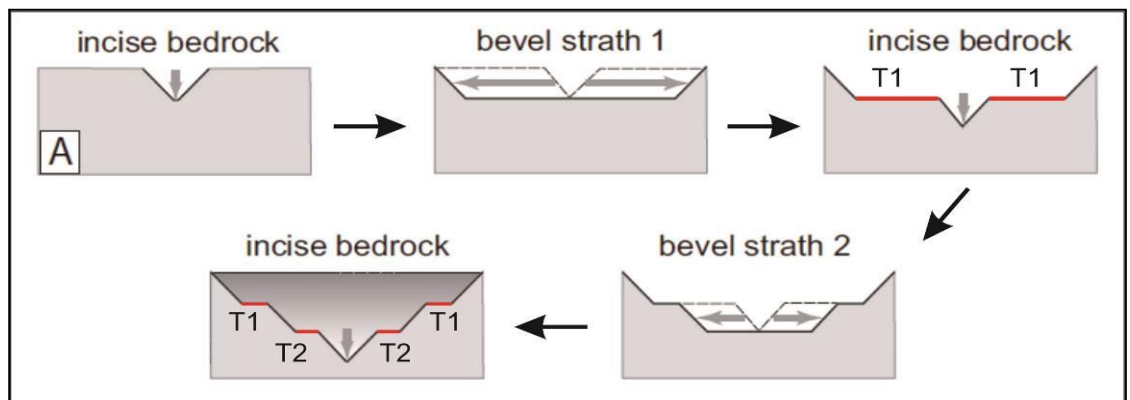


Figure 2.2 Formation of terrace levels due to the river incision and lateral erosion (Burbank, 2012)

We start the Erhjen river terrace mapping by a look at the 5m DEM map (**Figure 1.15**) from this map, we can generate a slope map based on Z information in the DEM map (**Figure 2.4**). This slope map will help us determine the flat surfaces along the Erhjen River that expected to be river terrace. We start to classify the terrace level based on its elevation by making topography profiles perpendicular and parallel to the river flow direction.

Topography profiles from upstream to downstream of Erhjen River will show if there is an anomaly. In the normal condition, the river terrace elevation will decrease as we go to the downstream and the slope of the terrace towards downstream relatively more gentle than the river slope.

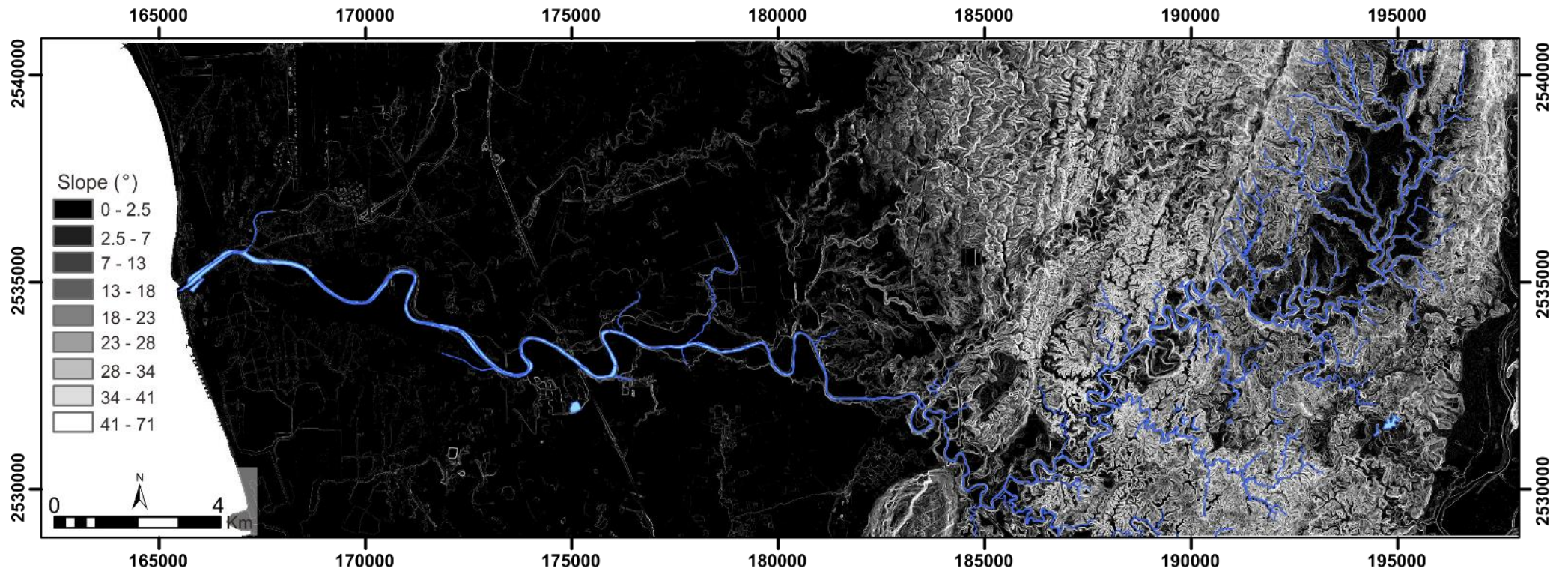


Figure 2.3 Slope map of the Erhjen River area based on 5m DEM

## 2.3 Tilted Terrace mapping

River terrace analysis could be able to detect an anomaly like discontinuities. Since Erhjen River passed by several geological structures, it is important to take a look at the terrace that has an anomaly due to the discontinuities such as fault and fold. In Chapter 1 we already take a look at the geological map of the Erhjen River. There are three geological structures that developed the midstream part of Erhjen River, especially the Gutingkeng Fault. In this research, we propose to redraw the Gutingkeng Fault based on the river terrace deposit tilt on the 1m DEM map of Erhjen River from Central Geological Survey.

The fault could be difficult to detect from the surface, in this case from the river terrace. First, we made several topographic profiles in the certain area that we expect that there is a fault by looking at the DEM, slope map, and geological map. From the topographic profiles, we can see the surface of the terrace. If the surface of the terrace is tilted in several degrees of the slope we can mark it and give some explanation of the tilted direction. Another indicator for us to able to draw the fault trace is if there is any scarp or topography offset. By drawing topographic profiles we also can see if there are any scarp or topography offset.

We marked the tilted terrace and measure its slope by using simple trigonometric function (Figure 2.4). We compare the tilted slope angle with the slope of the modern river. There are two comparisons: First, we compare the tilted angle of terrace slope with the euclidian river slope and the second we compare the tilted angle of terrace slope with the long river slope. The difference between these comparisons is in the distance of the river.

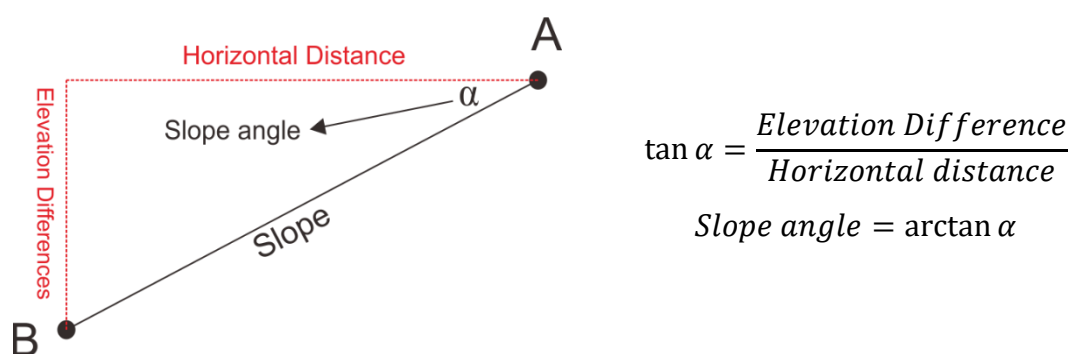


Figure 2.4 Slope calculation for the tilted terrace

The first comparison is we compare the slope of the tilted terrace with the shortest distance of the river without noticing the meander. And the second comparison is we calculate the distance of the river along the meander. The explanation is simplified in **(Figure 2.5)**. The purpose of this comparisons is we want to observe the location of the tilted terrace. The terrace will intend to tilt towards the river but, in the normal condition a single river terrace deposit will be flat or has a slope with no larger than the local river slope. Careful observation has been done in the midstream area of the Erhjen River in order to map the fault trace. We marked all the tilted terrace, measure it slopes and compare with the modern channel.

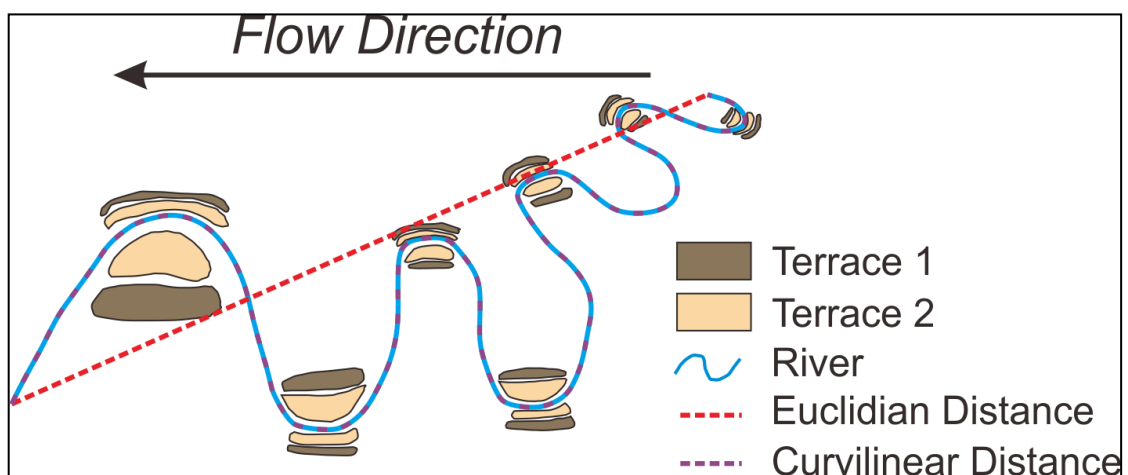


Figure 2.5 Sketch explaining curvilinear versus euclidian distance

After we marked the tilted terrace we start to draw the fault trace. We draw the fault trace on the 1m DEM **(Figure 2.6)** map which has better resolution in the elevation value. We observe an area that has a significant sharp gradient color along the terrace and we draw the topographic section based on the 5 m DEM. We only can get the .JPG format of 1m DEM from the Central Geological Survey, so our 1m DEM observation is limited when we want to draw the topographic profiles.

The tilted terrace is just narrowing the area of Gutingkeng fault zone, in other words, it is increasing the probability of the fault trace going in the predicted way as we thought.

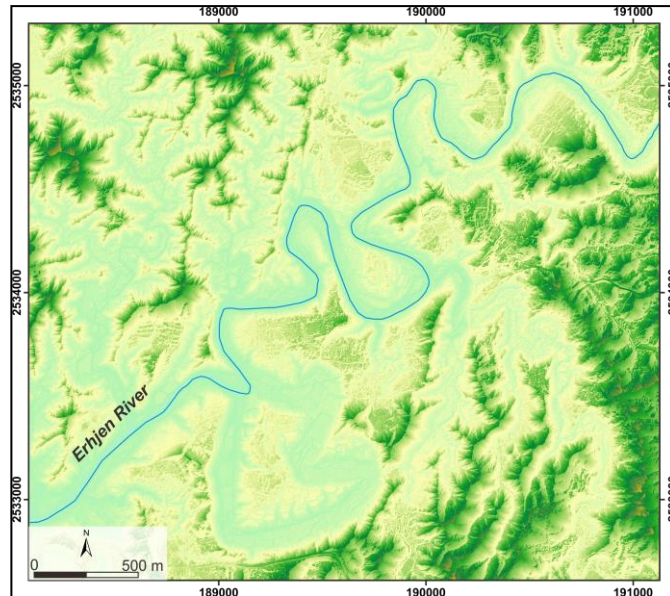


Figure 2.6 Screen capture of the 1-m DEM based on LiDAR data in the midstream segment of the Erhjen River

## 2.4 Radiocarbon Dating ( $^{14}\text{C}$ )

The science of tectonic geomorphology is very dependent on the time controls of the landscapes. To determine the rate of fault moves or the surface changes shape, we must specify the age of the offset feature. Two dating methods which are relative dating methods and absolute dating methods are already well-known. Since this research goal needs much more accuracy in the time controls, we use absolute dating methods. There are several absolute methods to establish the timing in the landscapes (**Table 2.1**).

Classifying the terrace is inaccurate when only based on the elevation. The age of the terrace will be the key data that we can use to classifying the terrace and correlate each of them. We add 8 radiocarbon dates in this research located mostly in the midstream part of Erhjen River where there is a lack of age data.

The purpose of using radiocarbon dates in this research is because the age of terrace deposit mostly will be Holocene (~10000 years BP) which is included in the range of the Radiocarbon dates which are 0 – 35 ka (Burbank, 2012). And the material that we used will be charcoal. Charcoal produced from the incomplete combustion of organic matter (Bird, 2013). This organic matter can be plants, animals, and any remnants from living things that carried by the river and deposited in the terrace along the river. The charcoal that is freshly deposited will be covered by the sediments in the lower elevation. That is why the terrace age is going younger as the elevation decrease.

Table 2.1 Absolute dating methods (Burbank, 2012). Red frame indicates the method that is used in this study

Method	Useful range	Materials needed	References
Radioisotopic ( <sup>14</sup> C)	35 ka	Wood, shell	Libby (1955), Stuiver(1970)
U-Th	10-350 ka	Carbonate	Ku (1976)
Thermoluminescence	30 – 300 ka	Quartz or feldspar	Berger (1988)
Optically Stimulated Luminescence	30 – 300 ka	Quartz silt	Aitken (1998)
Cosmogenic In Situ <sup>10</sup> Be, <sup>26</sup> Al	0-4 Ma	Quartz	Lal (1988), Nishiizumi et al. (1986)
He, Ne	Unlimited	Olivine, Quartz	Cerling and Craig (1994)
<sup>36</sup> Cl	0-4 Ma		Phillips et al. (1986)
Chemical Tephrochronology	0 – Several Ma	Volcanic Ash	Westgate and Gorton (1981)
Amino acid racemization	0-300 ka, temperature dependent		
Paleomagnetic identification of reversals	>700 ka	Fine sediments, volcanic flows	Cox et al. (1964)
Secular Variation	0 – Several Ma	Fine sediments	Creer (1962, 1967)
Biological Dendrochronology	0 – 10 ka	Wood	Fritss (1976)
Sclerochronology	0 – 1000 yr	Coral	Buddemeier and Taylor (2000)

## Chapter 3 : Results and Discussions

### 3.1 Erhjen River Terrace Classification Map

Numerous topographic profiles already created in order to classify the terrace in Erhjen River. The direction of the topographic profiles either perpendicular to the river flow or parallel with the river flow. On our mapping, we develop 4 major levels of terraces in the Erhjen River and 5 levels of sub-terraces based on the elevation difference between each terrace. The highest terrace in the upstream part which is the oldest terrace ranging from 80 – 85 meters above sea level labeled as T1a and the lowest labeled as T4a ranging from 65-70 meters above sea level. We can see in the upstream of the Erhjen River, the development of the terraces are wide, especially for the T3a, it spreads very wide, reaching more than 1.5 km in total width and continuous in both side of the river. Classifying the terrace in the upstream is relatively easy because the terrace risers recognizable from the DEM and there is no tilted terrace.

We make a 3D morphotectonic map of the upstream part in the Erhjen River with 3 topographic profiles to show how the terrace classification (**Figure 3.2**). Although the upstream part also passed by several geological structures, the terrace itself still flat and did not experience any disturbances. These geological structures did not cut through the terrace deposit.

As we go to the midstream of Erhjen River, the river starts to meander. It becomes the indicator if there is something in the middle part of the Erhjen River. The terrace deposit also becomes minor and several sub-levels of the terrace are formed such as T1b, T2b, T3b, etc. In chapter 1 we can see from the geological map that the midstream of Erhjen River passes through by 3 geological structure, which are Gutingkeng Fault, Lungchuan Fault, and Hsiakunshui Anticline. At this location, the terrace becomes harder to classify since there are more levels of elevation and many small terraces (**Figure 3.3**). These many levels are due to the geological structures that pass through the surface of the midstream part of Erhjen River.

Several tilted terrace also found in the midstream part and it supports our hypothesis that there is something control this terrace. We found 10 tilted terraces, measure its slope and compare the slope with the slope from the modern river (**Figure 3.6**).

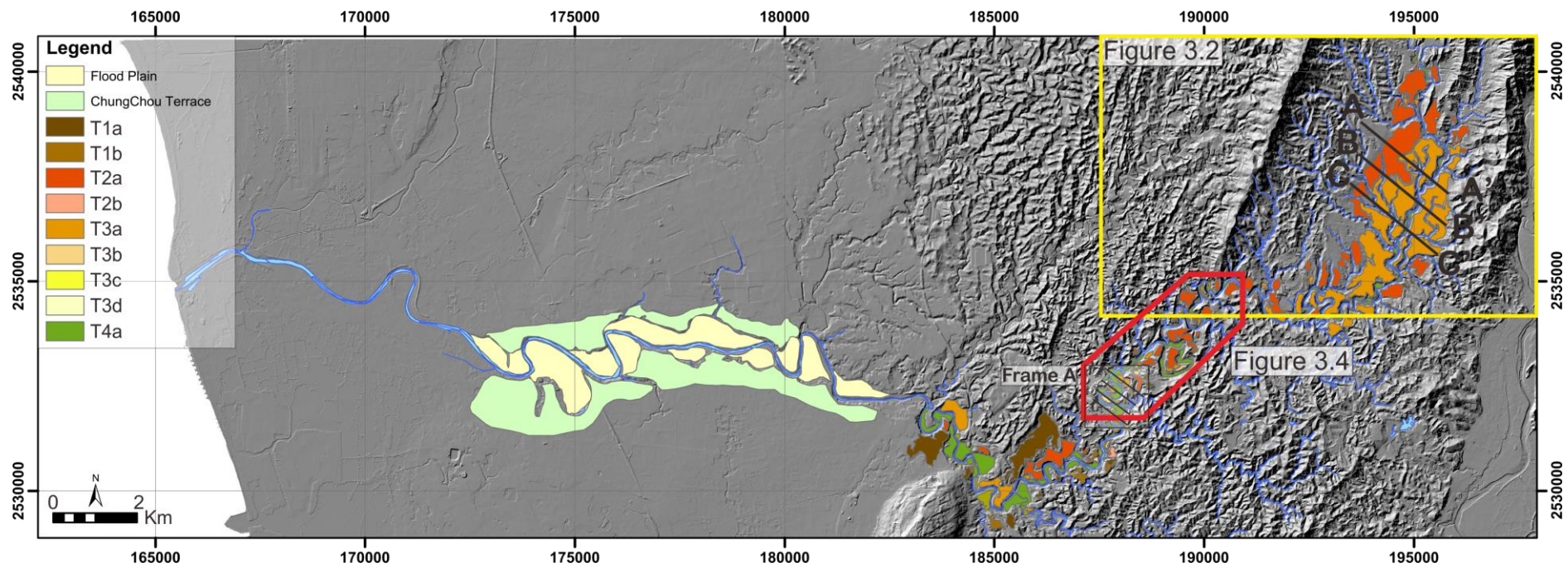


Figure 3.1 Erhjen River terrace map (Appendix A for bigger scale)

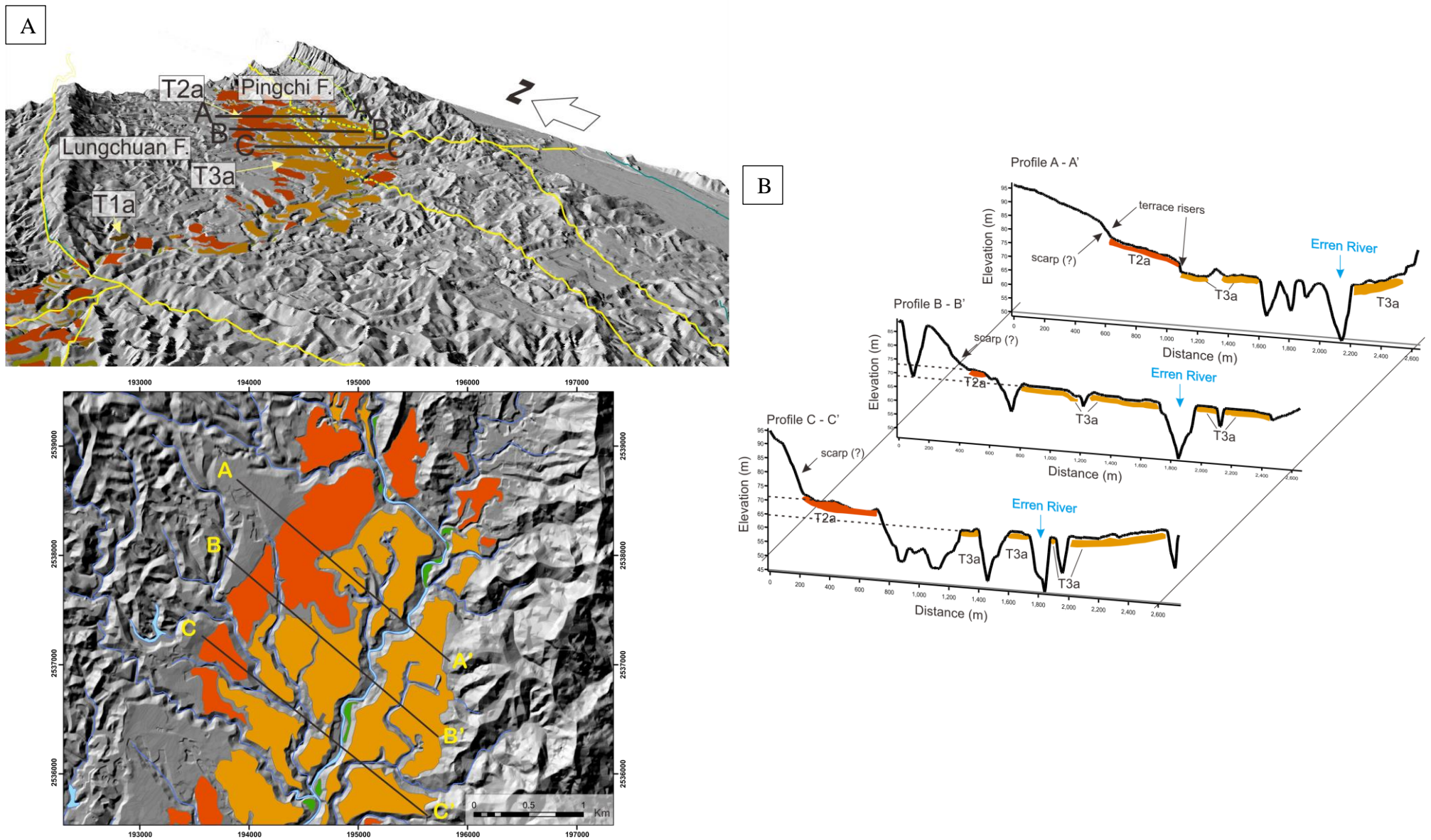


Figure 3.2 (A) 3D morphotectonic map of the upstream segment of the Erhjen River upstream with vertical exaggeration of 1.5x (times). (B) Topographic profiles showing two different levels of terrace deposit

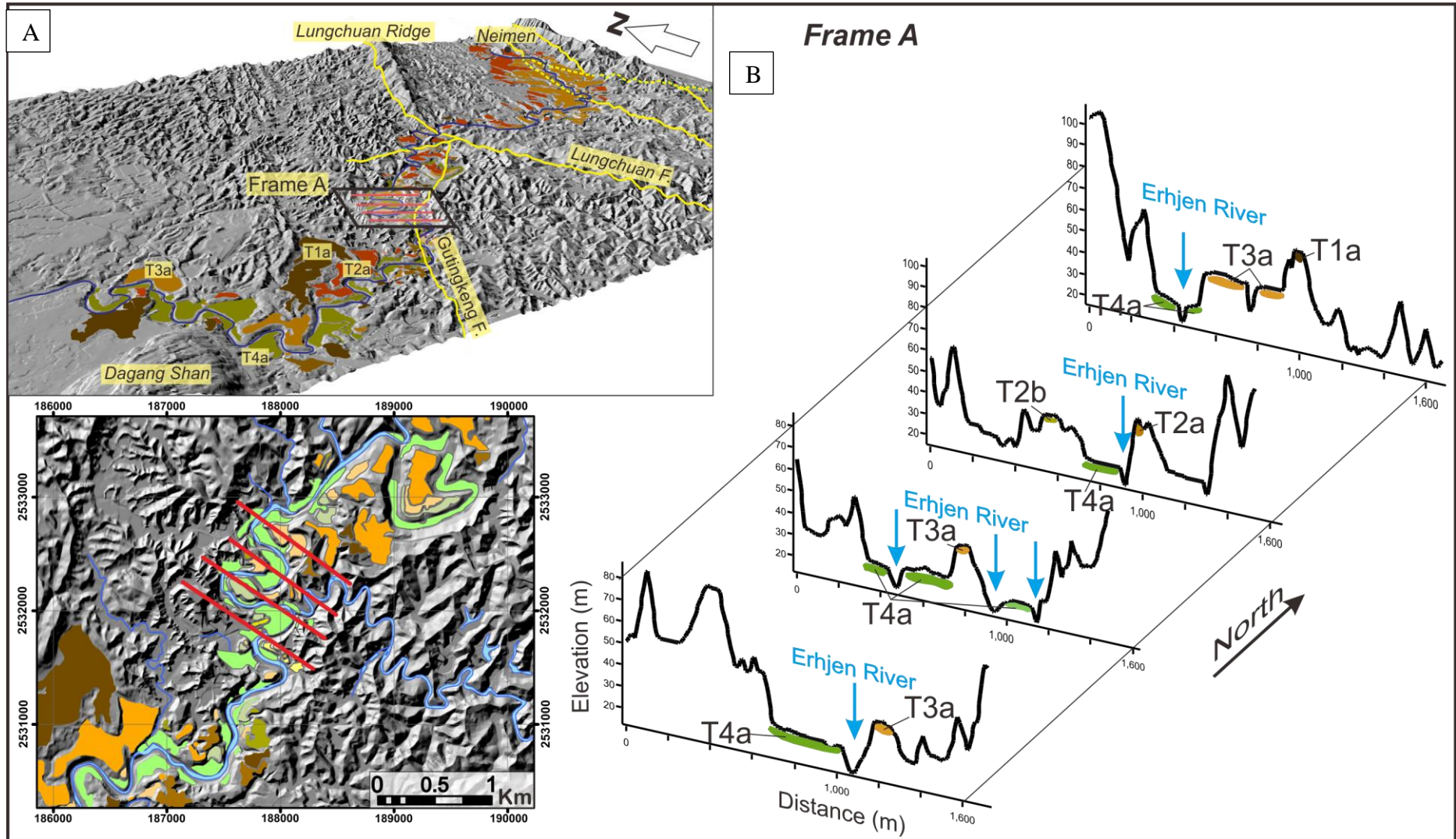


Figure 3.3 (A) 3D morphotectonic map of the Erhjen River midstream segment with vertical exaggeration of 1.5x (times). (B) Topographic profiles of 4 within frame A showing morphology of the Erhjen River midstream area

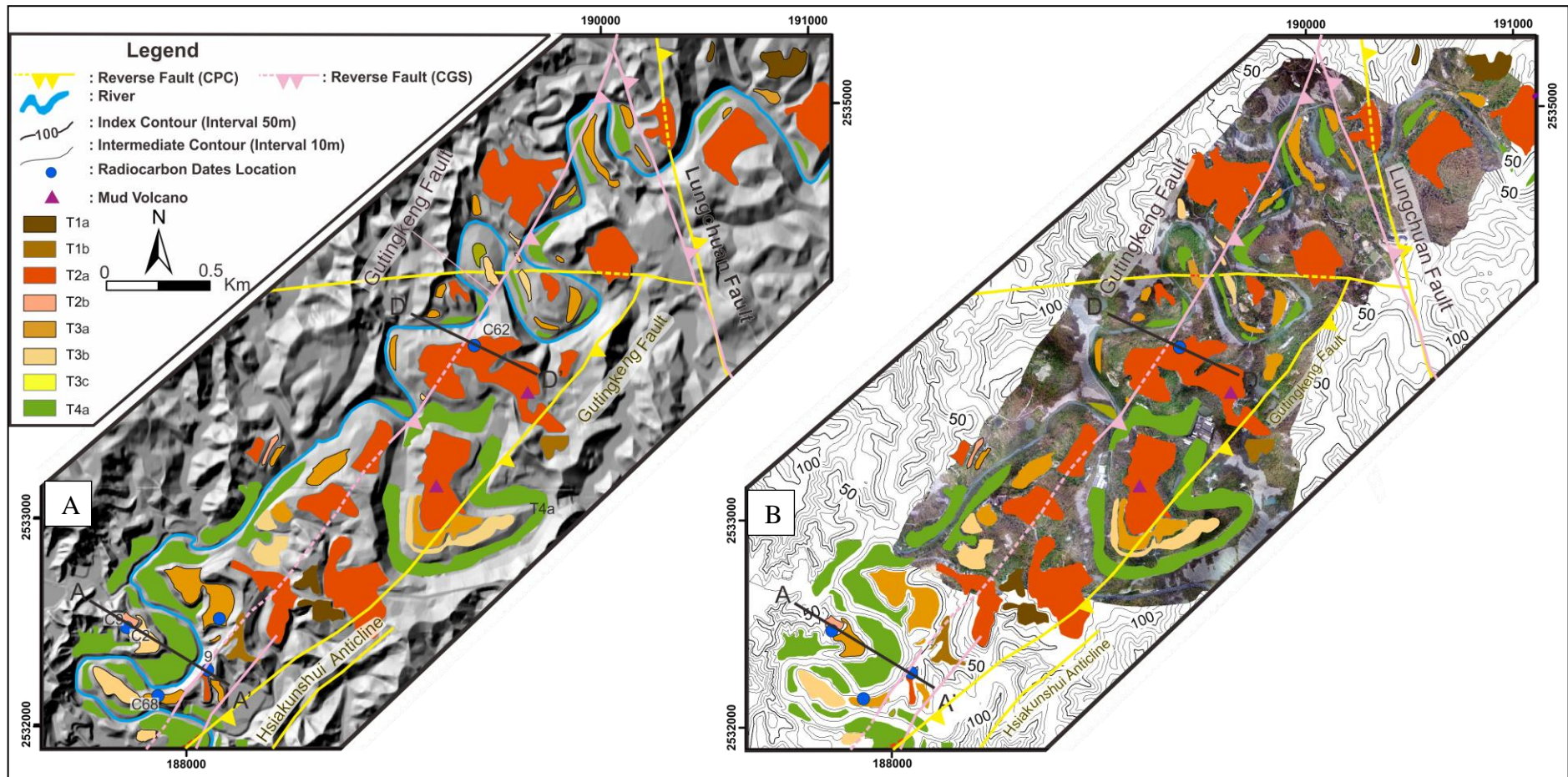


Figure 3.4 Midstream of Erhjen River terrace map. (B) Aerial photo of Erhjen River midstream segment

### 3.2 Radiocarbon Dating Results

In order to classify the fluvial terrace that becomes harder as we go to the midstream, we need another method. We use radiocarbon dating to dates the charcoal in the terrace deposit to get the age of the terrace. 28 radiocarbon dates from the previous study aided 7 more from this study have been conducted. Several locations have been selected for dates (**Figure 3.4**). Based on our dating results and a previous study, we can classify the terraces regarding their ages.

We also made a stratigraphic column in each sampling site. This stratigraphic column will help us to differentiate between the terrace deposit and soil. The stratigraphic column also becomes an indicator if the site is good enough to do the sampling. For example, you will not do the sampling in the soil. Because soil is a modern deposit which can not representative enough to show the ages of the terraces. But still, in the soil, we can found some paleo-civilization tools like bricks and ceramics from the predecessor. Sometimes the results of the radiocarbon dates are not as good as we wish. There is some limitation that we encounter. The result of the dating can be old and also can be young. This is due to the uncertainty of the sample we took, we are unable to detect if the sample was reworked or not. The results show that the T2a ages are ranging between 1010 to 1380 YBP, T3a between 800 to 870 YBP, and T4a younger than 800 YBP. However, from among all of the 34 radiocarbon dates, we only can rely on several samples. From the results, we also can see in sample 9, C2, C9, and C68 showing an interesting result.

The topographic profile has been drawn and showing that within 450 meters in distance between sample C2/C9 site and sample no.9 site, the age difference is very significant. In sample 9, C2, C9, and C68 we can see they are in a slightly different elevation level. We took the C2 and C9 sample in the same outcrop which is T2b while sample C68 was located in T3a and sample no. 9 in the T2a based on the previous study. The different ages between C2/C9 and sample no.9 are more than 1000 years BP, while the elevation differences between the terraces are only 2 meters. There is also 2 meters different elevation between C2/C9 location with C68 location and the age differences only  $\pm 200$  years which we can rely on this dating results. We measure three type of elevation that we will use this elevation to calculate the local incision rate. **One** is sample elevation, **Two** is terrace strath elevation, and **the last** is terrace elevation. Three of them are measured from the local riverbed

Table 3.1 Radiocarbon dates along the Erhjen River. The number of the sample correlates with the map in Appendix A. Samples with a number starting with capital “C” (grey column) are the samples from this study (conventional ages) while the others are from a previous study (Meng-Long Hsieh conventional ages – Unpublished data)

Coordinate (TWD 97)		Age (Years BP)	No.	Material	Terrace (This Study)	Terrace (Previous Study)	Sample H (from river bed) - (meter)	Strath H (meter)	Terrace H (meter)
X	Y								
195140.119	2540199.814	870±40	1	Plant Fragment	T3a	CP1	10	<8	15
194995.711	2540202.494	6750±90	2	Wood	-	-	13		
194824.095	2539231.71	4576±40	3	Plant Fragment	T2a	-	5	4	14
194882.052	2539422.827	597±47	4	Plant Fragment	T3a	-	10.5	-	
193193.395	2536855.995	8580±63	5	Plant Fragment	-	High Terrace	28	-	
193330.009	2534162.111	12426±59	6	Plant Fragment	T3a	-	13	10	20
190435.836	2532262.418	9817±51	7	Plant Fragment	-	-	43	42	47
187311.222	2531540.497	5060±140	8	Charcoal	-	-	61	60	66
188118.702	2532244.352	2020±40	9	Wood	T2a	KT1 - KT2	35	34	42
187469.105	2531605.671	1710±40	10	Wood	T3a	Minor Terrace - Modern floodplain	36	35	42
186971.675	2530492.67	2240±40	11	Wood	T1b	KT1	27	26	-
186952.941	2530511.512	2410±40	12	Wood	T2a	KT1	27	26	-
187898.015	2531735.557	1340±50	13	Wood	T4a	KT2	19	19	25
187501.096	2531139.825	1000±45	14	Wood	T4a	Minor Terrace - Modern floodplain	12	12	19
187500.083	2531032.783	387±20	15	Charcoal	-	-	15		19
184931.395	2529501.285	2270±50	16	Wood	T3a	KT1	15	15	27
184875.794	2529365.255	2160±50	17	Wood	T1b	KT1	17	17	27
184854.149	2529369.655	1680±40	18	Wood	T1b	KT1	23	17	27
184233.954	2530636.598	8390±60	19	Wood	T4a	High Terrace	23	-	35
184180.116	2530644.522	11350±70	20	Plant Fragment	T4a	High Terrace	26	-	34
184076.449	2530664.045	8260±60	21	Wood	-	High Terrace	22	-	30
184148.687	2531216.191	4020±50	22	Wood	-	-	16	12	27
184504.606	2531198.649	2220±50	23	Wood	-	-	12	10	27
184252.803	2531235.117	7820±60	24	Wood	-	-	30	-	36
184425.763	2532209.17	9370±50	25	Wood	-	-	24	21	41
184082.98	2532553.951	34080±430	26	Wood	-	-	15	9	
185151.32	2533588.422	10150±70	27	Wood	-	-	19	19	36
189398.643	2533826.232	200 ± 30	C31	Charcoal	T2a	CP2 - Minor Terrace	38	-	45
189087.493	2533007.08	103.03±0.38 pMC	C48	Charcoal	T3a	CP2	20	-	27
188617.592	2532537.179	130 ± 30	C35	Charcoal	T1a	High Terrace	46	-	49
188160.391	2532511.779	260 ± 30	C41	Charcoal	T3a	KT2	20	-	22
187709.54	2532460.979	1010±30	C2	Charcoal	T2b	KT2	33	28	39
187709.54	2532460.979	1010±30	C9	Charcoal	T2b	KT3	30	28	39
187868.29	2532124.428	800±30	C68	Charcoal	T3a	KT2	26	-	30
189398.643	2533826.232	1380 ± 30	C62	Charcoal	T2a	CP2 - Minor Terrace	38	-	40

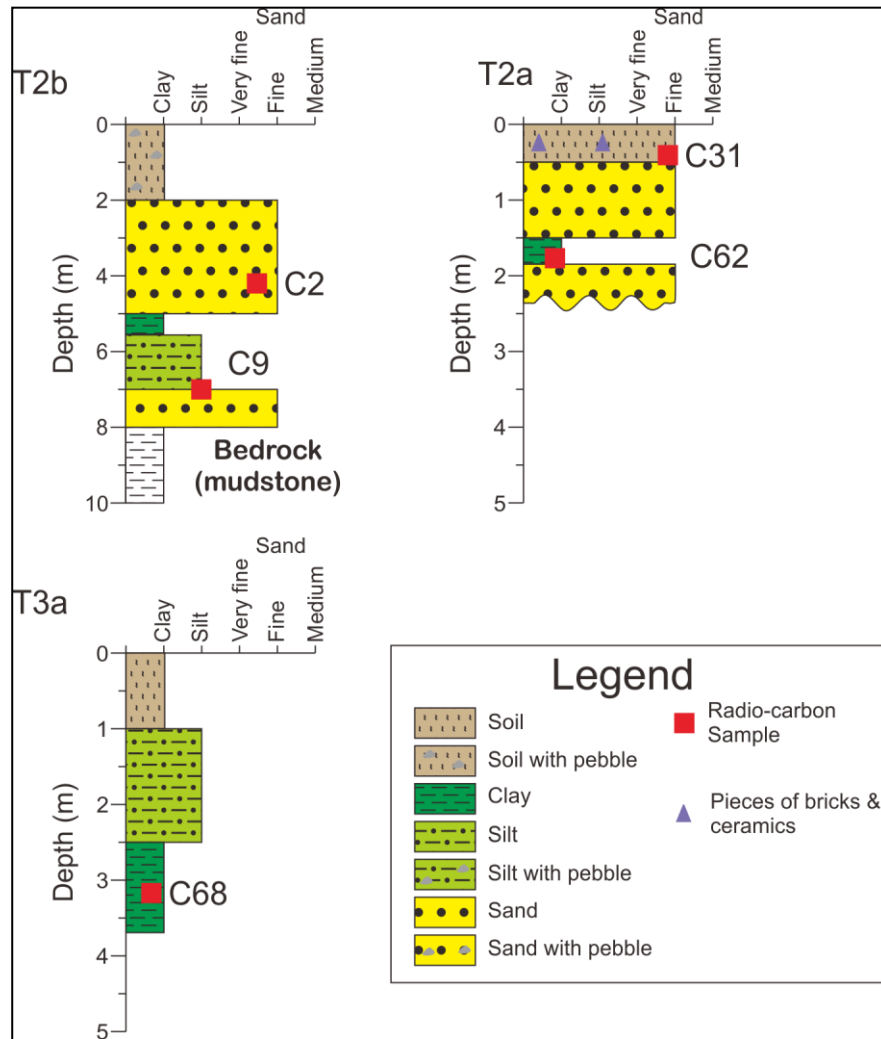


Figure 3.5 Stratigraphic column for each radiocarbon dating sites. (Lithology symbols and colors – USGS, 2006)

We also have to keep in mind that C2, C9, and C68 are located in the footwall of Gutingkeng fault while sample no.9 is located in the hanging wall based on CGS geological map. From this phenomenon, if we believe the dates are correct, we think that the T2b and T3a were uplifted. We know that Gutingkeng fault is an east-dipping reverse fault, but from the InSAR, we see that the west side was uplifted relative to the east side which suits well with our hypothesis based on the terrace analysis with the radiocarbon dates.

For sample C2 and C9 were located close to each other and different in elevation. The C2 was covered by fine sand deposit while C9 is muddier. We took C2 samples 4.2 meters from the T2b surface as we can see in the outcrop photo (**Figure 3.6**). C9 sample was located deeper, more than 5m from the T2b surface it is close to the strath terrace.

This sample covered with laminated sand and mud deposit which makes this is perfect for being sampled. A laminated structure in the terrace deposit indicate that the layer is well-preserved without any disturbances, thus it will become a good condition for charcoal to be deposited. And the age of the charcoal will represent the age of the place where it is deposited.

Meanwhile, the sample number C62 located in the tilted terrace T2a. In this area, we found some tools such as bricks, ceramics, etc. These bricks and ceramics were found 30 cm from the surface of T2a. Since T2a in this area was tilted we took a sample deeper than the layer that contains paleo-civilization tools. We took the C62 sample 1.8 meters below the T2a terrace (**Figure 3.6**).

The results from these radiocarbon dates can be used to calculate the incision rate of the Erhjen River. In the A-A' profile, the incision rate from 2 ka to recent is  $15.3 \pm 0.21$  mm /yr ; from 1 ka to recent is  $25.8 \pm$  mm/yr; from 0.8 ka to recent is  $27.5 \pm 0.2$  mm/yr. While D-D' profile showing almost similar results from 1 ka to recent the river incise  $26 \pm 0.18$  mm/yr. As we calculate the local incision rate we found that three places have similar local incision rate which are the C2 & C9, C68, and C62, while the no.9 sample has different local incision rate which is slower.

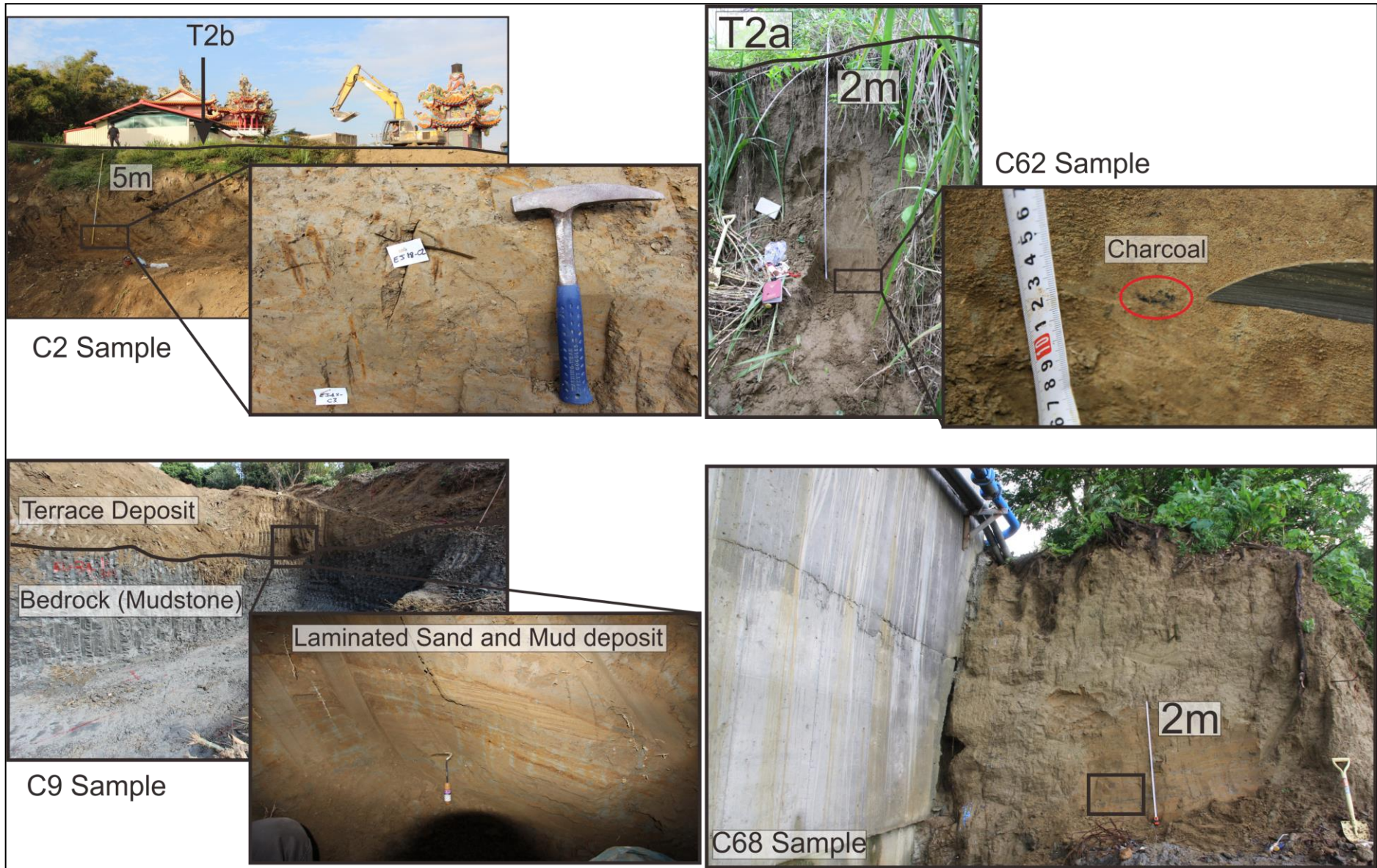


Figure 3.6 Outcrop photos where the C2, C9, C62, and C68 samples were taken.

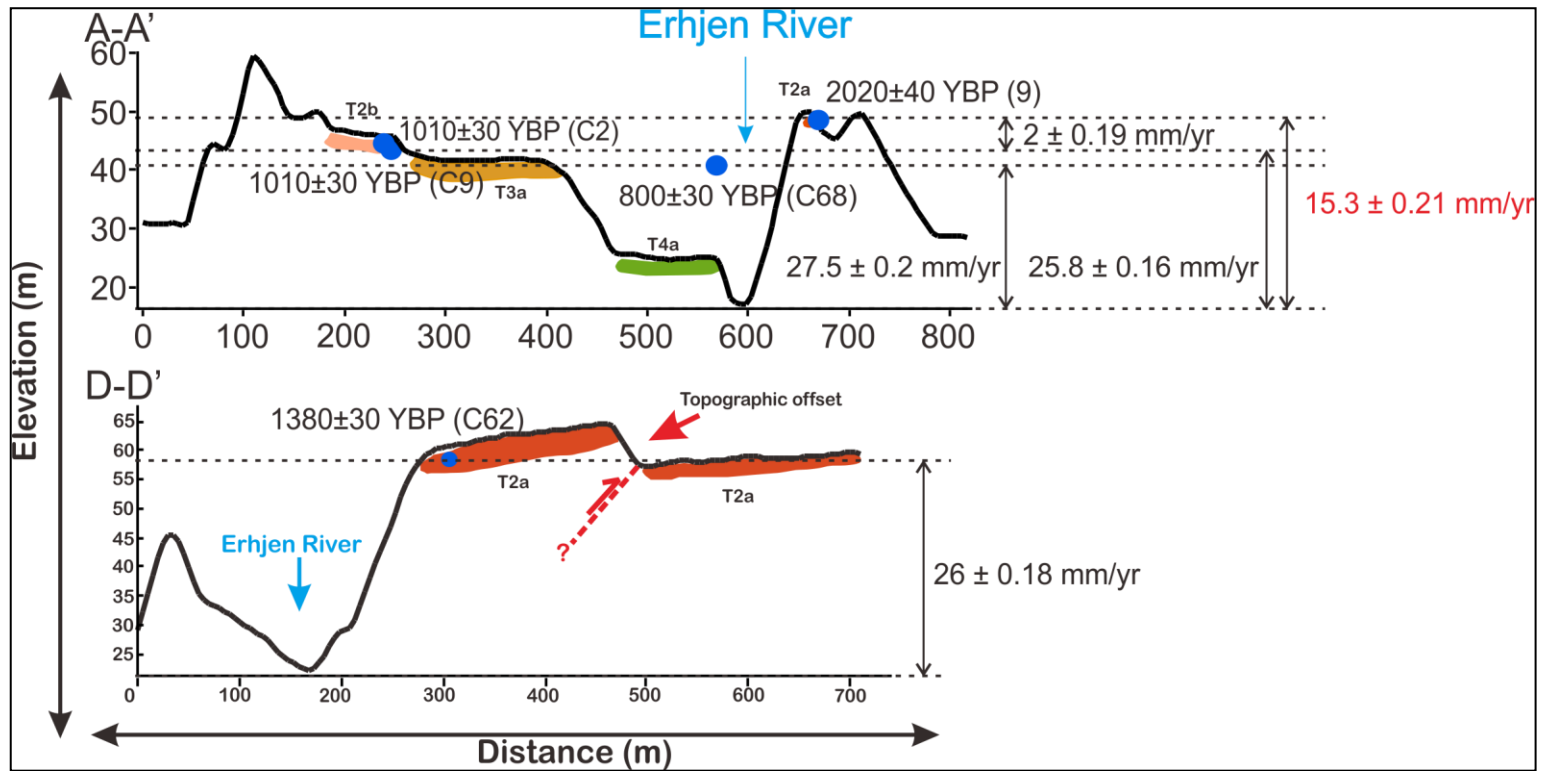


Figure 3.7 Topographic profiles of A-A', and D-D'. The age in C68 is projected into A-A' section (Map view in figure 3.4)

Another data showed by the radiocarbon dating the sample no. C62 (T2a terrace) the age of this terrace is  $1380 \pm 30$  years BP and the elevation difference of the terrace relative to the modern river is 38 meters. From this data, we can calculate how much the river incise. The local incision rate in this area is about 27 mm/yr which makes this incision rate value is close with another incision rate value in the C2, C9, and C68 area. Thus, we can conclude that in the midstream part of Erhjen River from 1 ka to recent is incising for about 20 – 30 mm/yr.

### 3.3 Tilted Terrace at the midstream of Erhjen River

Careful observation has been done by checking all of the terraces in the midstream area that passed by Lungchuan and Gutingkeng fault. We marked 10 tilted terrace (**Figure 3.8**) at the midstream part of Erhjen River and measure its slope, the slope of the tilted terrace will be compared with the local river slope. These tilted terraces will also become our foundation to draw the fault trace in the surface. We also create Euclidian topographic profiles of the Erhjen River terrace deposit from upstream to downstream to observe the distribution of the terrace, classify the age of each terrace groups and check if the Lungchuan fault or Gutingkeng fault affect the terrace and the Erhjen River itself.

We measure the slope of the terrace by using the simple trigonometric function. The parameters we need to calculate the slope is elevation and distance. We can get all of the parameter value we need by looking at the 5m DEM map.

Based on our measurements of the tilted terraces, the slope azimuth of the tilted terraces are dominantly in NW direction with a value ranging from  $1^\circ - 4^\circ$  with  $\pm 0.02$  uncertainty and mostly happened in T2a terrace. We draw the fault by connecting all of these terraces and still maintain the topographic value based on the 1m DEM map from Central Geological Survey. However, not all of the tilted terrace can be considered as an indicator if the fault is lying above the terrace surface. The data we can consider is the tilted terrace No.5 where we have the reliable radiocarbon dates and topography offset (**Figure 3.9**). In this terrace, we interpret this fault is a west dipping thrust fault. This makes sense since the west side of the fault in this terrace is tilted and uplifted. When we try to extend the fault trace to the south, it suits very well with terrace No. 6 or we called as a “B” terrace due to its B shape (**Figure 3.8**). The “B” terrace is the only terrace that tilted to the southwest which makes the northern part of this terrace has high elevation. Thus, we interpret that the Gutingkeng fault also passed this terrace.

Table 3.2 Slope measurements for the tilted terrace in the midstream segment of the Erhjen River. (Refers to **Figure 3.9**)

No	Terrace	Tilted Slope ( ° )	Uncertainty	Slope Azimuth ( ° )	Euclidian River Slope ( ° )	Curvilinear River Slope ( ° )
1	T2a	1.26	± 0.018	318	0.34	0.18
2	T2a	1.72	± 0.019	295	1.03	0.88
3	T3b	2.86	± 0.019	310	1.14	0.76
4	T3a	4.57	± 0.018	329	0.57	0.48
5	T2a	2.86	± 0.019	246	1.14	0.94
6	T2a	4.28	± 0.017	141	0.42	0.31
7	T2a	2.29	± 0.018	335	0.34	0.34
8	T3a	2.86	± 0.018	305	0.46	0.46
9	T2a	2.29	± 0.019	290	0.28	0.28
10	T3b	2.38	± 0.019	311	0.28	0.28

The tilted “B” terrace is proving that the Gutingkeng fault already affects the terrace since Erhjen River flows in this area. As we do the field survey in the south cliff of the “B” terrace, we found a dark color mudstone striking NE with 49° dipping to the east (**Figure 3.8**). We interpret this dark color mudstone layer as a shear zone of Gutingkeng fault. A darkening color of mudstone layer is an indicator of a transformation of smectite mineral into illite due to the pressure and temperature change during the fault event (Casciello et al., 2011).

From the field survey photo of the “B” terrace (**Figure 3.8**) we can recognize that in this area there are several levels of elevation that makes this terrace hard to classify. These several levels of elevation are artificially made for agriculture benefits so that we can not distinguish the between the terrace risers that occurred naturally or artificially. Several radiocarbon dates have been conducted in this area (**Appendix A and B**) but the results are not as we expected, so the classification of the terrace just based on the elevation level.

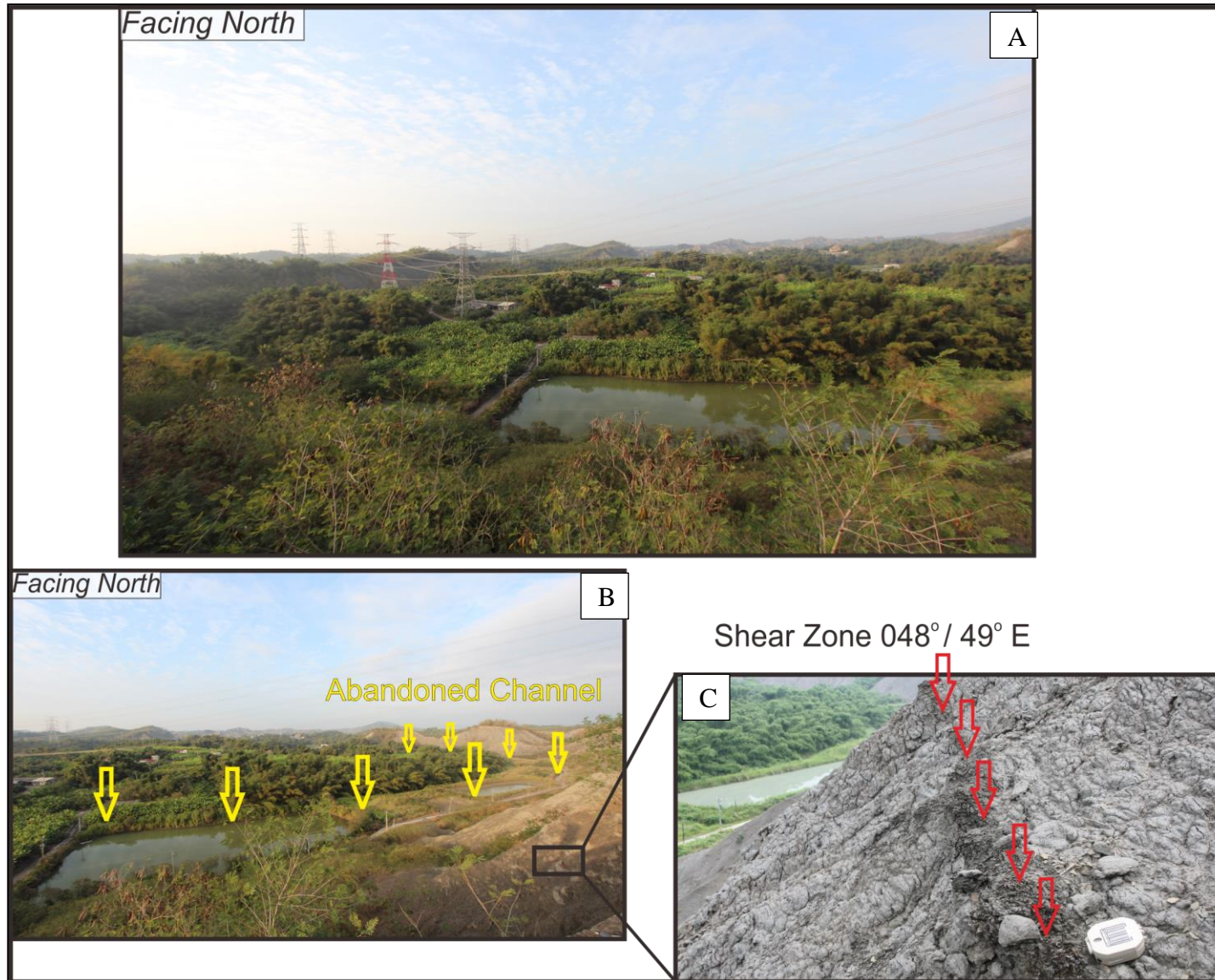


Figure 3.8 (A) The “B” terrace landscape field photo (B) Abandoned channel of Erhjen River (C) Shear zone of Gutingkeng fault

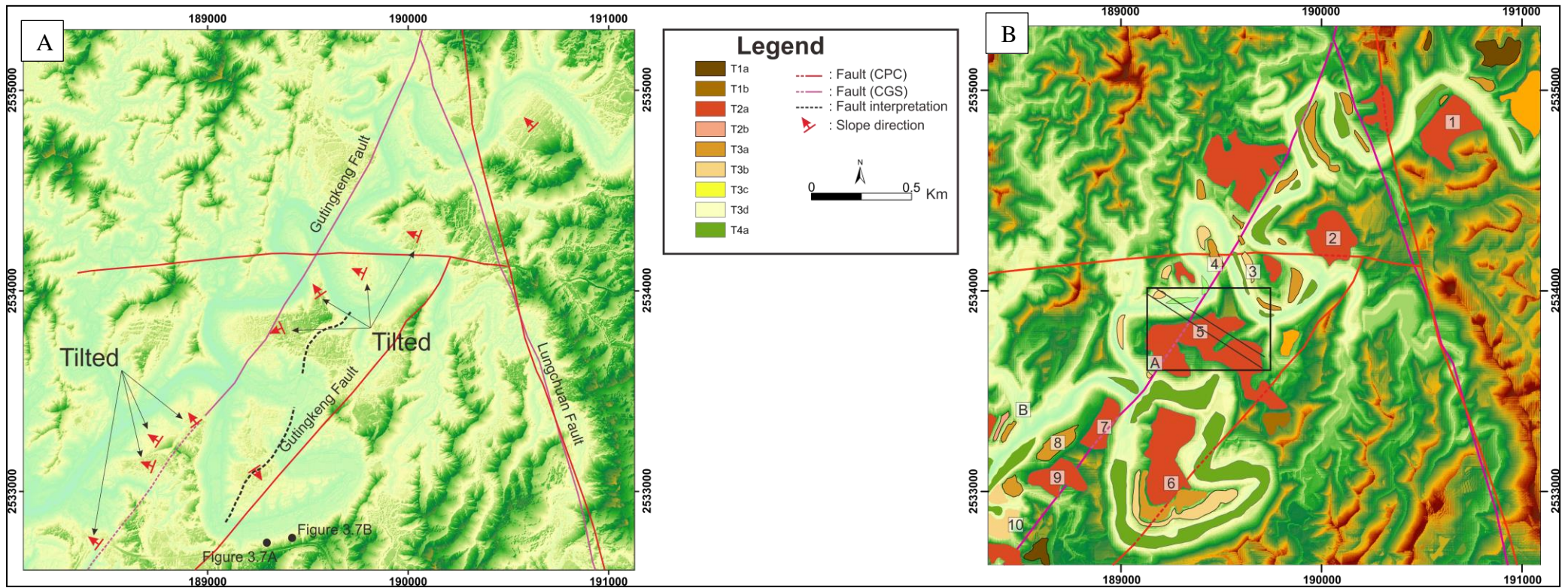


Figure 3.9 Interpretation on the fault trace based on the tilted terrace. (A) 1m DEM map. (B) 5m DEM map

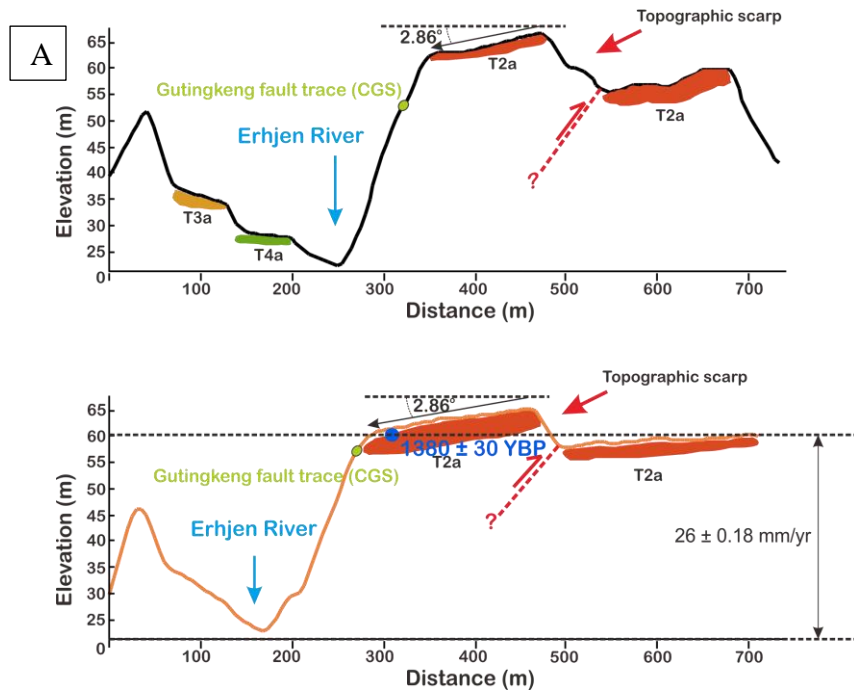


Figure 3.10 (A) Topographic profiles of frame "A" located in map **Figure 3.9**. (B) Field photograph of the topographic scarp

In frame A (**Figure 3.9**), we can see that the T2a terrace has a scarp with 2 – 5 meters different elevation. As we go to the south of the terrace, the different elevation starts to decreasing and then almost flat towards the edge of the south part of the terrace. We draw the Gutingkeng fault trace following this scarp up to the NE direction. This terrace has tilted  $2.86^\circ$  to the Southwest while the local euclidian slope of the river is  $1.14^\circ$ . This means that the terrace encounters some uplift due to the geological structure movement of Gutingkeng reverse fault while the river keeps incising the bedrock. In frame B, it looks flat on the topographic profiles but when we measure the slope we got  $2.29^\circ$  and  $2.86^\circ$  of slope angle and compared to the river that only has  $0.2^\circ - 0.4^\circ$ .

Another terrace profile has been created by projecting the terrace to the A-A' Euclidian axis of the downstream to upstream in order to understand the distribution of all the terrace deposit and classify the age of the terrace in the Erhjen River (**Figure 3.11**). From this profile, we can see that the sub-group level of terraces is start developed in the midstream where the geological structures appear (Gutingkeng fault and Lungchuan fault). This profile helps us to determine the continuation of the terrace and calculate the total slope. We also know that there is a lack of radiocarbon dating data in the area between the Gutingkeng fault and Lungchuan fault, that is why we decide to take several samples in that area.

We measure the total euclidian slope of each terrace from the mountain front. Mountain front is the boundary between Coastal Plain and Western Foothills. From these measurements, we will know if the terrace has deformed or not by comparing the terrace slope with the modern river slope.

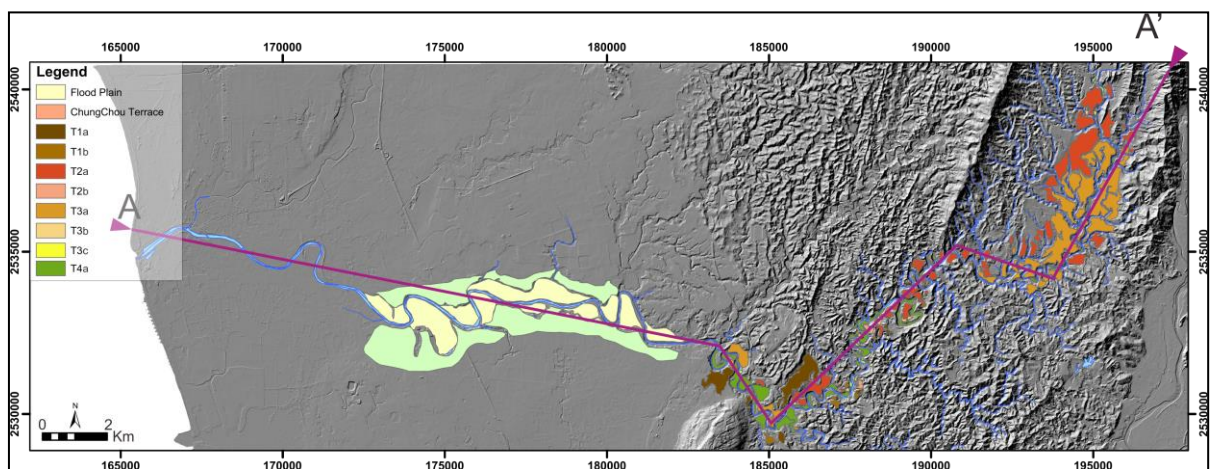


Figure 3.11 Euclidian section of A-A' used to project the terraces along the Erhjen River (Appendix A for bigger scale)

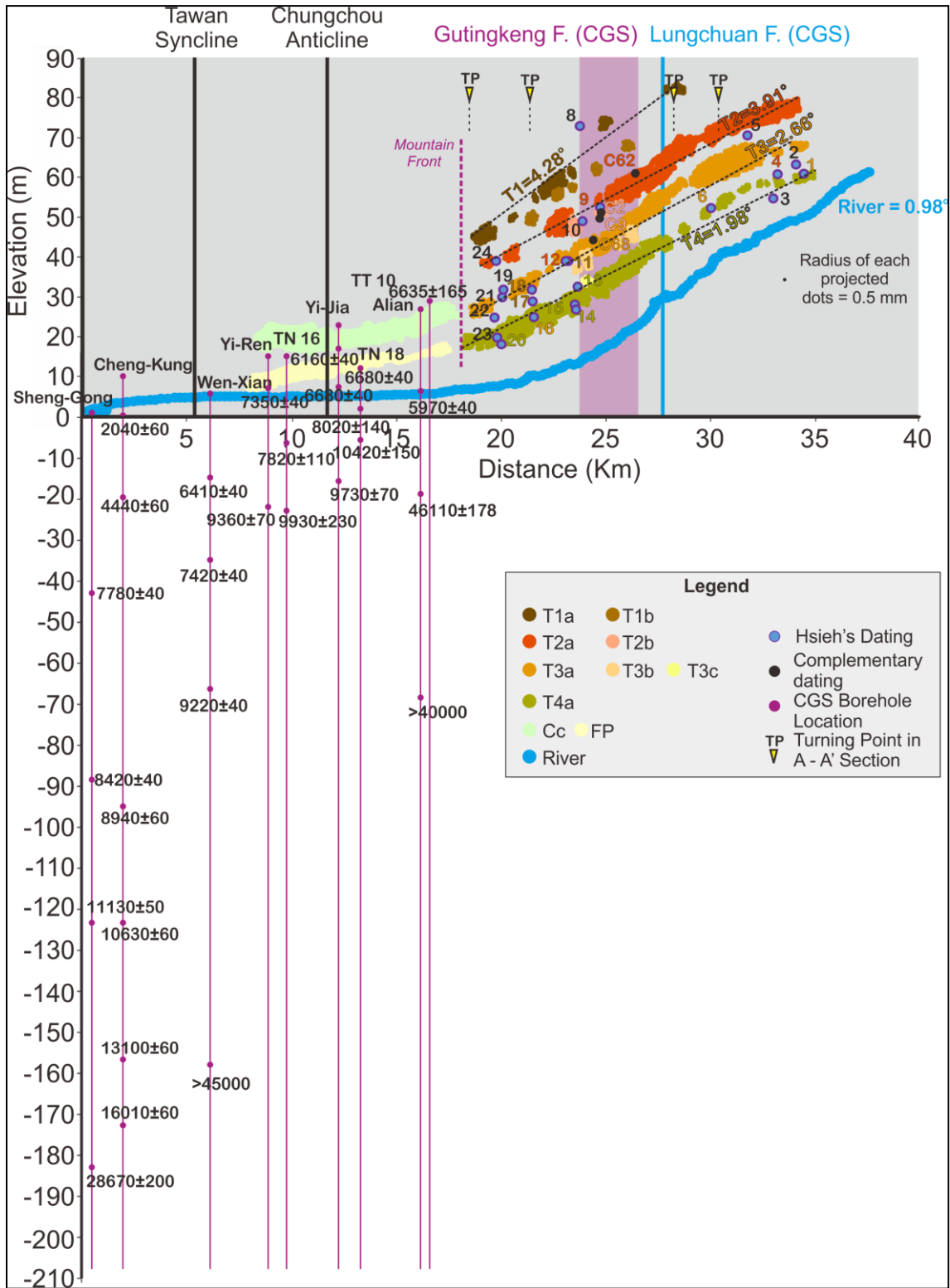
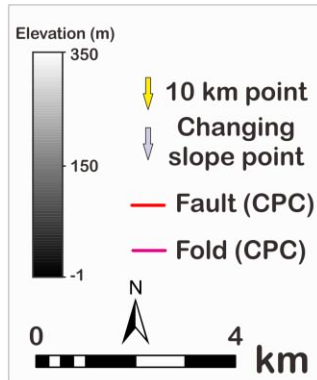
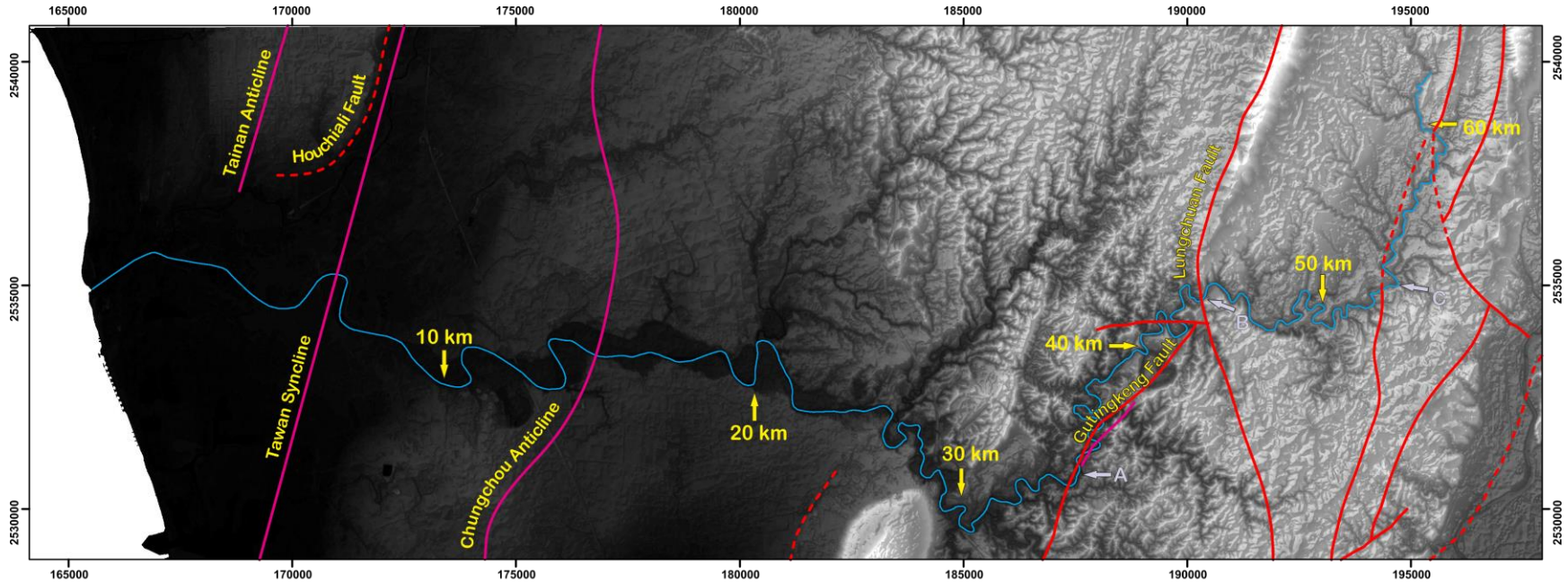


Figure 3.12 Projected topographic profile A-A' (See location in **Figure 3.11**). The code number of radiocarbon dates refers to table 3.1. The number on each borehole represents the conventional age with Years Before Present (YBP) as the unit. Location of CGS borehole data in appendix: A. Details of each borehole data are in the table 3.3



Erhjen River curvilinear Profile

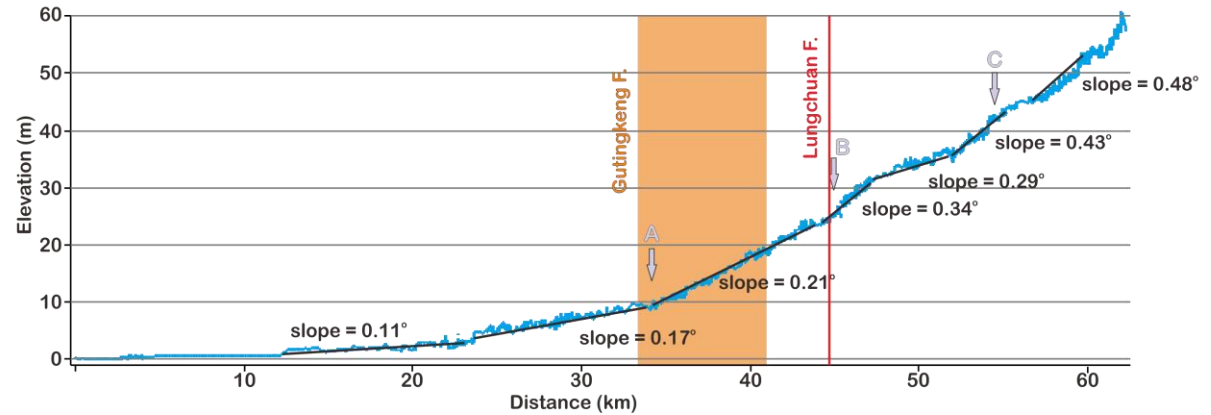


Figure 3.13 Curvilinear topographic profile along the Erhjen River

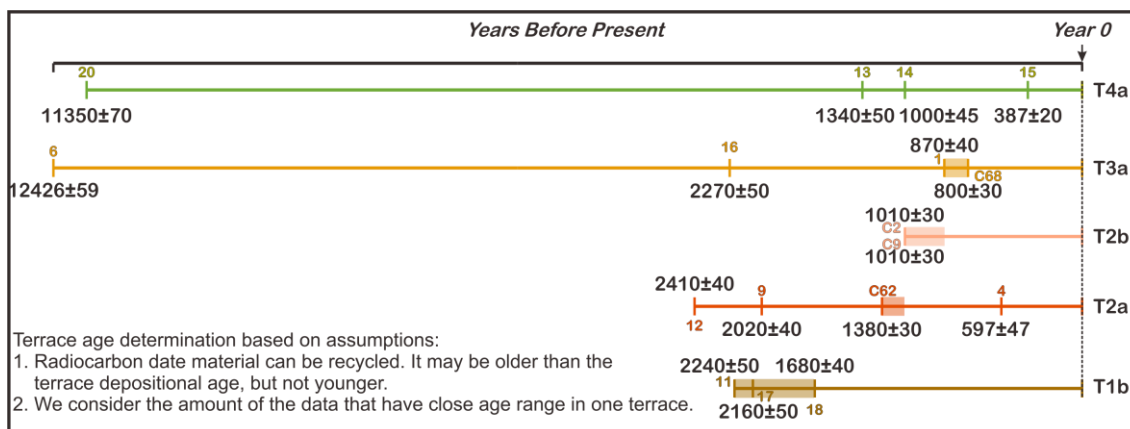


Figure 3.14 Schematic diagram of <sup>14</sup>C dates for each group of terrace age based on Hsieh & Knuepfer (2001) and this study

Table 3.3 Central Geological Survey borehole data (Central Geological Survey, borehole sites refer to map in Figure 3.13)

Borehole Sites	Depth (m)	Age ( Years BP)	Sedimentation Rate (mm/year)
Sheng-Gong	44.7	7780 ± 40	5.7
	89.3	8420 ± 40	10.6
	123.7	11130 ± 50	11.1
	183.6	28670 ± 200	6.4
	246.7	47950 ± 2270	5.1
Cheng-Kung	9.9	2040 ± 60	4.9
	29.4	4440 ± 60	6.6
	105.1	8940 ± 60	11.8
	134.5	10630 ± 60	12.7
	166.9	13100 ± 72	12.7
	182.7	16010 ± 80	11.4
Wen-Xian	20.6	6410 ± 40	3.2
	40.5	7420 ± 40	5.5
	70.7	9220 ± 40	7.7
	163.4	>45000	
	216.8	>45000	2.6
Yi- Ren	22.3	7350 ± 40	3
	35.9	9360 ± 70	3.9
Yi - Jia	4.8	6160 ± 40	0.8
	15.4	6680 ± 40	2.3
	38.7	9730 ± 70	4
Alian	20.2	5970 ± 60	3.4
	46.6	46110 ± 178	1
	66.9	>40000	0.7

The borehole data from Central Geological Survey in the coastal plain provide us several ages and sedimentation rates on each borehole sites at a different depth (**Table 3.3**). From this information we can get an insight that in the coastal plain within less than 50 meters depth the sedimentation rates are ranging from 0.8 – 5.7 mm/year during ~7000 Years BP – 2000 Years BP. If we correlate the sedimentation rate from this data to the regional sedimentation rate from a previous study (**Figure 1.4**) it has a similarity that as time goes by the sedimentation rate is increasing.

On the other hand, if we put the timeline for each radiocarbon dates on each group of terrace (**Figure 3.14**), we can determine the age of each terrace with several assumptions. Based on our determination, we can say the youngest terrace is T4a with the age younger than  $800 \pm 30$  Years BP, then T3a with the age 800 – 870 Years BP, followed by T2b with the exact  $1010 \pm 30$  Years BP, and T2a in sometime between 1010 – 1380 Years BP, the last and oldest terrace is T1b with the age range between 1600 – 2240 Years BP. Based on our slope calculation with the euclidian axis, we found that T1a has the steepest slope which has value for about  $4.28^\circ$  followed by T2a with  $3.91^\circ$  then T3a with  $2.66^\circ$  and T4a is the most gentle terrace with the  $1.98^\circ$  slope. The Erhjen River slope also changes become steeper as it passes the Lungchuan fault. If we compare the slope on the west side and east side of Lungchuan fault the result is showing that river slope in the east side of Lungchuan fault has a value  $0.8^\circ$  while the west side is  $1.9^\circ$ . From the calculation of the slope, we know that T1a has the steepest slope among the other terraces. This is due to the T1a formed earlier thus, it encounters more deformation resulting in the steep slope. As in the coastal plain where the Cc and the FP developed very well. In Cc with only 8 – 10 meter different elevation from its highest terrace to the lowest, it spreads to more than 5 km same case also happen with the FP. A curvilinear profile of Erhjen River also shows several slope changes. We record three slope changes and three of them are located near the fault. In the upstream, the slope of the river is  $0.38^\circ$ . Then, the slope changes near the Pingchi fault become  $0.24^\circ$  followed by another change starting from Lungchuan fault, the river slope become  $0.21^\circ$

T2a, T3a, and T4a terraces are the most continuous terrace since we can connect them from upstream to downstream comparing to T1a that are not develop in several areas. T2a, T3a, and T4a slope of the terraces are changing and the slope steepens where the Gutingkeng fault and Lungchuan fault occurred.

### 3.4 Discussion

The initiation of the major terrace surface in the lower Erhjen River Basin is more dependent on increases in bedload yield from hillslopes, triggered by catastrophic rainfall events (Hsieh & Knuepfer, 2001). Erhjen River made the highest suspended load carrier with the value of  $1.3 \times 10^7$  t/year (Hydrological Year Book of Taiwan, R.O.C). It carries gravel bedload, probably from Miocene sandstone/shale ridges (Hsieh & Knuepfer, 2001). This high value of the suspended load and climate change become the reasons why the Erhjen River has high incision rate, reaching up to 3 cm/year from 0.8 ka to recent based on the radiocarbon dating results in the midstream part of Erhjen River. Despite the fact that Erhjen River incision rate was fast due to climate change, several hypotheses also could be the factor of fast incision rate in the Erhjen River. These hypotheses will be based on two assumptions. **The first assumption** is some of the ages that located in the midstream is not representative. From **Figure 3.7**, we know that we have three ages that have close range which is the 0.8 ka – 1.3 ka. The only age that we suspect to be not representative is the 2 ka. If the 2 ka age is expected to be younger (close with the age of 1.3 ka) the local incision rate will be also similar with the other three sites. Thus, the river condition is not disturbed or we can say there is no anomaly in the river. **The second assumption** is all ages in the midstream are true/representative. In **the second assumption**, we can generate four hypotheses. **First hypothesis** is related to sea level fall. If the sea level fall, the river will try to catch the base level/sea level. Thus, the stream of the river will stronger which cause the incision of the river is increasing. **Second hypothesis** is there is fault activity that change after 1 ka. As we can see in the **Figure 3.7** local incision rate was recorded 2 mm/yr during 2 ka – 1 ka then it suddenly increasing 10 times become more than 20 mm/yr. **Third hypothesis** is there is some changes in river slope. If the slope of the river is changing and become steeper, the river stream will also increase. Causing the incision rate become fast. **Fourth hypothesis** is we interpret there is another fault in-between the sampling sites of 2 ka (east side of the river banks) with the 1 ka (west side of the river banks) we will discuss each of the hypothesis in this section.

Leveling data have been provided in the research location from Ching et al (2015) helps us to take a look of which area that has the bigger uplift rate. We project these leveling benchmark points into the 280° azimuth Z-Z' axis (**Figure 3.16**) and plot in the data to the uplift rate versus distance graph. We observe the leveling data during 2004 –

2010 and 2010 - 2016 and separate into two periods based on the two earthquake events which are  $M_w$  6.4 Jiashian Earthquake (March 4<sup>th</sup>, 2010) and  $M_w$  6.4 Meinong Earthquake (February 5<sup>th</sup>, 2016). **The first period**, during 2004 – 2010 the highest uplift rate was reached by station G478 with 24.2 mm/yr followed by the three benchmark stations G477, J109, and J110 with each value 21.24 mm/yr, 20.3 mm/yr, and 20.9 mm/yr. **The second period**, during 2010 – 2016 the highest uplift rate was same which is G477, reaching 19.8 mm/year followed by G478 and J109 station with uplift rate 19.26 mm/yr and 19.1 mm/yr. As we take a look on the graph, in the **second period** all of the benchmark stations were uplifted. As the Jiashian earthquake and Meinong earthquake occur, the leveling benchmark points near Gutingkeng fault increasing rapidly (**Figure 3.17**).

As we observed the highest uplift rate stations, all of them were located in the east side of the Erhjen River (**Figure 3.19**). These leveling data will support another hypothesis that both side of the river is uplifted. We compare the uplift rate in the midstream area with local incision rate and the result is the local incision rate still bigger than the uplift rate.

As we think the **First hypothesis** which is sea level fall, we have to check the global sea level and local sea level change. Global sea level has fluctuated widely in recent geologic past. It stood 4-6 meters above the present during the last interglacial period, 125,000 years ago (Gornitz, 2007). As we see in **Figure 3.16** the relative sea level has increased to approximately 120 meters since 20,000 years ago. Increasing sea level alleged due to the climate warming resulting in the massive ice sheet that covered parts of North America, Northern Europe, and several other regions during the last ice age melt. By the mid-Holocene period, 6000 – 5000 years ago, the glacial melting rate becomes slower. In Taiwan itself based on the observation during 1950 – 2000 the sea level around Taiwan also increase. Showed by the 2 stations in Kaohsiung and Penghu with 2.41 mm/yr and 6.06 mm/yr (**Figure 3.15**). With this information we can clearly discard this hypothesis.

Meanwhile the **Second hypothesis**, we interpret that the terrace in the west side of the riverbed is uplifted at about 23 meters relative to the riverbed. This value is calculated from the terrace elevation compare to the riverbed.

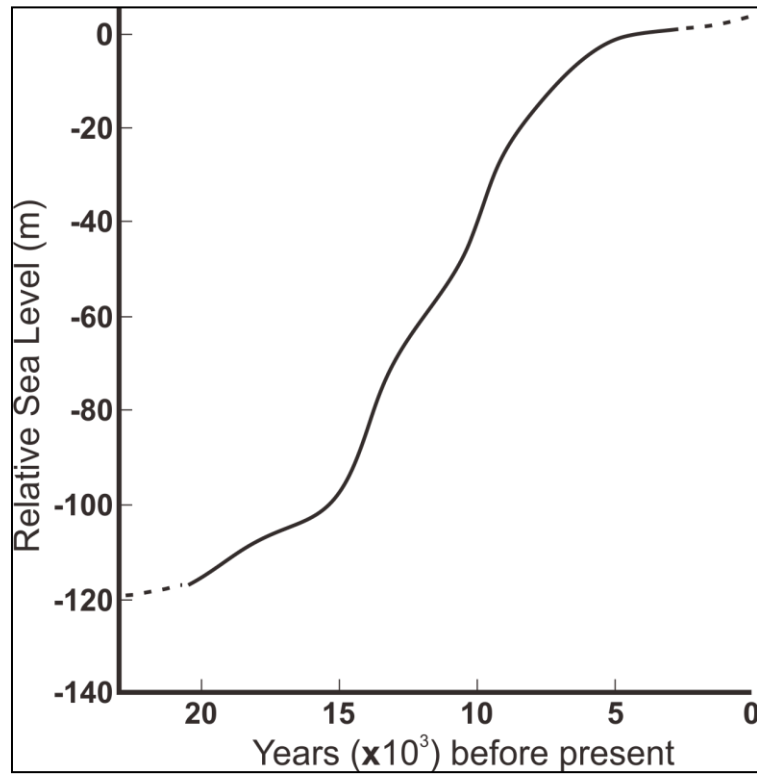


Figure 3.16 Generalized curve of sea level rise since the last ice age (Courtesy of Vivien Gornitz - NASA, 2007)

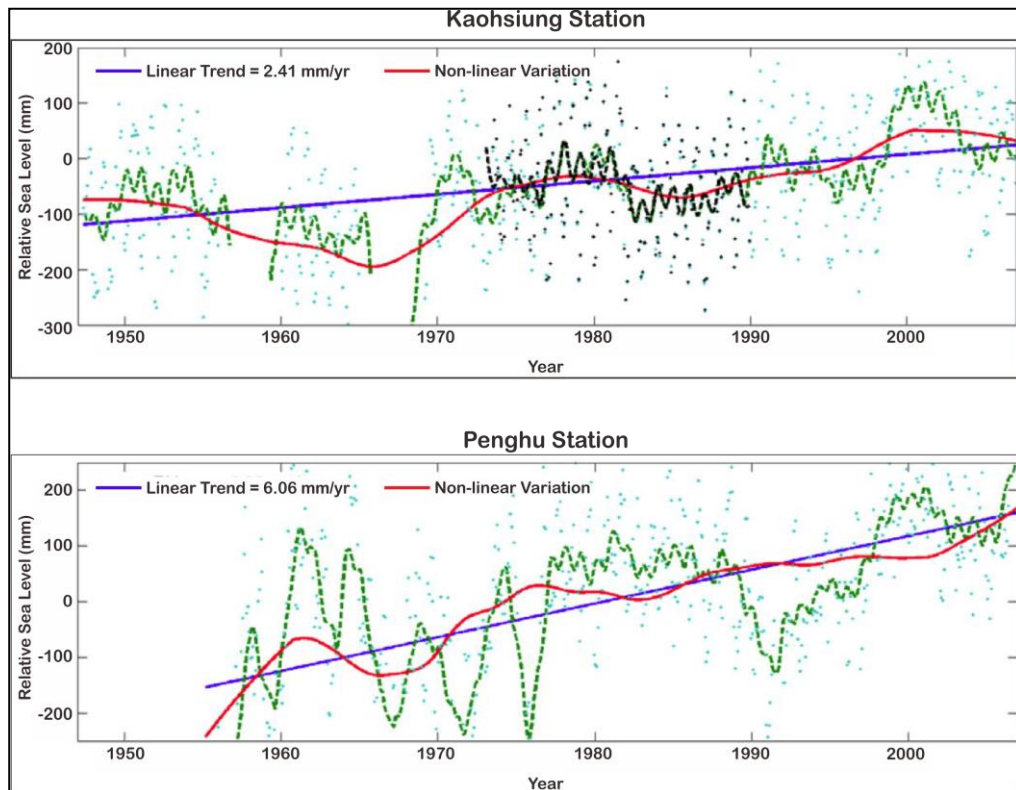


Figure 3.15 Sea level observation around Taiwan based on Kaohsiung & Penghu Station (Tseng, 2009)

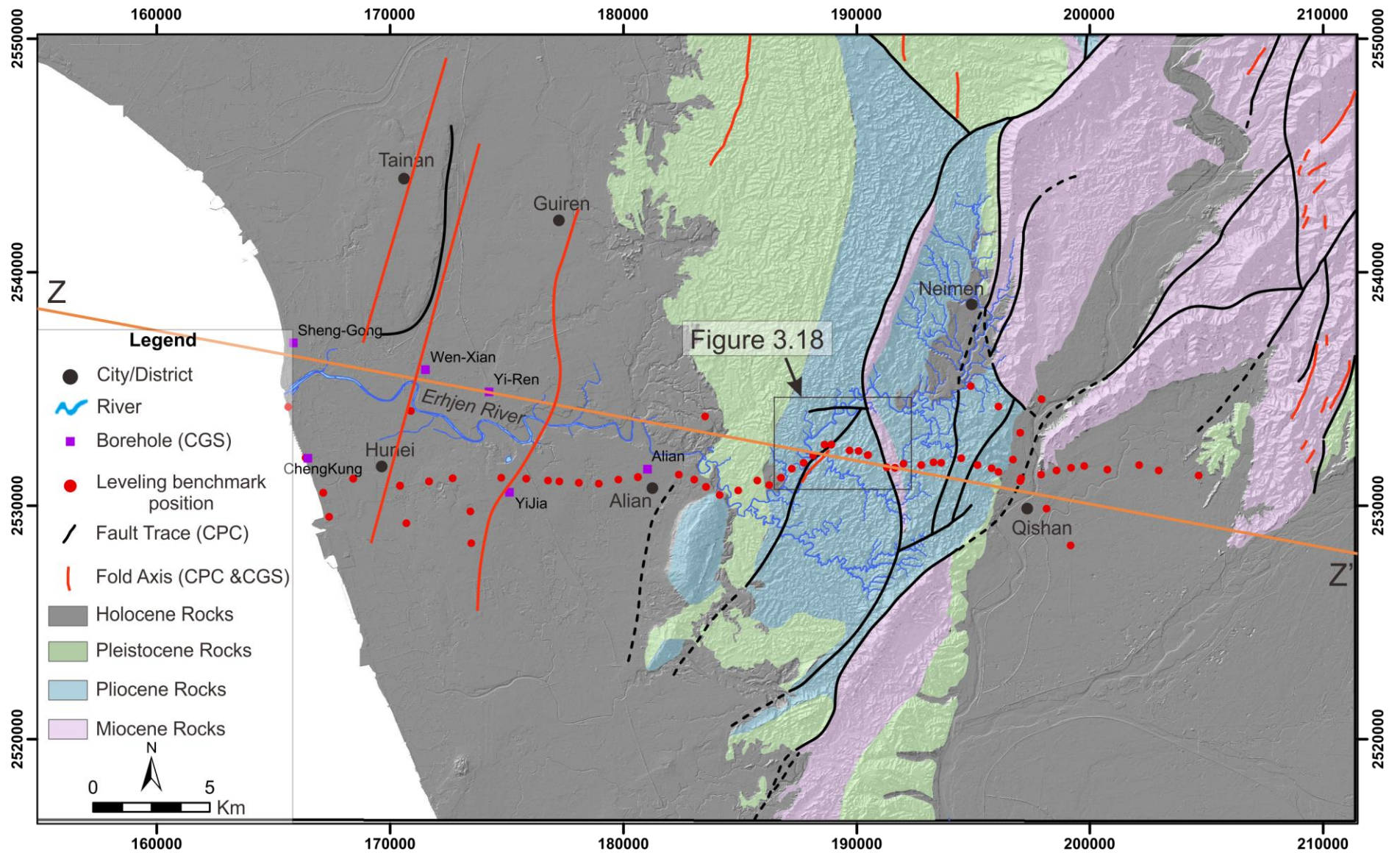


Figure 3.17 Location of the leveling benchmark and 280° azimuth projection axis Z-Z' with geological map as the background (Appendix: B for bigger map)

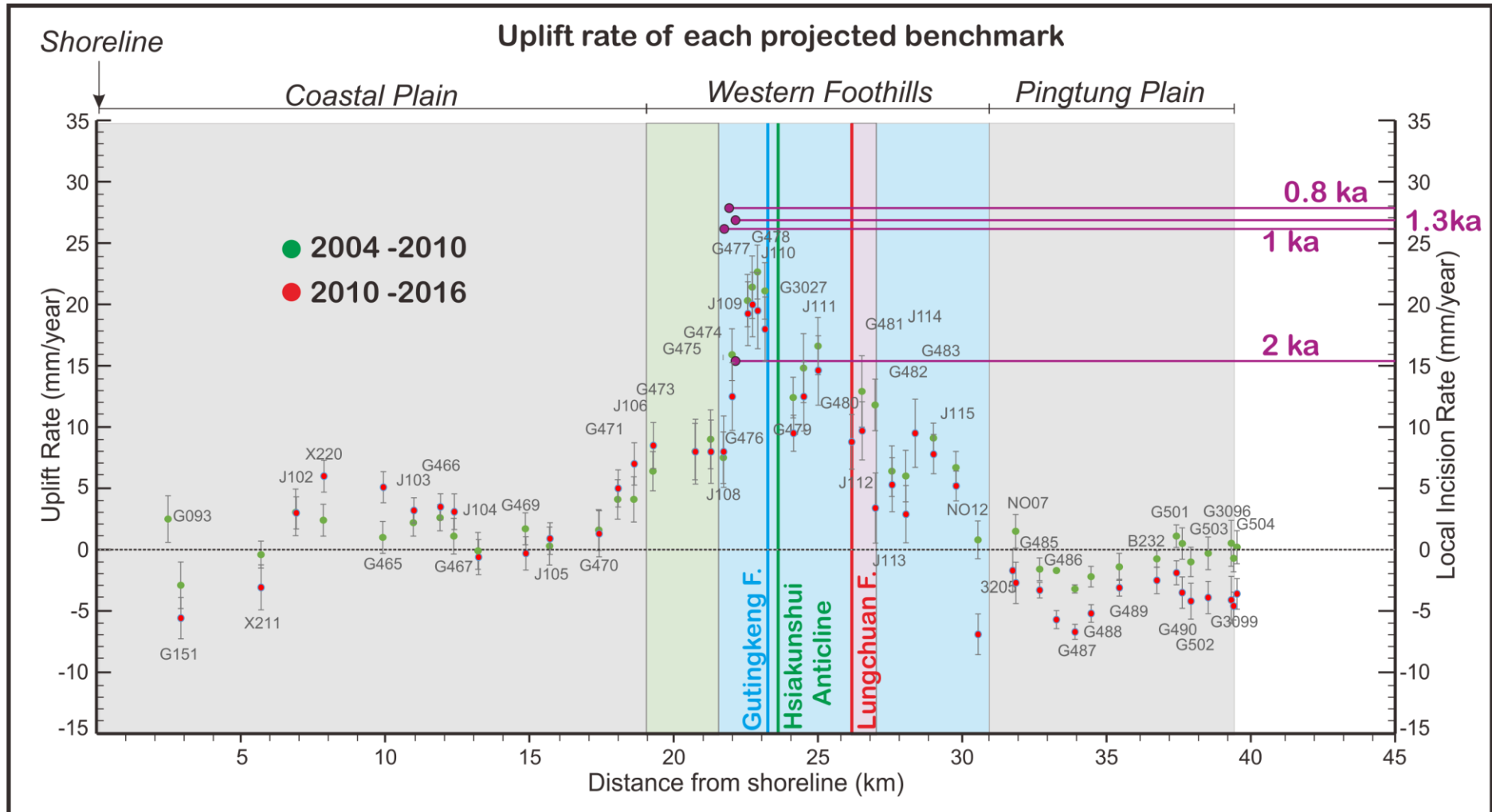


Figure 3.18 Projection of benchmark leveling point position to the Z-Z' axis. The colors in the graph and the geological structure are based on the CPC geological map

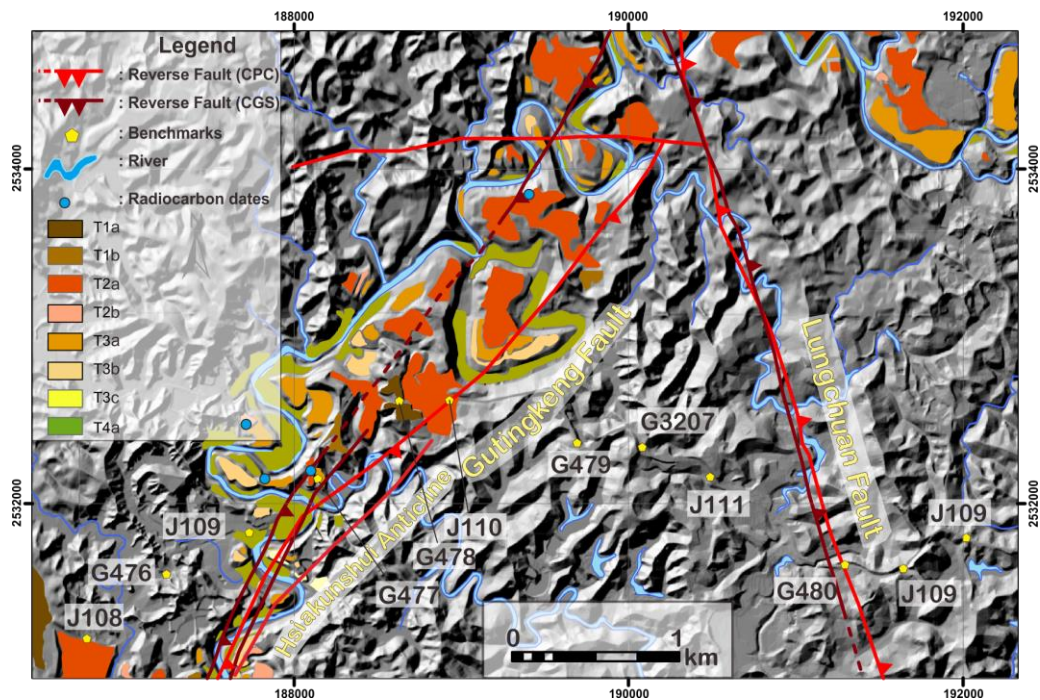


Figure 3.19 The location of the highest uplift leveling benchmark point in the midstream segment of the Erhjen River

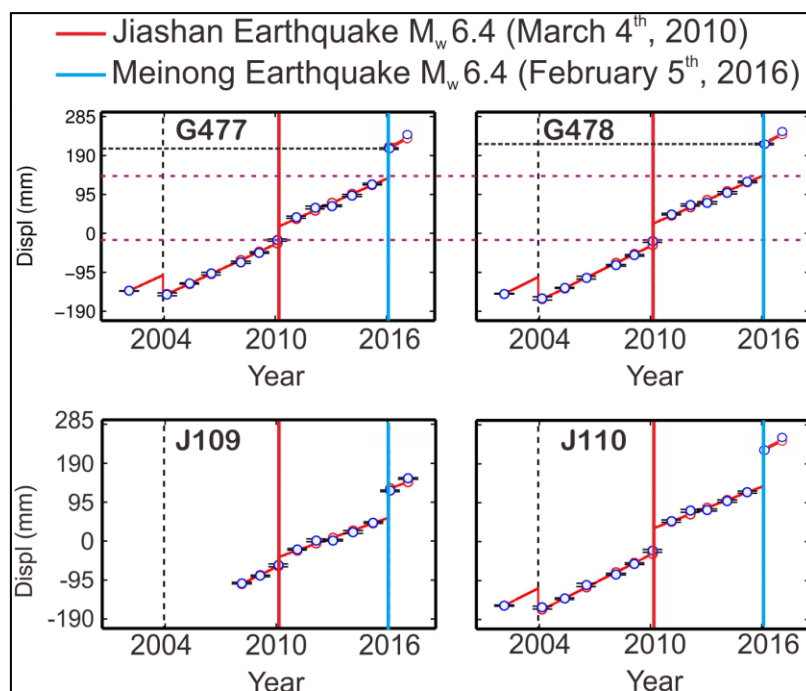


Figure 3.20 Leveling data time series for benchmarks G477, G478, J109 and J110 (Courtesy of Ching Kuo-En, 2018)

As we take a look at the curvilinear profiles of Erhjen River with its terrace deposits, we can see that the Erhjen River slope becomes steeper in the west side of Lungchuan fault. This phenomenon will support the **Third hypothesis** which is the increasing slope of Erhjen River. We calculate Erhjen River slope in the east side (upstream – midstream) is  $0.9^{\circ}$  while the west side (midstream – downstream) of Lungchuan fault is  $1.5^{\circ}$ .

In the **fourth hypothesis**, there is another reverse fault interpreted dipping to the east between both sides of the river in the A-A' (**Figure 3.21**). Another west dipping fault also interpreted in the tilted terrace T2a. As we try to map this fault trace, it is hard to correlate since we only draw fault based on the topographic offset and tilted terrace. This interpretation is weak since we do not have any age in the bedrock, we can not tell which rock is older or younger. The previous study's Gutingkeng fault trace is based on the *Gephyrocapsa oceanica* nannofossils first appearance datum (FAD) which is located in the east side of Gutingkeng fault at the zonation of NN 18, Late-Pliocene (Martini's zonation 1971) while the west side marked by the last appearance datum (LAD) of *Helicosphaera selli* at the zonation of late NN 19, Early-Pliocene (Martini's Zonation 1971) (Horng, 1994). All of those fossils will be the indicator that the west part of the Gutingkeng fault is younger than the east part, which marks a Gutingkeng fault is an east-dipping reverse fault.

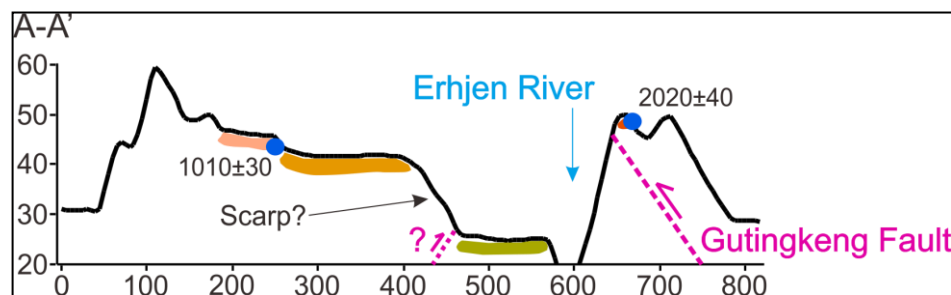


Figure 3.21 The location of interpreted reverse fault

Another observation on the ages in the CGS borehole showing that they can be correlated with the age in the terrace that located in the east part of Mountain Front. Within 100 m depth (except in the Alian, which is closest to the Mountain Front) the ages are in range between 6000 – 9000 years BP, especially those which are near the surface of Chungchou terrace the ages even have close range with 6000 – 7000 years BP. If we take a look at the ages in the Cheng-kung (coastal plain) borehole which is 2000 years BP it can be correlated with the age of the terrace in the downstream which is also dominated by 2000 years BP.

Based on our observation of the terrace deposit, leveling data, and radiocarbon dating we found that the **second hypothesis** (Fault activity change after 1ka), **third**

**hypothesis** (there are changes in river slope), **and fourth hypothesis** (another fault occurred in-between the sampling sites) are most likely to occur in this area. The incision rate of the river due to the tectonic tilting or uplifted area in both sides of the river terraces which caused the river slope increase should increase the tendency of a river to incise. While the **first hypothesis** is less likely to occur because of the sea level rise reaching up to 120 meters and the results of nannofossils which become an indicator of the dip of the fault.

Meanwhile the **First assumption** is also most likely to occur. As we compare our radiocarbon dates we found that the only one dates that has 2 ka age compare to other radiocarbon dates that located nearby. This 2 ka age can be recycled and if it is recycled, the age would be similar with the other three sites.

This means that tectonic becomes the dominant factor in the control of the Erhjen River terrace deposit. We do not deny climate factor does not affect the Erhjen River, it does affect the Erhjen River. Climate events such as rainy season and typhoon can increase the quantity of the water in Erhjen River. An increasing amount of water in the river will also increase the incision rate of the river to erode the body of the river.

### **3.5 Limitation**

We already see and measure how the terrace can be affected by the geological structure. We calculate local incision rate based on the elevation and radiocarbon. But somehow, we encounter some limitation that we cannot avoid.

In the first step of terrace classification, we only can rely based on the elevation level. We classify the terrace that has high elevation level the oldest terrace and vice versa. Until we have  $^{14}\text{C}$  radiocarbon to determine the age of the terrace. The radiocarbon dates help us to classify in more detail the age of each terrace. But still, due to the limited time and resources, we only date several places that important for us. Radiocarbon dates only cover local area. So our incision rate based on the radiocarbon dates is applied in the local area of the Erhjen River. And also some material that we dates are reworked so we can not rely upon all of the radiocarbon dates.

The aerial photo is less used, because aerial photo will also take picture of the trees. Trees become obstacle when we want to observe the flat surface area along the side

of the river. But it is useful when we encounter some uncertainties in the DEM. For example, not all of the flat surface are natural. It can be artificial and made by the human. When we conduct the field survey, the aerial photo will show us the condition in a certain area. Several areas we are unable to visit due to the inaccessible road, so we just do the reconnaissance based on the aerial photo.

Another part that becomes our concern is the drawing of the Gutingkeng fault trace. We cannot draw the Gutingkeng fault trace just based on the tilted terrace and topographic scarp/offset. Several geological profiles are needed to know the deformation in the Gutingkeng fault. However geological profiles in this research area could be an objective in the future work.

## Chapter 4 : Conclusions

Our surveillance on the Erhjen River terrace deposit has given us the insight about the modern geological event in this river. Based on our observation, four major terraces and four sub-groups of terraces are developed in the Erhjen River. These terraces became our tools to determine what happened in this area. Our  $^{14}\text{C}$  radiocarbon date results are the age of each terrace are different the youngest terrace is T4a with the age younger than  $800\pm 30$  Years BP, then T3a with the age  $800 - 870$  Years BP, followed by T2b with the exact  $1010\pm 30$  Years BP, and T2a in sometime between  $1010 - 1380$  Years BP, the last and oldest terrace is T1b with the age range between  $1600 - 2240$  Years BP.

Some tilted terraces have been found in the midstream area of Erhjen River. These tilted terraces become an indicator of the movement of the geological structure which is developed in this area. Lungchuan fault and Gutingkeng fault are the geological structures that affect these tilted terraces. We measure the slope of 10 tilted terraces in the midstream of Erhjen River with a value ranging from  $1^\circ - 4^\circ$  and developed mostly in T2a terraces. We also mapped the Gutingkeng fault trace on the surface of the terrace deposit.

We calculate incision rate at three sites in the midstream of Erhjen River. The incision rate calculation is based on the radiocarbon dates and elevation of the sample from the modern channel. The first site is in the C2, C9, and sample no. 9 areas showing that from the  $2020\pm 40$  years BP (T2a) to  $1010\pm 30$  years BP (T2b) Erhjen River erodes for about 2 mm/year, then it increases to 20 mm/year from  $1010\pm 30$  to recent, it is increasing 10 times larger. The other sites are located in the C62 (T2a) sample, from this sample we can conclude that during the 1380 Years BP to recent the incision rate is about 2.8 mm/year. In the location of C68 (T3a) sample, we calculate the incision rate is about 2.5 mm/year. From all of these differences in radiocarbon dates result, we can simplify during the 1 ka to recent the incision rate in the upper midstream part of Erhjen River is about 20 – 30 mm/year.

We know that Erhjen River keeps incising the bedrock but we also have to consider that the midstream part of Erhjen River is uplifted. Based on the leveling data observation from the previous study shows that the leveling station in the west side of Gutingkeng fault record the highest uplift with 25.1 mm/year during 2004 – 2010 and 34.2 mm/yr during 2010 - 2016.

Euclidian topographic profile of terrace deposit from upstream to downstream has been made. From these profiles, we also can determine the slope of each terrace from upstream to downstream. Based on our calculation on the Euclidian profiles, we get the T1a slope is 4.28°, T2a is 3.91°, T3a is 2.66°, and T4a is 1.98°. T1a is the steepest terrace since it encounters the geological structure longer than the other terrace. As we can see on the profiles, the slope of the Erhjen River become steeper in the west side of the Lungchuan fault. From this phenomenon, we can understand that the Gutingkeng and Lungchuan also do affect the Holocene deposit, in this case, the terrace deposit.

Since our goal is to get a better understanding of the Holocene deformation in the Gutingkeng fault, we do provide several hypotheses that can lead to understand the deformation. But however, in this study it is hard to say that we did not answer completely the question of our objectives. We need geological profile in a certain location to know the condition below the surface of the deformation of the footwall of Gutingkeng fault. Several geological profiles near the research area provided by previous studies can be a reference to draw the geological profiles for future work.

## References

- Biete, C., Alvarez-Marron, J., Brown, D., & Kuo-Chen, H. (2018). The Structure of Southwest Taiwan: The Development of a Fold-and-Thrust Belt on a Margins Outer Shelf and Slope. *Tectonics*, 37(7), 1973–1993. <https://doi.org/10.1029/2017TC004910>
- Bird, M. I. (2013). Charcoal. *Encyclopedia of Quaternary Science: Second Edition*, (December 2013), 353–360. <https://doi.org/10.1016/B978-0-444-53643-3.00047-9>
- Burbank, D., Anderson, R. (2001). *Tectonic Geomorphology*.
- Casciello E, Pappone G., Z. a. (2002). Structural features of a shear-zone developed in an argillaceous medium : the southern portion of the Scorciabuoi fault (Southern Apennines). *Bollettino Società Geologica Italiana, Volume Spe*, 659–667.
- Chen, W., Ridgway, K. D., Chen, Y., & Shea, K. (2001). Systems of the Pliocene-Pleistocene collisional marine foreland basin of Taiwan, (10), 1249–1271.
- Chen, Y. C., Sung, Q., & Cheng, K. Y. (2003). Along-strike variations of morphotectonic features in the Western Foothills of Taiwan: Tectonic implications based on stream-gradient and hypsometric analysis. *Geomorphology*, 56(1–2), 109–137. [https://doi.org/10.1016/S0169-555X\(03\)00059-X](https://doi.org/10.1016/S0169-555X(03)00059-X)
- Chiang, C. S., & Yu, H. S. (2006). Morphotectonics and incision of the Kaoping submarine canyon, SW Taiwan orogenic wedge. *Geomorphology*, 80(3–4), 199–213. <https://doi.org/10.1016/j.geomorph.2006.02.008>
- Ching, K. E., Gourley, J. R., Lee, Y. H., Hsu, S. C., Chen, K. H., & Chen, C. L. (2016). Rapid deformation rates due to development of diapiric anticline in southwestern Taiwan from geodetic observations. *Tectonophysics*, 692, 241–251. <https://doi.org/10.1016/j.tecto.2015.07.020>
- Church, J. A., & White, N. J. (2011). Sea-Level Rise from the Late 19th to the Early 21st Century. *Surveys in Geophysics*, 32(4–5), 585–602. <https://doi.org/10.1007/s10712-011-9119-1>

- Church, M. (2013). Refocusing geomorphology: Fieldwork in four acts. *Geomorphology*, 200, 184–192. <https://doi.org/10.1016/j.geomorph.2013.01.014>
- Delcaillau, B., Deffontaines, B., Floissac, L., Angelier, J., Deramond, J., Souquet, P., Lee, J. F. (1998). Morphotectonic evidence from the lateral propagation of an active frontal fold; Pakuashan anticline, foothills of Taiwan. *Geomorphology*, 24(4), 263–290. [https://doi.org/10.1016/S0169-555X\(98\)00020-8](https://doi.org/10.1016/S0169-555X(98)00020-8)
- Diao, H., Kobayashi, H., & Koketsu, K. (2018). Rupture process of the 2016 Meinong, Taiwan, earthquake and its effects on strong ground motions. *Bulletin of the Seismological Society of America*, 108(1), 163–174. <https://doi.org/10.1785/0120170193>
- Hopkins, A. J., & Snyder, N. P. (2016). Performance evaluation of three DEM-based fluvial terrace mapping methods. *Earth Surface Processes and Landforms*, 41(8), 1144–1152. <https://doi.org/10.1002/esp.3922>
- Hsieh, M. L., Ching, K. E., Chyi, S. J., Kang, S. C., & Chou, C. Y. (2014). Late Quaternary mass-wasting records in the actively uplifting Pa-chang catchment, southwestern Taiwan. *Geomorphology*, 216, 125–140. <https://doi.org/10.1016/j.geomorph.2014.03.040>
- Hsieh, M.-L., & Knuepfer, P. L. K. (2001). Late Holocene river terraces in the Erhjen River basin, southwestern Taiwan; an example of river response to active uplift and climate change. *Geological Society of America, 1997 Annual Meeting Abstracts with Programs - Geological Society of America*, 29, 344. [https://doi.org/10.1016/S0169-555X\(00\)00105-7](https://doi.org/10.1016/S0169-555X(00)00105-7)
- Hsieh, M.-L., & Knuepfer, P. L. K. (2002). Synchronicity and morphology of Holocene river terraces in the southern Western Foothills, Taiwan: A guide to interpreting and correlating erosional river terraces across growing anticlines. *Geological Society of America, 2002 Annual Meeting Abstracts with Programs - Geological Society of America*
- Hsu, Y. J., Lai, Y. R., You, R. J., Chen, H. Y., Teng, L. S., Tsai, Y. C., ... Su, H. H. (2018). Detecting rock uplift across southern Taiwan mountain belt by integrated

- GPS and leveling data. *Tectonophysics*, 744(February), 275–284.  
<https://doi.org/10.1016/j.tecto.2018.07.012>
- Hsu, Y. J., Yu, S. B., Kuo, L. C., Tsai, Y. C., & Chen, H. Y. (2011). Coseismic deformation of the 2010 Jiashian, Taiwan earthquake and implications for fault activities in southwestern Taiwan. *Tectonophysics*, 502(3–4), 328–335.  
<https://doi.org/10.1016/j.tecto.2011.02.005>
- Hsu, Y. J., Yu, S. B., Simons, M., Kuo, L. C., & Chen, H. Y. (2009). Interseismic crustal deformation in the Taiwan plate boundary zone revealed by GPS observations, seismicity, and earthquake focal mechanisms. *Tectonophysics*, 479(1–2), 4–18.  
<https://doi.org/10.1016/j.tecto.2008.11.016>
- Huang, S. T., Yang, K. M., Hung, J. H., Wu, J. C., Ting, H. H., Mei, W. W., ... Lee, M. (2004). Deformation front development at the northeast margin of the Tainan basin, Tainan-Kaohsiung area, Taiwan. *Marine Geophysical Researches*, 25(1–2), 139–156. <https://doi.org/10.1007/s11001-005-0739-z>
- Huang, M. H., Dreger, D., Bürgmann, R., Yoo, S. H., & Hashimoto, M. (2013). Joint inversion of seismic and geodetic data for the source of the 2010 march 4, Mw6.3 Jia-Shian, SW Taiwan, earthquake. *Geophysical Journal International*, 193(3), 1608–1626. <https://doi.org/10.1093/gji/ggt058>
- Jia, L., Zhang, X., He, Z., He, X., Wu, F., Zhou, Y., Zhao, J. (2015). Late Quaternary climatic and tectonic mechanisms driving river terrace development in an area of mountain uplift: A case study in the Langshan area, Inner Mongolia, northern China. *Geomorphology*, 234, 109–121. <https://doi.org/10.1016/j.geomorph.2014.12.043>
- Kumar, Satish. (2005). Quaternary geomorphic events and river terraces in Northwest Himalaya: a case study of the Beas basin India. Unpublished master thesis
- Lacombe, O., Angelier, J., Chen, H. W., Deffontaines, B., Chu, H. T., & Rocher, M. (1997). Syndepositional tectonics and extension-compression relationships at the front of the Taiwan collision belt: A case study in the Pleistocene reefal limestones near Kaohsiung, SW Taiwan. *Tectonophysics*, 274(1–3), 83–96.  
[https://doi.org/10.1016/S0040-1951\(96\)00299-5](https://doi.org/10.1016/S0040-1951(96)00299-5)

- Le Béon, M., Huang, M.-H., Suppe, J., Huang, S.-T., Pathier, E., Huang, W.-J., Hu, J.-C. (2017). Shallow geological structures triggered during the Mw 6.4 Meinong earthquake, southwestern Taiwan. *Terrestrial, Atmospheric and Oceanic Sciences*, 28(5), 663–681. <https://doi.org/10.3319/TAO.2017.03.20.02>
- Li, T., Chen, J., Thompson, J. A., Burbank, D. W., & Yang, X. (2013). Quantification of three-dimensional folding using fluvial terraces: A case study from the Mushi anticline, northern margin of the Chinese Pamir. *Journal of Geophysical Research: Solid Earth*, 118(8), 4628–4647. <https://doi.org/10.1002/jgrb.50316>
- Miller, K. G. (2008). Sea level change, last 250 million years. *Encyclopedia of Paleoclimatology and Ancient Environments*, (Ed V. Gornitz, Ed. (Springer, Berlin, 2008)), 879–887.
- Monforte, P. M., Oliveira, U. R., & Rocha, H. M. (2015). Failure Mapping Process: an Applied Study in a Shipyard Facility. *Brazilian Journal of Operations & Production Management*, 12(1), 124. <https://doi.org/10.14488/BJOPM.2015.v12.n1.a12>
- Mouthereau, F., Lacombe, O., Deffontaines, B., Angelier, J., & Brusset, S. (2001). Deformation history of the southwestern Taiwan foreland thrust belt: Insights from tectono-sedimentary analyses and balanced cross-sections. *Tectonophysics*, 333(1–2), 293–322. [https://doi.org/10.1016/S0040-1951\(00\)00280-8](https://doi.org/10.1016/S0040-1951(00)00280-8)
- Necea, D., Fielitz, W., Kadereit, A., Andriessen, P. A. M., & Dinu, C. (2013). Middle Pleistocene to Holocene fluvial terrace development and uplift-driven valley incision in the SE Carpathians, Romania. *Tectonophysics*, 602, 332–354. <https://doi.org/10.1016/j.tecto.2013.02.039>
- Oldknow, C. J., & Hooke, J. M. (2017). Alluvial terrace development and changing landscape connectivity in the Great Karoo, South Africa. Insights from the Wilgerbosch River catchment, Sneeuwberg. *Geomorphology*, 288, 12–38. <https://doi.org/10.1016/j.geomorph.2017.03.009>
- Sandmann, S., Nagel, T. J., Froitzheim, N., Ustaszewski, K., & Münker, C. (2015). Late Miocene to Early Pliocene blueschist from Taiwan and its exhumation via forearc extraction. *Terra Nova*, 27(4), 285–291. <https://doi.org/10.1111/ter.12158>

- Sequences, C. (1984). © 1984 The International Association of Sedimentologists. ISBN : 978-0-632-01286-2. <https://doi.org/10.1002/9781444303810>
- Shalaby, A., & Shawky, M. (2014). Morphotectonics of Kid drainage basin, Southeastern Sinai: A landscape evolution coeval to Gulf of Aqaba - the Dead Sea rift. *Journal of African Earth Sciences*, 100, 289–302. <https://doi.org/10.1016/j.jafrearsci.2014.06.025>
- Shyu, J. B. H., Sieh, K., Avouac, J. P., Chen, W. S., & Chen, Y. G. (2006). Millennial slip rate of the Longitudinal Valley fault from river terraces: Implications for convergence across the active suture of eastern Taiwan. *Journal of Geophysical Research: Solid Earth*, 111(8). <https://doi.org/10.1029/2005JB003971>
- Sibuet, J. C., & Hsu, S. K. (2004). How was Taiwan created? *Tectonophysics*, 379(1–4), 159–181. <https://doi.org/10.1016/j.tecto.2003.10.022>
- Strick, R. J. P., Ashworth, P. J., Awcock, G., & Lewin, J. (2018). Morphology and spacing of river meander scrolls. *Geomorphology*, 310, 57–68. <https://doi.org/10.1016/j.geomorph.2018.03.005>
- Tsai, M.-C., Shin, T.-C., & Kuo, K.-W. (2017). Pre-seismic strain anomalies and coseismic deformation of Meinong earthquake from continuous GPS. *Terrestrial, Atmospheric and Oceanic Sciences*, 28(5), 763–785. <https://doi.org/10.3319/TAO.2017.04.19.01>
- Tziavou, O., Pytharouli, S., & Souter, J. (2018). Unmanned Aerial Vehicle (UAV) based mapping in engineering geological surveys: Considerations for optimum results. *Engineering Geology*, 232(November 2017), 12–21. <https://doi.org/10.1016/j.enggeo.2017.11.004>
- Vandenberghe, J. (2015). River terraces as a response to climatic forcing: Formation processes, sedimentary characteristics, and sites for human occupation. *Quaternary International*, 370, 3–11. <https://doi.org/10.1016/j.quaint.2014.05.046>

- Yang, K.-M., Huang, S.-T., Wu, J.-C., Ting, H.-H., & Mei, W.-W. (2006). Review and New Insights on Foreland Tectonics in Western Taiwan. *International Geology Review*, 48(10), 910–941. <https://doi.org/10.2747/0020-6814.48.10.910>
- Yu, H. S. (2004). Nature and distribution of the deformation front in the Luzon Arc-Chinese continental margin collision zone at Taiwan. *Marine Geophysical Researches*, 25(1–2), 109–122. <https://doi.org/10.1007/s11001-005-0737-1>

## **Appendix**

## **Appendix A: Terrace Map (Attached)**

## **Appendix B: Leveling Data Station Map (Attached)**